

CHAPTER 3
RESULTS & DISCUSSION

3.0. Mini river section

3.1. Soil composition

The U. S. Department of Agriculture has classified soil based on size of its constituents. They are

Clay	< 0.002 mm
Silt	0.05 – 0.002 mm
Medium sand	0.5 – 0.25 mm

The composition of soils collected from Angad, Amrapura and Chamunda nagar sections along the Mini river are given in Table 3.1, 3.2 and 3.3 respectively. The sand content was found to be higher in all the three sections.

Table 3.1. Soil composition of Angad section (22° 23' 02 N 073° 05' 9 E)

Sample No	Sand(%)	Silt(%)	Clay(%)
1	52	30	18
2	48	24	28
3	57	22	21
4	48	28	24
5	51	24	25
6	58	20	22
7	48	32	20
8	57	31	12
9	61	27	22
10	60	28	12
11	48	31	21
12	57	27	16
13	40	32	28
14	45	32	23
15	61	27	12
16	60	21	19
17	46	32	22
18	48	27	25
19	51	34	15
20	49	37	14
21	51	39	10
22	52	40	08
23	61	32	07
24	54	38	08
25	49	35	16
26	57	31	12
27	51	30	19
28	48	39	13
29	56	32	12

Table 3.2. Soil composition of Amrapura section (22° 21' 02 N 73° 04' 41 E)

Sample No	Sand(%)	Silt(%)	Clay(%)
1	45	29	26
2	58	30	12
3	49	28	23
4	53	21	26
5	58	22	20
6	61	22	17
7	56	32	12
8	54	26	20
9	49	30	21
10	52	27	21
11	49	40	11
12	47	38	15
13	61	30	09
14	54	35	11
15	47	38	15
16	54	36	10

Table 3.3. Soil composition of Chamunda nagar section (22° 23' 42 N 073° 05' 55 E)

Sample No	Sand(%)	Silt(%)	Clay(%)
1	54	20	26
2	55	20	25
3	61	21	18
4	54	17	29
5	52	22	26
6	62	21	17
7	49	29	22
8	34	52	14
9	37	54	09
10	32	50	18
11	29	61	10
12	33	47	20
13	30	52	18
14	23	55	22
15	32	62	06
16	34	52	14
17	36	50	14
18	51	29	20
19	54	21	25
20	65	20	15
21	49	29	22
22	47	33	20
23	35	52	13
24	40	42	18
25	48	28	24

3.2. Colloidal properties

The litholog of the Rayka, Jaspur, Dodka and Mujpur section is given in Figure 3.1, 3.3, 3.5 and 3.7 respectively. These lithologs implies the sequence of sediment deposition along the river bed over long period of time. The sediment samples were collected at the intervals of 0.25m in all these four sampling sites and analyzed for the pH, colloidal concentration, electrical conductivity and particle size distribution. This analysis was carried out to find the variation of particle size with respect to the sediment sequence and depth.

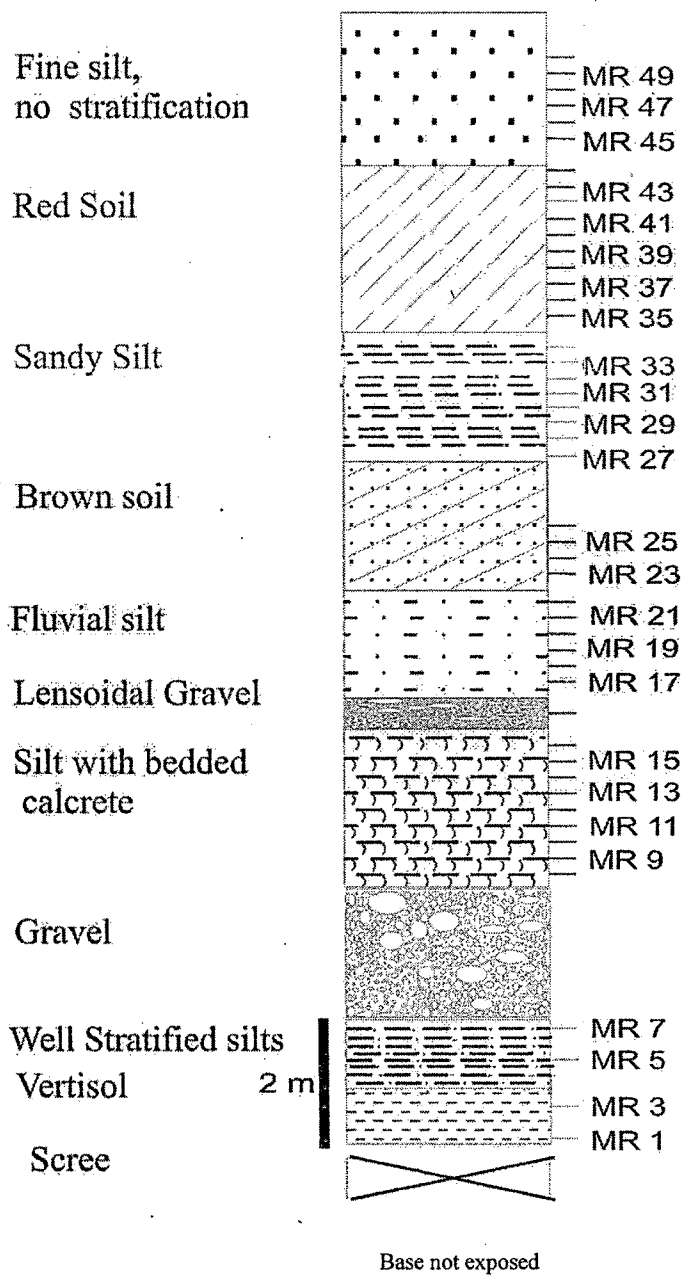


Figure 3.1. Litholog of the Rayka section (21° 29' 52 N 73° 9' 54 E)

Table 3.4. Properties of colloidal suspension of Rayka section

Sample No	pH	Colloidal concentration(mg/L)	Colloid size distribution(nm)	Electrical conductivity (mS/cm)
MR 1	6.90	1600	179.4±65.1	2.10
MR 2	7.43	800	150.2±0.7	1.99
MR 3	7.24	1200	112±3.4	2.11
MR 4	7.42	1000	90.0±5.8	2.19
MR 5	7.41	1000	85.6±0.4	2.17
MR 6	7.53	1800	60.5±0.0	2.19
MR 7	7.35	1800	31.1±0.2	2.18
MR 8	7.43	2000	72.5±0.3	2.08
MR 9	7.24	1800	45.8±23.1	2.34
MR 10	7.10	1600	25.7±3.2	2.32
MR 11	7.22	800	44.6±1.0	2.15
MR 12	7.28	1000	57.4±5.4	2.44
MR 13	7.25	1400	103.2±2.3	2.23
MR 14	7.15	1400	108.5±3.9	2.33
MR 15	7.21	1000	64.1±1.8	2.32
MR 16	7.03	400	59.6±0.7	0.41
MR 17	7.39	800	67.3±0.8	2.60
MR 18	7.46	1600	57.7±1.1	2.49
MR 19	7.11	2000	61.0±12.1	2.75
MR 20	7.03	2400	59.8±9.8	2.74
MR 21	7.06	2000	77.0±1.4	2.96
MR 22	7.76	1200	101.3±36.6	2.65
MR 23	7.49	2000	515.5±0.5	2.56
MR 24	7.37	1800	79.7±0.8	2.47
MR 25	7.36	2400	92.8±0.4	2.73
MR 26	7.44	1400	113.1±0.7	2.50
MR 27	7.28	1900	89.0±23.2	2.25
MR 28	7.30	1800	60.0±0.0	2.44
MR 29	7.10	2000	143.2±30.8	2.28
MR 30	7.34	1400	175.6±0.3	2.35
MR 31	7.54	1600	222.8±1.2	2.50
MR 32	6.91	1200	176.1±42.3	2.30
MR 33	7.18	1200	124.0±2.5	2.41
MR 34	7.43	2000	51.5±0.8	2.35
MR 35	7.10	2000	56.7±7.9	2.34
MR 36	7.40	400	58.3±0.4	0.43
MR 37	7.56	1200	60.4±10.9	2.39
MR 38	7.51	2200	64.9±3.0	2.43
MR 39	7.88	1000	78.4±21.0	2.46
MR 40	7.37	800	81.3±43.2	2.43
MR 41	7.51	1200	25.9±1.8	2.42
MR 42	7.30	1400	121.2±3.9	2.36
MR 43	7.06	1400	110.5±0.6	2.19
MR 44	7.34	1400	67.3±0.3	2.10
MR 45	7.50	2000	84.2±4.2	2.38
MR 46	7.24	2000	95.2±38.5	2.19
MR 47	7.51	1800	70.2±0.3	2.14
MR 48	7.30	1400	49.5±0.7	2.18
MR 49	7.07	1000	108.1±1.5	2.30

Table 3.5. ICP- AES analysis of colloidal suspensions

Sample No	Electrical conductivity(mS/cm)	Al (ppm)	Fe (ppm)	Ca (ppm)	Mg (ppm)	Si (ppm)
MR15	2.39	0.0385	0.0076	21.13	23.39	12.22
MR16	0.41	0.0341	NIL	16.35	5.406	5.112
MR17	2.34	0.0293	NIL	21.43	24.39	11.98
MR35	2.60	0.0234	NIL	13.00	8.066	9.754
MR36	0.43	0.0234	NIL	19.49	3.684	3.921
MR37	2.32	0.0222	NIL	28.63	15.80	10.46

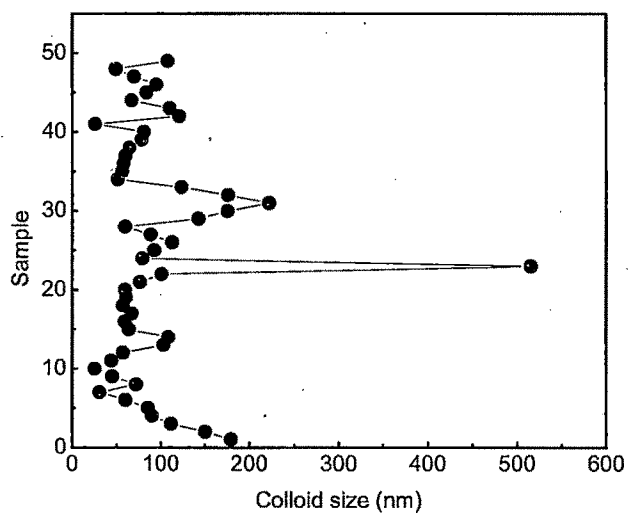
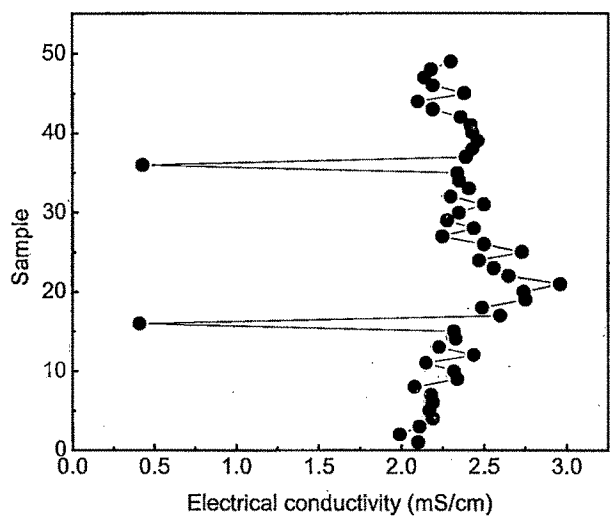


Figure 3.2. Electrical conductivity and colloid size of Rayka section

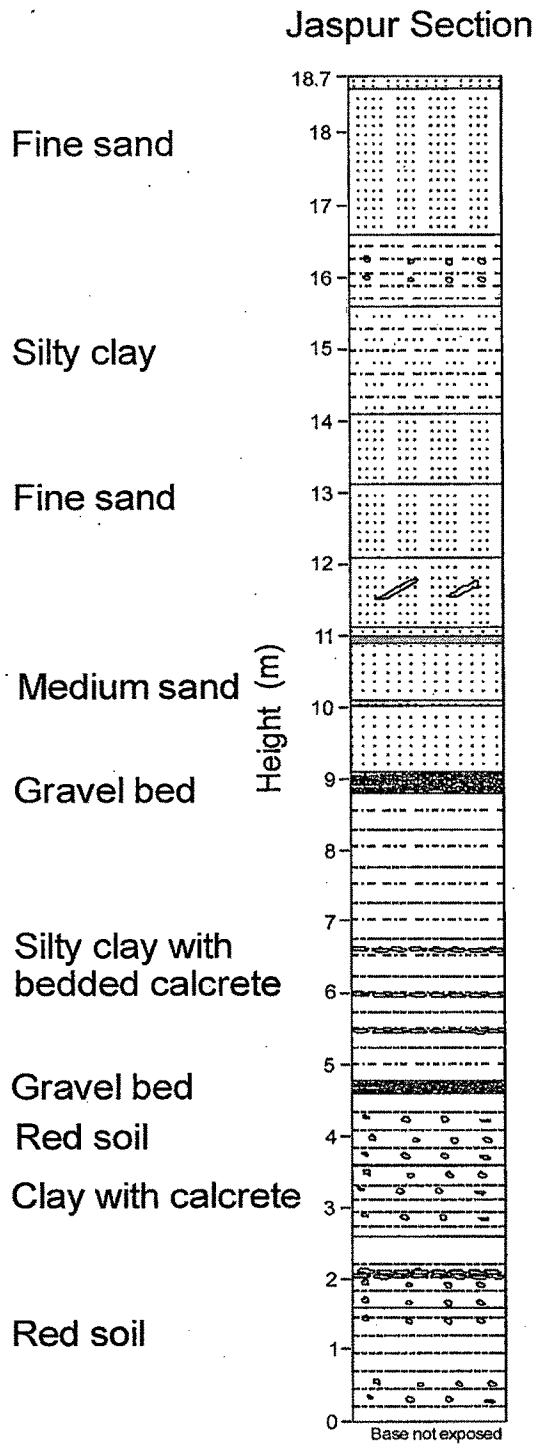


Figure 3.3. Litholog of the Jaspur section (22° 18' 31 N 73° 02' 69 E)

Table 3.6. Properties of colloidal suspensions of Jaspur section

	pH	Colloidal concentration (mg/L)	Colloid size distribution (nm)	Electrical conductivity (μ S/cm)
MJ 1	7.04	2400	103.6 \pm 46.5	3.25
MJ 2	7.02	2000	110.3 \pm 63.3	2.68
MJ 3	7.10	2000	112.5 \pm 48.5	2.53
MJ 4	6.99	2000	85 \pm 30.2	2.31
MJ 5	6.98	1800	76.6 \pm 2.0	2.32
MJ 6	6.98	1800	68.8 \pm 12.1	2.42
MJ 7	6.97	1900	39.7 \pm 13.2	2.52
MJ 8	7.05	2200	163.9 \pm 11.7	2.37
MJ 9	7.08	1800	61.7 \pm 10.3	2.34
MJ 10	7.04	1600	54.6 \pm 9.2	2.29
MJ 11	7.05	2000	181.1 \pm 29.6	2.35
MJ 12	7.11	1800	131.3 \pm 3.8	2.34
MJ 13	7.12	1400	120.4 \pm 12.8	2.28
MJ 14	7.13	1800	48.4 \pm 32.7	2.34
MJ 15	7.11	1600	195.3 \pm 63.3	2.29
MJ 16	7.10	1400	178.5 \pm 23.8	2.19
MJ 17	7.11	1800	92.7 \pm 31.1	2.30
MJ 18	7.14	1800	89.2 \pm 12.5	2.36
MJ 19	7.01	2000	146.0 \pm 41.7	2.45
MJ 20	7.23	2000	45.6 \pm 19.8	2.40
MJ 21	7.21	2000	153.1 \pm 9.8	2.37
MJ 22	7.13	1800	44.7 \pm 33.1	2.38
MJ 23	7.08	1800	180.7 \pm 29.8	2.35
MJ 24	6.92	1600	68.4 \pm 8.7	2.29
MJ 25	6.98	1600	45.5 \pm 35.2	2.24
MJ 26	7.04	2000	96.9 \pm 19.6	2.33
MJ 27	7.05	1800	135.1 \pm 27.7	2.22
MJ 28	7.03	2200	170.8 \pm 21.4	2.41
MJ 29	7.07	1800	100.3 \pm 12.4	2.29
MJ 30	7.12	2000	78.5 \pm 46.8	2.26
MJ 31	7.03	2000	108.6 \pm 8.1	2.33
MJ 32	7.03	1800	55.4 \pm 0.0	2.32
MJ 33	7.04	2200	64.0 \pm 21.6	2.76
MJ 34	7.18	1600	103.5 \pm 7.9	2.22
MJ 35	7.20	1400	66.9 \pm 0.0	2.22
MJ 36	7.11	1200	85.5 \pm 22.4	2.17
MJ 37	7.12	1400	201.3 \pm 85.6	2.29
MJ 38	7.14	1600	114.6 \pm 42.3	2.23
MJ 39	7.01	1600	109.9 \pm 67.8	2.16
MJ 40	6.98	1400	61.9 \pm 43.6	2.21
MJ 41	7.14	2000	45.5 \pm 10.5	2.36
MJ 42	7.10	2000	39.1 \pm 22.2	2.31
MJ 43	7.12	1400	88.0 \pm 23.2	2.28
MJ 44	7.02	1400	129.0 \pm 31.7	2.23
MJ 45	7.03	1600	25.3 \pm 10.3	2.27
MJ 46	7.04	1200	34.5 \pm 11.3	2.28
MJ 47	7.01	1200	45.5 \pm 10.2	2.19
MJ 48	7.09	1000	65.2 \pm 22.1	2.04
MJ 49	6.91	1400	52.4 \pm 22.5	2.16
MJ 50	6.86	1400	114.5 \pm 43.4	2.15
MJ 51	6.87	1800	190.4 \pm 26.0	2.21
MJ 52	6.90	1600	114.9 \pm 6.7	2.12

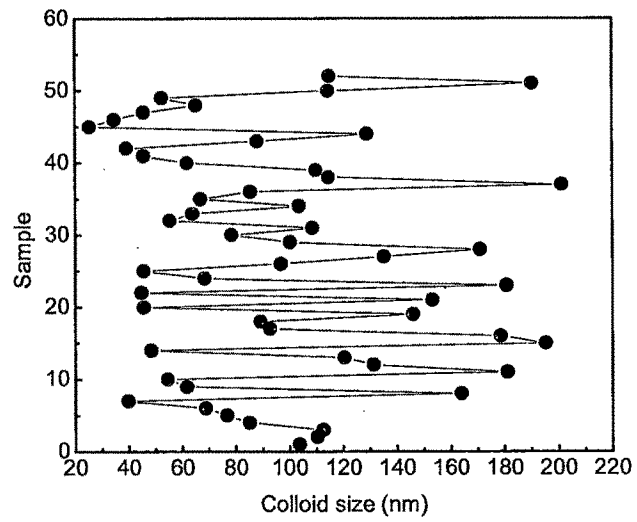
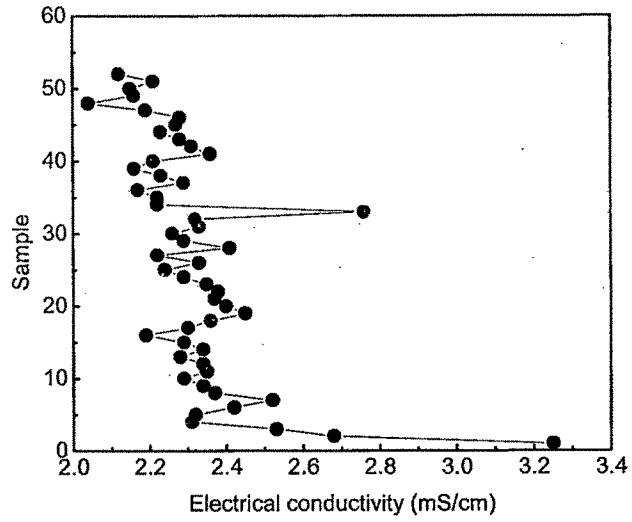


Figure 3.4. Electrical conductivity and colloid size of Jaspur section

Dodka section

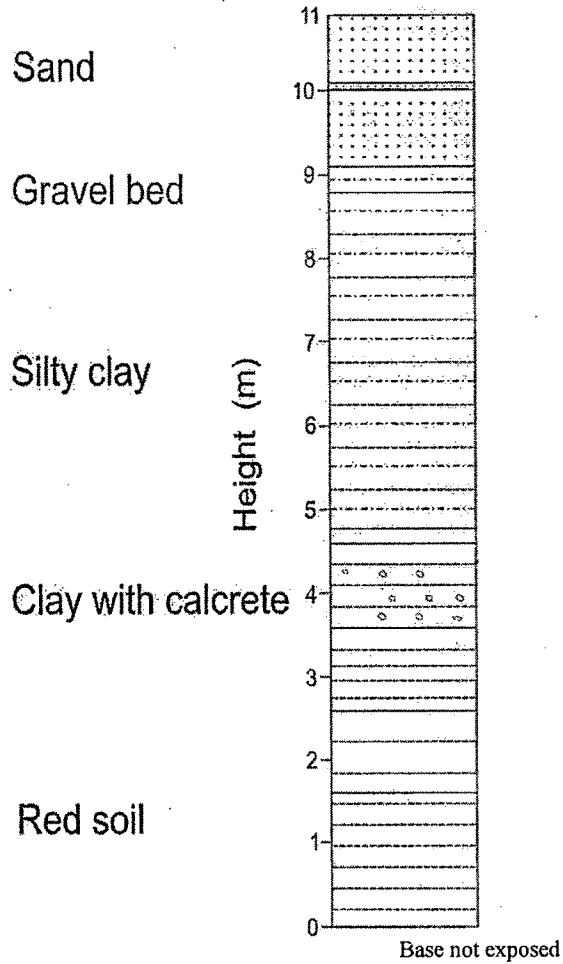


Figure 3.5. Lithlog of Dodka section (22° 21' 05 N 73° 09' 52 E)

Table 3.7. Properties of colloidal suspensions Dodka section

S No	pH	Colloidal concentration (mg/L)	Colloid size distribution (nm)	Electrical conductivity (mS/cm)
MD 1	6.98	2000	108.1±4.8	1.321
MD 2	6.87	1600	112.2±21.8	1.342
MD 3	6.89	2200	145.0±31.9	1.321
MD 4	6.98	2200	156.5±20.2	1.329
MD 5	7.02	2000	89.4±12.1	1.356
MD 6	6.89	1800	78.0±4.5	1.346
MD 7	6.72	1600	123±43.8	1.354
MD 8	6.78	2400	189.2±12.9	1.365
MD 9	6.81	2600	123.2±32.0	1.421
MD 10	6.91	2800	129.1±21.0	1.432
MD 11	7.08	2800	157.8±11.3	1.421
MD 12	7.08	2200	176.4±4.3	1.432
MD 13	6.76	2200	134.6±3.9	1.374
MD 14	6.88	2400	98.0±2.8	1.387
MD 15	6.93	2000	87.9±1.2	1.349
MD 16	7.20	1800	67.7±11.2	1.356
MD 17	7.17	2000	92.5±4.0	1.352
MD 18	7.16	2200	45.8±2.8	1.367
MD 19	7.21	2200	58.0±3.8	1.387
MD 20	6.90	2000	76.8±32.9	1.389
MD 21	6.99	1800	38.9±1.8	1.453
MD 22	6.93	2400	45.8±8.5	1.459
MD 23	6.91	2600	110.6±10.3	1.432
MD 24	6.88	2400	129.8±12.8	1.419
MD 25	6.76	2000	145.6±13.2	1.391
MD 26	6.79	1800	187.3±34.9	1.379
MD 27	6.87	1800	176.5±6.5	1.378
MD 28	7.04	2400	154.5±5.0	1.389
MD 29	7.01	2200	132.9±2.3	1.345
MD 30	7.09	2000	143.2±6.8	1.348
MD 31	7.14	1600	134.9±0.0	1.378
MD 32	7.21	2800	135.6±0.0	1.398
MD 33	7.23	3000	114.8±8.9	1.492
MD 34	7.29	3400	165.2±18.5	1.490

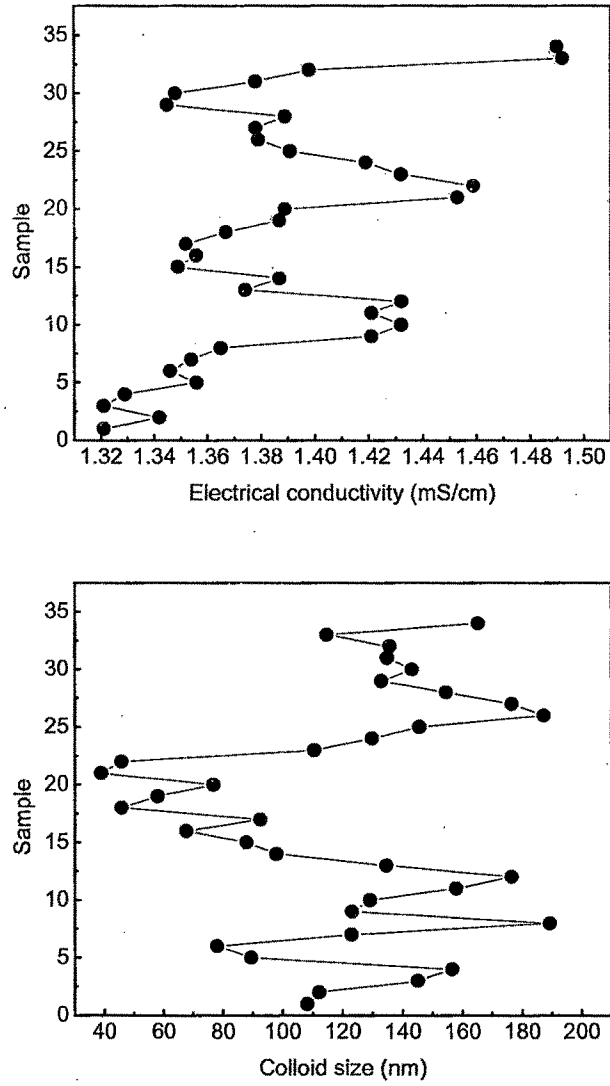


Figure 3.6. Electrical conductivity and colloid size of Dodka section

Mujpur section

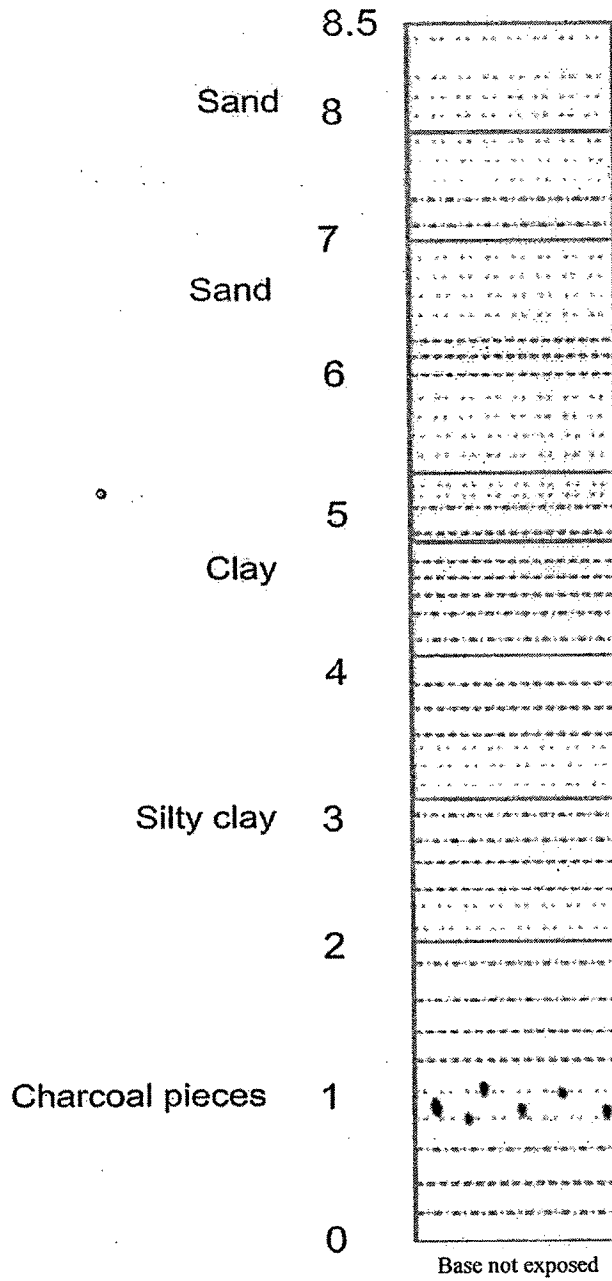


Figure 3.7. Litholog of the Mujpur section (22° 15' 18 N 72° 59' 10 E)

Table 3.8. Properties of colloidal suspensions of Mujpur section

S. No	pH	Colloidal concentration (mg/L)	Colloid size distribution (nm)	Electrical conductivity (mS/cm)
MM 1	7.11	2800	87.5±3.7	1.432
MM 2	7.23	2600	76.4±12.1	1.356
MM 3	7.21	2600	34.8±0.0	1.386
MM 4	7.06	2400	56.2±2.4	1.358
MM 5	6.98	2200	78.6±20.1	1.392
MM 6	6.87	2000	122.3±11.2	1.456
MM 7	6.95	2000	154.8±21.0	1.438
MM 8	6.88	2600	165.2±11.0	2.432
MM 9	7.03	2600	187.2±9.8	1.412
MM 10	7.05	2000	123.4±2.1	1.421
MM 11	7.12	3400	145.3±10.0	2.765
MM 12	7.10	4000	78.6±12.1	1.876
MM 13	7.08	3000	55.6±3.4	1.789
MM 14	6.85	3400	39.8±1.2	2.834
MM 15	6.92	3400	45.5±1.8	2.134
MM 16	6.96	3400	54.1±1.0	2.234
MM 17	7.18	4200	67.2±7.8	2.321
MM 18	7.10	4200	89.6±1.8	2.723
MM 19	7.08	4400	78.9±1.3	2.875
MM 20	7.05	4400	95.4±11.2	2.887

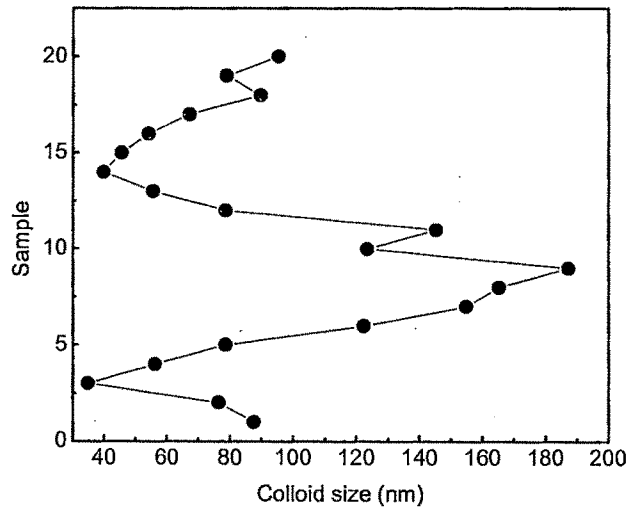
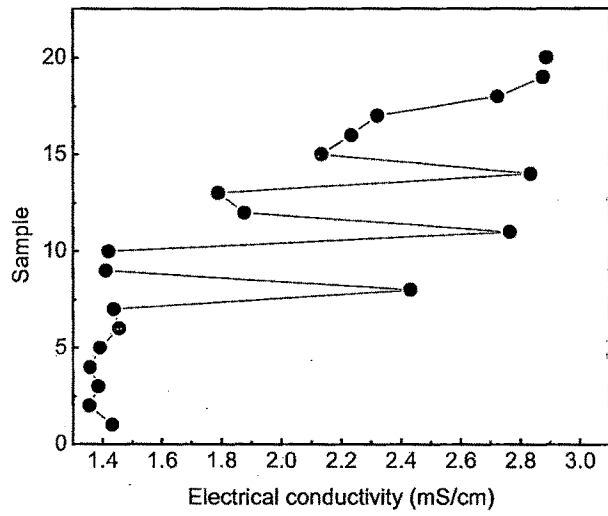


Figure 3.8. Electrical conductivity and colloid size of Mujpur section

The properties of colloidal suspensions of all four sections namely Rayka, Jaspur, Dodka and Mujpur are given in Table 3.4, 3.6, 3.7 and 3.8 and Figure 3.2, 3.4, 3.6 and 3.8.

3.2.1. pH

It has been observed that pH of the colloidal suspensions of all the samples of Rayka section are above 7 except sample No1 and 32. In case of Jaspur section most of the samples show pH values of above 6.9. While the Dodka samples showed the pH of above 6.9, the pH of colloid suspensions of Mujpur section is above 7, if not all. This shows the slight alkaline nature of sediments of all four sections.

3.2.2. Colloid concentration

The results of colloidal concentration shows the quantity of colloids present in sediment samples and it also varies for the samples of single section. The data provided for the sediment samples of whole section are helpful in understanding the properties of soil colloids at different intervals.

3.2.3. Colloid size distribution

The results show that the colloidal particles are highly polydisperse with respect to size which means that each sample has the particles of varying size. This varied size distribution can be attributed to the formation nature of this colloids from original parent geologic material by weathering process. Weathering means the transformation of one product into another by various factors such as physical mechanism (temperature, hydration, effect of salt crystallization) and the chemical mechanisms (dissolution, hydrolysis, oxidation-reduction). In this process large mineral fragments are transformed into smaller ones of varying size. It has been reported that the coarse grained aquifer material may contain up to 5% clay sized materials that may be detrital (present in the original parent geologic material) or authigenic (formed by geochemical alteration of primary minerals).

In Rayka type section, sample No 7 has small particles while sample No 23 showed maximum size of colloids. Such wide size distribution in a particular single section indicates the formation nature of colloids by weathering. The monodispersity of colloids was found in samples 6 and 28. In the case of Jaspur section, the sample No

45 and 37 contains particles of minimum and maximum size with samples 32 and 35 showing monodispersity. In the case of Dodka section, samples 21 and 8 has the particles of minimum and maximum dimension with 31 and 32 consist of mono disperse particles.

The Mujpur section samples 9 and 3 have colloids of minimum size with monodispersity and maximum size respectively.

3.2.4. Electrical conductivity

The Electrical conductivity of colloidal suspensions of Rayka section samples are above 2 mS/cm, except samples 16 and 36, whose EC values turned out to be 0.41 mS/cm and 0.43 mS/cm respectively. Such low Electrical conductivity of these two samples could be attributed to the low concentration of indicator elements of colloids such as Si, Al and Mg present as compared to other samples. The element content of colloids determined by ICP-AES analysis is given in Table 3.5. To confirm the observed low Electrical conductivity and colloid concentration ICP-AES analysis was carried out for samples 15 to 17 and 35 to 37. The concentration of indicator elements Si, Al, Ca and Mg is relatively low for samples 16 and 36 which also showed low colloidal concentration as compared to other samples.

Though the Electrical conductivity of distilled water is $1\mu\text{S}/\text{cm}$, the Electrical conductivity of colloidal suspensions reaches above 2 mS/cm. Such exponential increase in Electrical conductivity indicates the presence of surface charge on the colloids.

In case of Jaspur section, Electrical conductivity values of grater than 3 mS/cm is observed for sample No 1 and it shows the decreasing trend upto sample No 4. Though the Electrical conductivity values of colloidal suspensions of Rayka and Jaspur section reaches above 2 mS/cm, the EC values of Dodka and Mujpur section falls below 1.5 mS/cm, except few samples at the bottom of the Mujpur section.

3.3. Mini river section

Table 3.9. Properties of colloidal suspensions of Angad section (22° 23' 02 N 073° 05' 9E)

Sample No	pH	Colloid concentration (mg/L)	Colloid size distribution (nm)	Electrical conductivity (mS/cm)
MiAN1	7.89	1100	137.1±0.9	0.489
MiAN 2	7.99	1200	133.1±0.4	0.493
MiAN 3	7.84	1000	67.0±0.4	0.370
MiAN 4	7.80	1300	56.8±0.6	0.403
MiAN 5	7.88	1100	89.0±0.1	0.314
MiAN 6	7.94	1400	84.5±0.8	0.488
MiAN 7	7.96	1300	141.3±0.2	0.335
MiAN 8	7.88	1200	140.0±0.2	0.312
MiAN 9	7.83	1200	133.3±0.2	0.321
MiAN 10	7.83	1000	154.6±1.1	0.301
MiAN 11	7.82	800	144.1±0.4	0.246
MiAN 12	7.88	800	167.0±0.4	0.232
MiAN 13	7.59	800	20.4±1.2	0.226
MiAN 14	7.81	1200	119.4±0.1	0.366
MiAN 15	7.56	1300	138.0±0.2	0.387
MiAN 16	7.98	900	71.1±0.1	0.258
MiAN 17	7.90	900	123.1±0.1	0.244
MiAN 18	8.04	2000	137.4±0.2	0.610
MiAN 19	7.78	1000	134.7±0.1	0.288
MiAN 20	7.74	1200	135.8±0.1	0.336
MiAN 21	7.68	1400	190.2±5.7	0.415
MiAN 22	7.73	2000	83.6±0.5	0.699
MiAN 23	7.70	1200	143.9±0.2	0.310
MiAN 24	7.54	2200	123.0±0.1	0.773
MiAN 25	7.76	2400	141.6±0.4	1.551
MiAN 26	7.72	3500	142.0±0.1	3.120
MiAN 27	7.65	4000	125.5±0.2	4.110
MiAN 28	7.62	4400	43.7±0.3	4.610
MiAN 29	7.48	2600	44.0±0.3	2.320

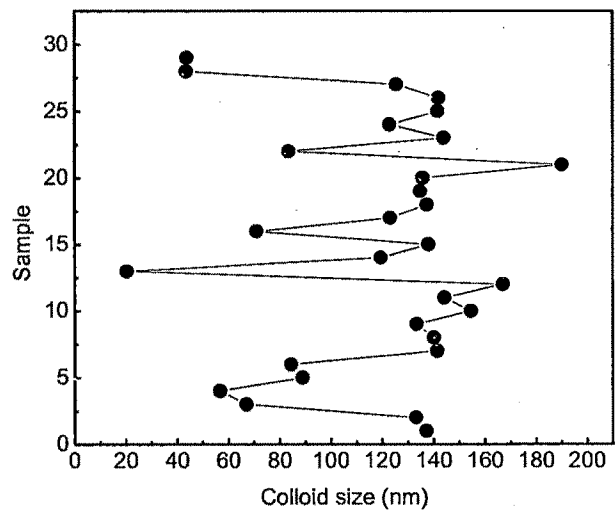
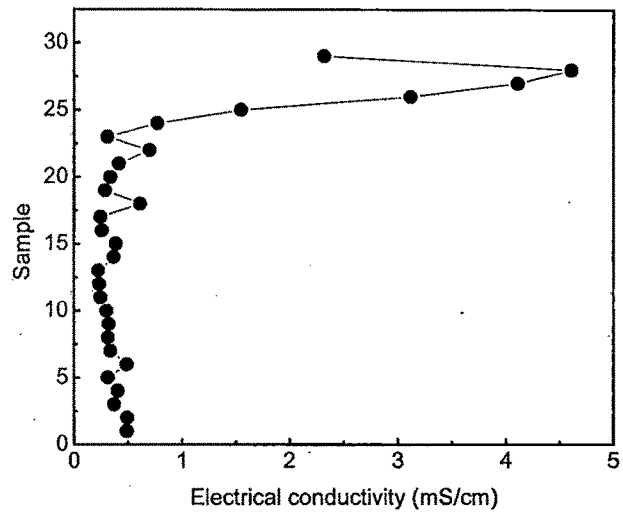


Figure 3.9. Electrical conductivity and particle size of colloids of Angad section

Table 3.10. Properties of colloidal suspensions of Amrapura section (22° 21' 02 N
73° 04' 41 E)

Sample No	pH	Colloid concentration (mg/L)	Colloid size distribution (nm)	Electrical conductivity (mS/cm)
MiAM 1	7.68	800	28.7±6.5	0.293
MiAM 2	7.85	800	83.6±0.7	0.297
MiAM 3	7.88	1200	132.5±0.1	0.340
MiAM 4	7.76	1200	142.4±0.6	0.325
MiAM 5	7.67	1000	116.4±1.1	0.317
MiAM 6	7.81	800	78.9±0.1	0.289
MiAM 7	7.87	1800	99.8±0.9	0.408
MiAM 8	7.84	1600	128.2±0.1	0.345
MiAM 9	7.71	2500	134.9±0.4	0.630
MiAM 10	7.64	2000	131.9±0.2	0.490
MiAM 11	7.79	2000	101.0±0.5	0.455
MiAM 12	7.96	2400	122.3±3.9	0.556
MiAM 13	7.82	2400	36.5±0.6	0.583
MiAM 14	7.80	2200	137.4±0.0	0.433
MiAM 15	7.70	1000	130.4±0.0	0.335
MiAM 16	7.73	1000	123.8±0.1	0.288

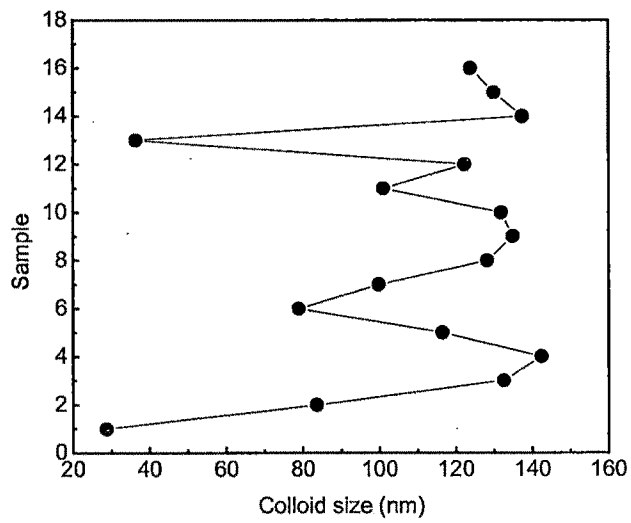
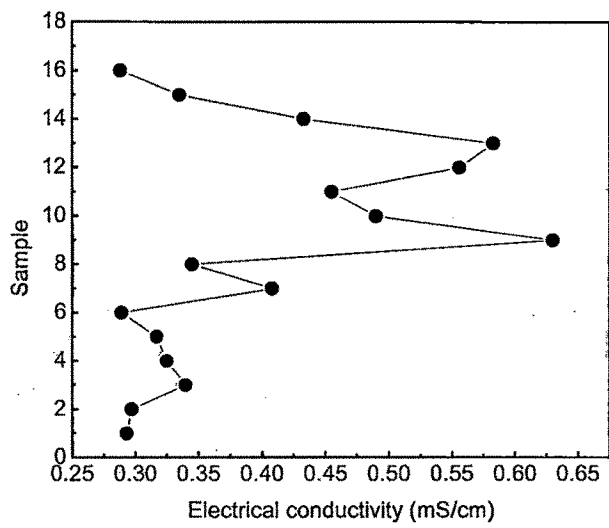


Figure 3.10. Electrical conductivity and particle size of colloids of Amrapura section

Table 3.11. Properties of colloidal suspensions of Chamunda nagar section (22° 23' 42 N 073° 05' 55 E)

Sample No	pH	Colloid concentration (mg/L)	Colloid size distribution (nm)	Electrical conductivity (mS/cm)
MiC1	7.99	1200	133.5±0.8	0.489
MiC 2	7.96	1400	53.0±0.2	0.580
MiC 3	7.89	1200	184.6±2.5	0.483
MiC 4	8.08	1200	74.4±0.7	0.478
MiC 5	7.99	1400	264.1±0.0	0.504
MiC 6	8.07	1400	48.7±0.4	0.531
MiC 7	8.22	2000	136.5±0.1	0.705
MiC 8	7.98	2000	131.1±0.1	0.682
MiC 9	8.03	2000	121.4±0.4	0.669
MiC 10	8.05	2400	136.1±0.3	0.738
MiC 11	8.05	2000	124.1±0.1	0.635
MiC 12	8.24	2000	132.4±0.5	0.663
MiC 13	8.25	2800	141.7±0.3	0.814
MiC 14	8.19	2800	44.6±0.2	0.889
MiC 15	8.16	2800	51.8±0.3	0.873
MiC 16	8.13	2400	82.2±0.1	0.734
MiC 17	8.33	2000	135.0±0.4	0.688
MiC 18	8.36	2400	68.1±0.9	0.714
MiC 19	7.98	2000	79.5±0.6	0.664
MiC 20	8.26	2400	101.3±0.7	0.752
MiC 21	7.99	2500	81.4±2.3	0.774
MiC 22	8.10	3400	134.3±0.5	1.141
MiC 23	8.11	1400	87.3±0.7	0.682
MiC 24	8.02	1600	132.8±0.5	0.638
MiC 25	8.11	2000	61.2±0.5	0.841

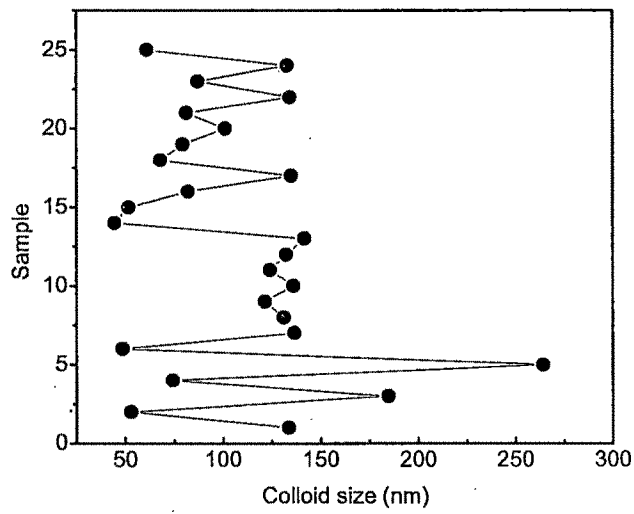
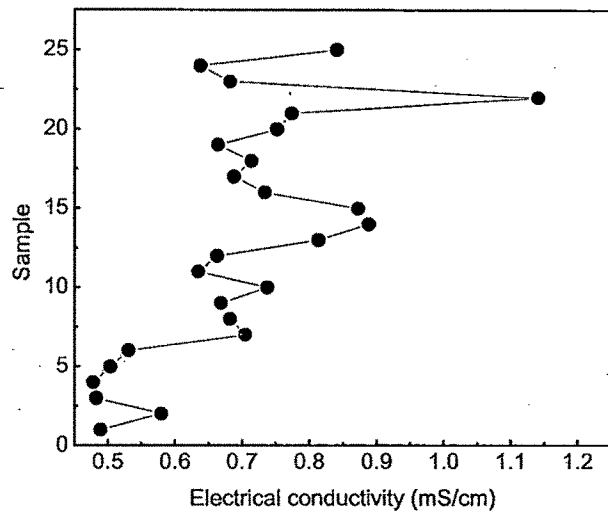


Figure 3.11. Electrical conductivity and particle size of colloids of Chamunda nagar section

The properties of colloidal suspensions of Angad, Amrapura and Chamunda nagar are given in Table and Figure 3.9, 3.10 and 3.11 respectively.

3.3.1. pH

It has been observed that pH of the colloidal suspensions of Angad and Amrapura samples are above 7.8 except few samples. But in case of Chamunda nagar pH>8 is obtained except few samples which showed pH of less than 8. Such a high pH values indicate the high alkaline nature of sediments of these three section.

3.3.2. Electrical conductivity

The EC values of colloidal suspensions of Angad samples vary from 0.226 mS/cm to 4.610 mS/cm. The high concentration of colloids observed for the bottom most sediments of Angad has contributed to the increase in the EC of few samples above 3 mS/cm. Such high electrical conductivity is also an indicator of sediment contamination. The continuous flowing of industrial effluents up to the particular level in the river would have contributed to high EC for the bottom most sediments.

While the Electrical conductivity values of Amrapura sediments varied from 0.288 mS/cm to 0.630 mS/cm, the variation in the EC values of Chamunda nagar samples was 0.478 to 1.141 mS/cm.

3.3.3. Colloid size distribution

The particle size distribution of colloids varies from one section to another. But the polydisperse nature of colloid suspensions of the mini river sediments is relatively less than the Mahi river sediments.

The Angad section samples 13 and 21 have colloids of small and big size and there is no monodispersity found in all these samples. The Amrapura and Chamunda nagar samples 1, 14 and 4, 5 have the colloids of small and big dimension.

3.4. Characterization of colloids in water samples

3.4.1. Colloid size distribution

It is well known that the sediments, organic matter, clay and iron oxides are potential source of colloids in natural environments. During the surface run off, these particles are washed away to the river environments and subsequently into the aquifer system. Thus, studying the size distribution of colloids in surface and ground water samples would be useful to find the origin of colloids in nature.

The ground and river water samples were collected from five different locations along the mini river which are given below. The ground water level (m) is given in brackets.

GW- Ground water, RW- River water

GW 1: Chamunda nagar (14m), GW 2: Rampura (09m), GW 3: Angad (16 m), GW 4: Lalpura (12 m) and GW 5: Amrapura (10m).

RW 1: Chamunda nagar, RW 2: Chamunda nagar, RW 3: Angad, RW 4: Amrapura and RW 5: Singrot

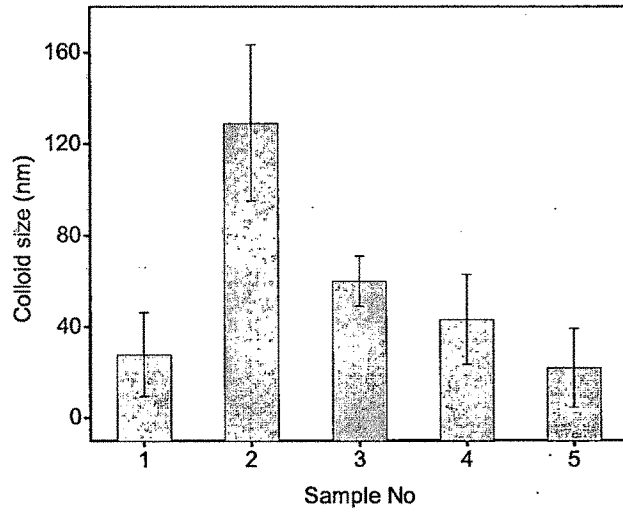
3.4.2. Sample preparation

The collected water samples were filtered with whatmann 40 filter paper and centrifuged at 750 RPM for 15 minutes. The supernatant samples were used for the size distribution analysis by static light scattering technique.

The size distribution of colloids in river water is given in Figure 3.12. While the size distribution of particles in sample No 2 of river water is higher, the sample No 5 has particles of small size. The Rayleigh ratio was calculated from $1/R_{\theta}$ value obtained at angles of 45° , 90° and 135° . The Rayleigh ratio (R_{θ}) value is higher for sample 1 followed by sample 2.

The size distribution of colloids in ground water is given in Figure 3.13. The analysis results shows that the size distribution of particles are high in all the samples, except sample No 4 of ground water, which has particles of monodisperse in nature. Rayleigh ratio (R_{θ}) value of sample 2 is higher than other water samples.

Size of River water colloids



Calculation of Rayleigh ratio

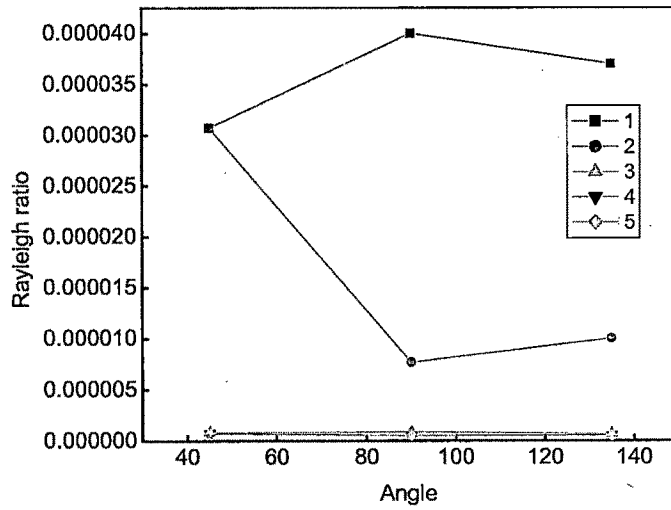
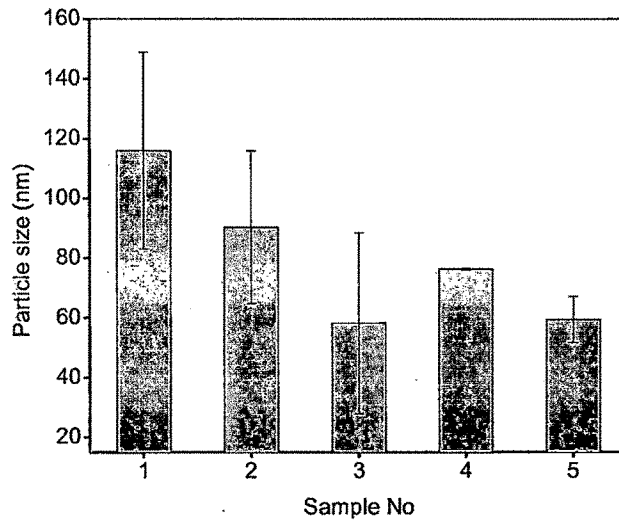


Figure 3.12. Size distribution of river colloids and its Rayleigh ratio

Size of ground water colloids



Calculation of Rayleigh ratio

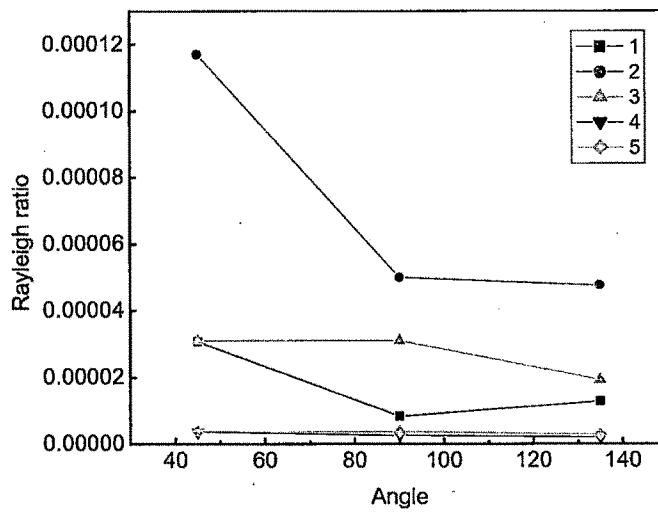


Figure 3.13. Size distribution of ground water colloids and its Rayleigh ratio

3.4.3. Aquatic colloids (Mahi river)

Scanning Electron Microscopy

The Scanning electron microscopy (SEM) image of aquatic colloids isolated from two samples 1 and 2 are given in Figure 3.14a and b, which shows its surface morphology.

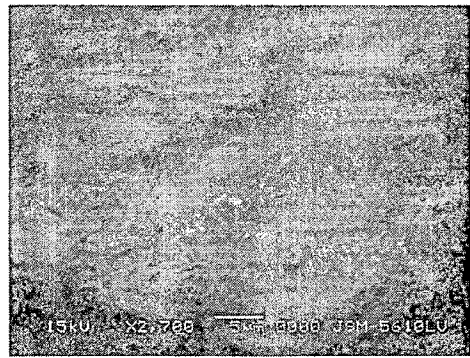
3.4.4. Elemental analysis of aquatic colloids

The elemental content of aquatic colloids was determined on a Scanning Electron Microscopy combined Energy Dispersive X-Ray instrument (SEM-EDS) and the images are shown in Figure 3.15. The percentage of elements is given Table 3.12.

The carbon content is relatively higher in both samples a and b followed by calcium and Silicon. The high carbon content in the samples is an indication of the presence of significant quantity of organic matter in water samples with the silica. The presence of Fe and Al based mineral colloids in water samples has been proved with the results presented here, despite its low content.

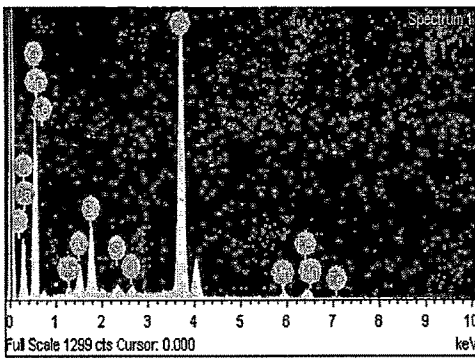


(a)

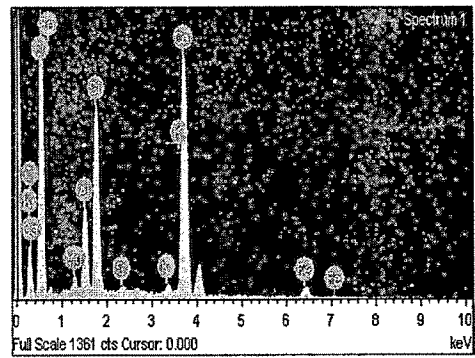


(b)

Figure 3.14. SEM image of Mahi river colloids



(a)



(b)

Figure 3.15. SEM combined EDS image of colloids

Table 3.12. Elemental content of aquatic colloids

(a)

Element	Weight %	Atomic %	Compound %
C	11.52	19.01	42.21
Mg	0.43	0.35	0.72
Al	1.22	0.89	2.30
Si	3.38	2.38	7.23
S	0.48	0.30	1.20
Cl	0.44	0.25	0.00
Ca	28.15	13.92	39.38
Mn	1.90	0.69	2.46
Fe	3.16	1.12	4.06
O	49.32	61.09	

(b)

Element	Weight %	Atomic %	Compound %
C	11.77	18.56	43.11
Mg	0.55	0.43	0.91
Al	3.21	2.25	6.06
Si	7.95	5.36	17.01
S	0.26	0.16	0.66
K	0.45	0.22	0.54
Ca	19.70	9.31	27.57
Fe	3.22	1.09	4.14
O	52.89	62.62	

3.5. X – Ray diffraction analysis of colloids

A variety of minerals in sediments exist as colloidal particles. So, the colloids separated from sediments were characterized to identify the minerals by X-ray diffraction analysis (Panalytical, X'per PRO, Cu K, 2.2KW Max). The X-ray diffraction spectra of colloids separated from sediments of Rayka and Jaspur section is given in Figure 3.16 and 3.17 respectively. The primary minerals identified are Quartz, calcite and kaolinite from 2θ values 27, 30 and 28 respectively reported in literature (151). The calcite content is relatively less in the colloids of Jaspur section. The type of minerals identified in colloids separated from sediments is found to be similar irrespective of their sampling site. Quartz is found to be the dominant primary mineral in all the colloidal samples.

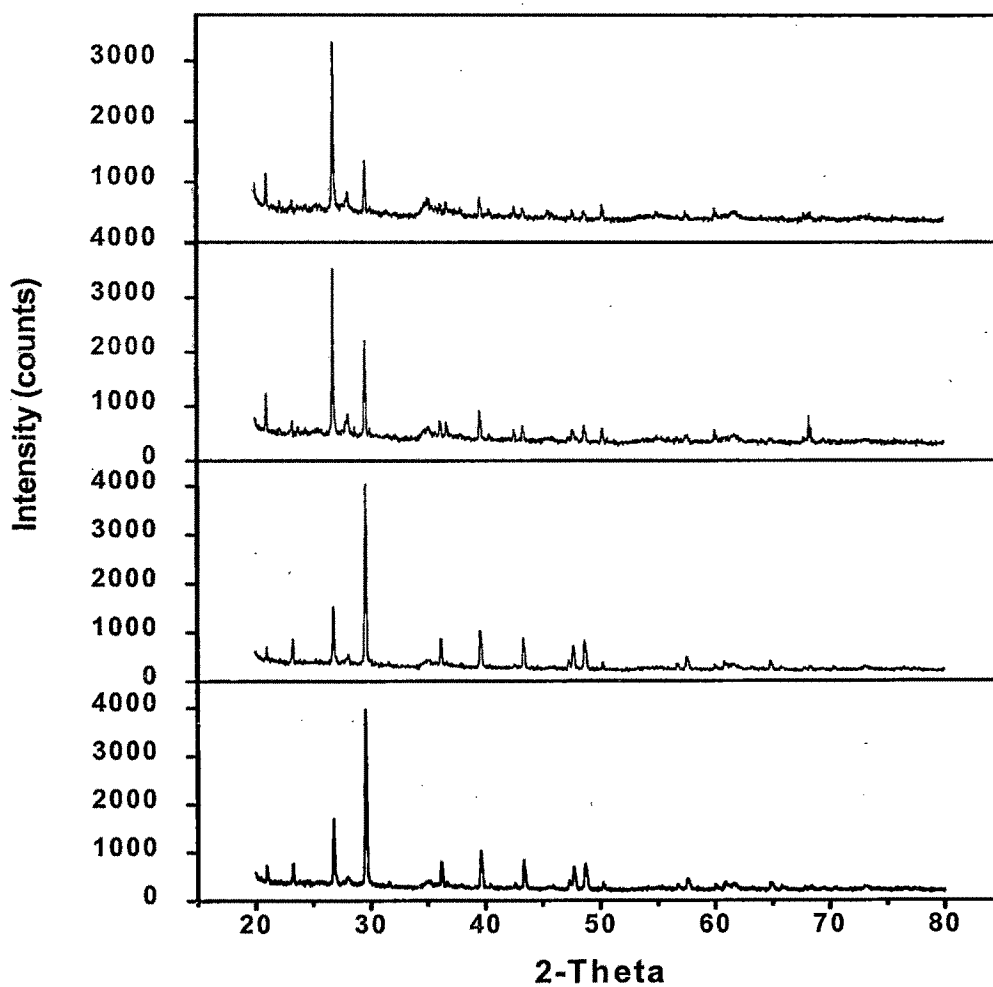


Figure 3.16. X ray diffraction analysis of colloids of Rayka section

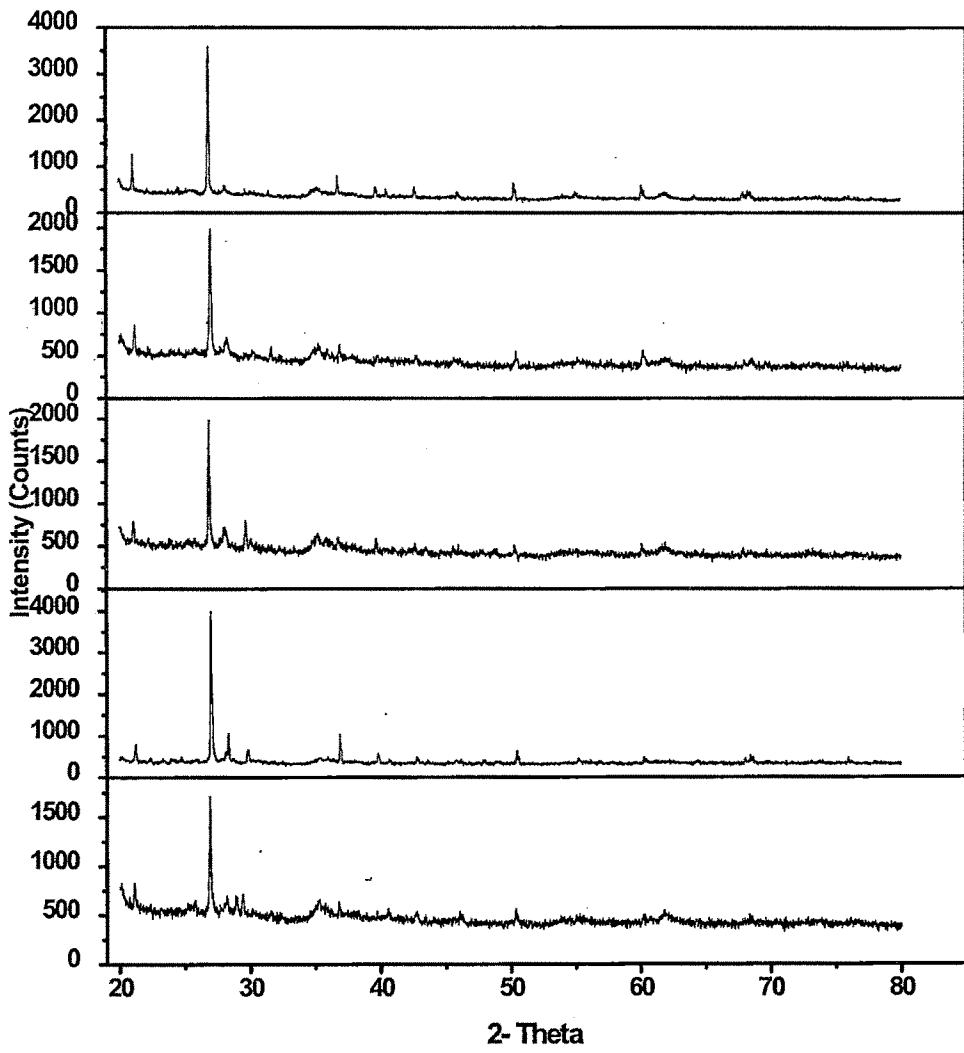


Figure 3.17. X ray diffraction analysis of colloids of Jaspur section

3.6. Transmission electron microscopy (TEM)

Transmission electron microscopy image of colloidal particles is shown in Figure 3.18. It can be seen from TEM images that the particles are highly irregular in shape. The rod and hexagonal shaped particles proves the existence of clay minerals as colloids. The hexagonal shaped particles show the presence of kaolinite mineral in the suspension.

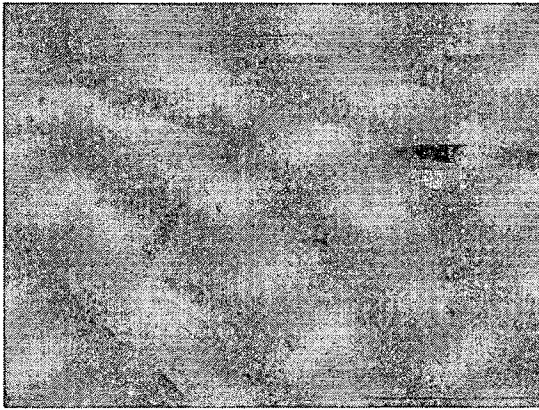
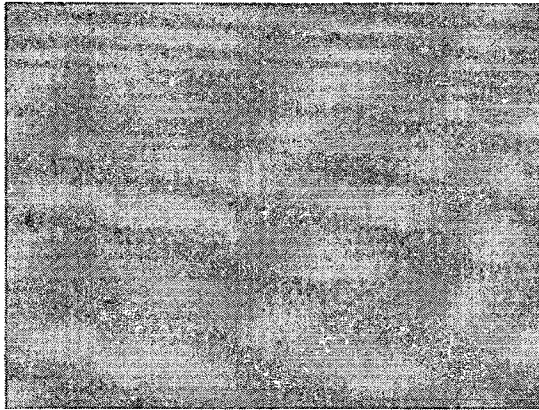


Figure 3.18. Transmission Electron Microscopy image of colloidal particles

3.7. Colloid mobilization

3.7.1. Rayka section

Six sediment samples (MR 15,16 & 17, 35,36 & 37) of Rayka section, that differed considerably in electrical conductivity and colloidal concentration were used for the colloid release experiments and its physical properties are given in Table 3.13. The average packed height of the sediment column was 15 cm. The infiltration experiments consisted of leaching with distilled water using a dropping funnel at the top of the soil column with the water flowing out at a constant rate of 0.3 mL/min to ensure a uniform release of colloidal particles. The effluent was collected at the bottom of the column at regular time intervals for measuring colloidal concentration. This was done by drying the collected solution at 100°C as per the procedure of Kjaergaard et al (150).

The breakthrough curve of colloidal particles mobilized with distilled water from the sediments is given in Figure 3.19. The mass balance of the colloids was calculated at 5 minutes interval for the flow rate of 0.3 mL/min of distilled water. The cumulative mass and C/C_0 of the colloids was calculated using mass balance of the colloids and the data are given in Table 3.14. For the experiments performed with sample 15 significant amount of colloidal particles were found in the effluent at five pore volumes after which colloidal concentration reached a maxima of about 9600 mg/L at around 35 pore volumes followed by gradual decrease in colloidal concentration. The appearance of primary minimum at about 20 pore volumes could be due to the straining of colloidal particles in the sediment column. The observed decrease in colloidal concentration after 35 pore volumes is due to the finite supply of mobilized colloidal particles from the sediment packed column and the colloidal concentration attains a low level because of depletion of mobile colloids in the column.

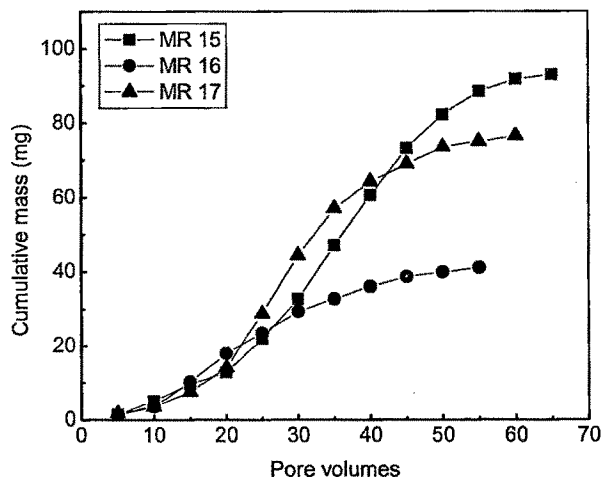
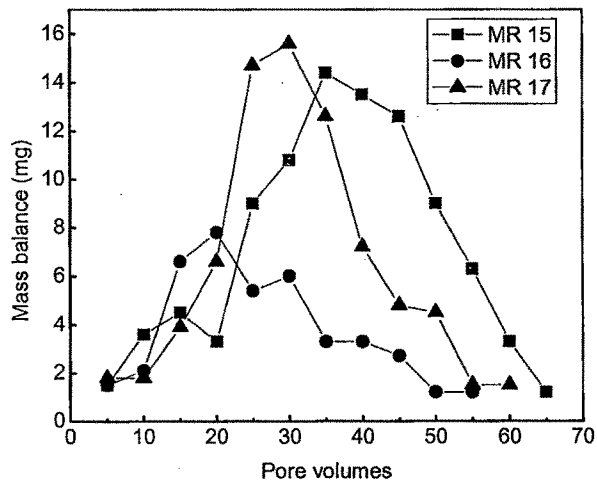
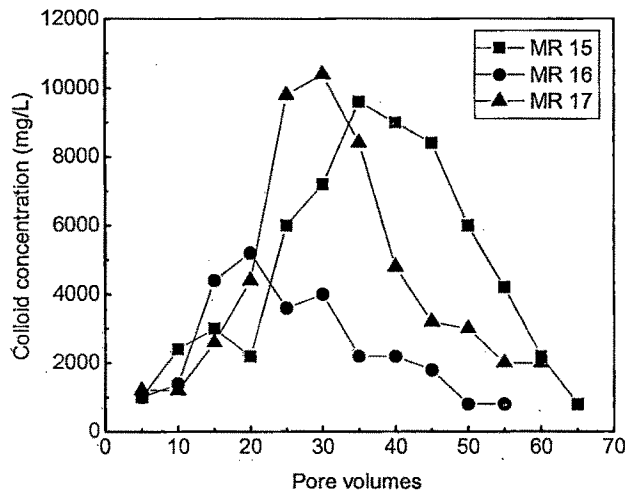
In the case of sample 16, the maximum colloidal concentration of about 5200 mg/L is observed at about 20 pore volumes and then starts to decrease to a low level. A sudden jump in colloidal concentration is observed after 10 pore volumes indicating the mobility of colloids in the sediment column. Though the observed release trend of colloids is same, the colloidal concentration obtained for sample 15 is high than sample 16. The low colloidal concentration of sample 16 in the column experiment substantiates the results of elemental analysis of colloidal suspensions of sediments 15

and 16. The increase in colloidal particle concentration with time is expected as the influent water soaks the sediments for a longer time and so the dispersion of binding agents such as silica, iron oxide and carbonate that binds colloidal material to larger mineral grains would be more. The cumulative mass calculated from the mass balance of the colloids is 93 mg and 41.1 mg for sample 15 and 16 respectively. From these cumulative mass relative mass of colloids (C/C_0) were calculated and presented. The peak in the colloidal concentration was observed for all the samples followed by decline in concentration.

The breakthrough curves of colloids mobilized from other samples are shown in Figure 3.19. The breakthrough curves clearly indicate the release of colloids from sediments with flowing water and their mobility in column. Although the experiments are performed in a similar manner with the constant flow rate maintained throughout the experiments, the maxima of colloidal concentration are obtained at different pore volumes. As the discrete colloids present in the sediments are released early with distilled water, the colloidal concentration peaks at low porevolume. However the peak observed at high pore volumes could be due to the presence of fewer amounts of discrete colloids and the slow dissolution of cementing agents that binds the colloids on mineral grains that make them to move slowly causing the shift in the peak.

Table 3.13. Characterization of the sediments of Rayka section

Properties	MR 15	MR 16	MR 17	MR 35	MR 36	MR 37
Organic carbon (g/kg)	1.8	2.2	2.2	2.8	1.5	2.2
CEC (mmol/kg)	20	20	14	30	17	15
Bulk density (kg/L)	1.5	1.6	1.6	1.8	1.9	1.7
Pore volume (cm ³)	50	45	48	48	50	45
Porosity	0.26	0.23	0.25	0.25	0.26	0.23



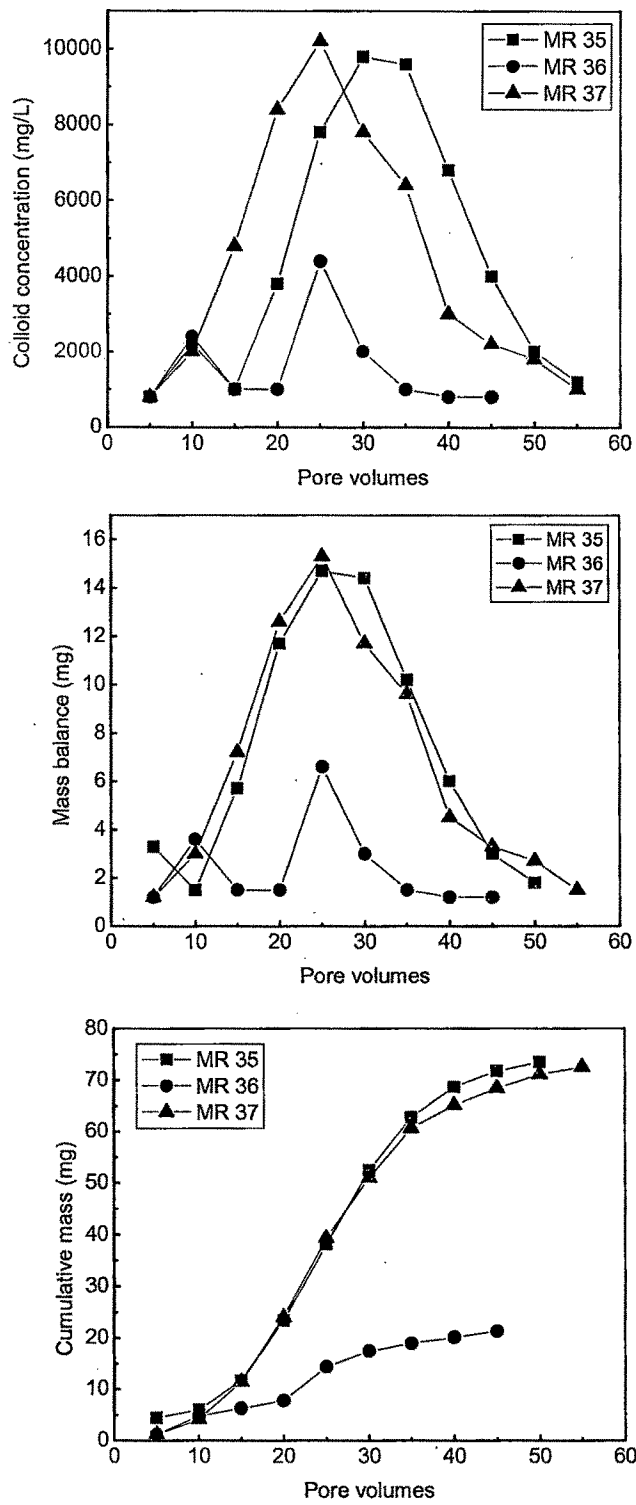


Figure 3.19. Breakthrough curves of colloid mobilization experiments from Rayka sediments

Table 3.14. Mass balance calculations for the colloid release experiments

Pore volume	Mass balance(mg)			Cumulative mass (mg)			C/Co		
	MR 15	MR 16	MR17	MR 15	MR 16	MR 17	MR 15	MR 16	MR 17
5	01.5	1.5	1.8	01.5	01.5	1.8	0.016	0.036	0.0235
10	03.6	2.1	1.8	05.1	03.6	3.6	0.054	0.087	0.0470
15	04.5	6.6	3.9	09.6	10.2	7.5	0.103	0.248	0.0980
20	03.3	7.8	6.6	12.9	18.0	14.1	0.138	0.437	0.1843
25	09.0	5.4	14.7	21.9	23.4	28.8	0.235	0.569	0.3764
30	10.8	6.0	15.6	32.7	29.4	44.4	0.351	0.715	0.5803
35	14.4	3.3	12.6	47.1	32.7	57.0	0.506	0.795	0.7450
40	13.5	3.3	7.2	60.6	36.0	64.2	0.651	0.875	0.8392
45	12.6	2.7	4.8	73.2	38.7	69.0	0.787	0.941	0.9019
50	09.0	1.2	4.5	82.2	39.9	73.5	0.883	0.970	0.9607
55	06.3	1.2	1.5	88.5	41.1	75.0	0.951	1.000	0.9803
60	03.3		1.5	91.8		76.5	0.987		1.000
65	01.2			93.0			1.000		

Pore volume	Mass balance(mg)			Cumulative mass (mg)			C/Co		
	MR 35	MR 36	MR 37	MR 35	MR 36	MR 37	MR 35	MR 36	MR 37
5	3.3	1.2	1.2	4.5	1.2	1.2	0.0612	0.056	0.0165
10	1.5	3.6	3.0	6.0	4.8	4.2	0.0816	0.225	0.0578
15	5.7	1.5	7.2	11.7	6.3	11.4	0.1591	0.295	0.157
20	11.7	1.5	12.6	23.4	7.8	24.0	0.3183	0.366	0.3305
25	14.7	6.6	15.3	38.1	14.4	39.3	0.5183	0.676	0.5413
30	14.4	3.0	11.7	52.5	17.4	51.0	0.7142	0.816	0.7024
35	10.2	1.5	9.6	62.7	18.9	60.6	0.8530	0.887	0.8347
40	6.0	1.2	4.5	68.7	20.1	65.1	0.9346	0.943	0.8966
45	3.0	1.2	3.3	71.7	21.3	68.4	0.9755	1	0.9421
50	1.8		2.7	73.5		71.1	1		0.9793
55			1.5			72.6			1

3.8. Adsorption of cationic and anionic dyes on soil colloids in aqueous solution



The adsorption of alizarin red and methylene blue dyes on colloids from aqueous solution has been investigated and the structure of these dyes is shown in Figure 3.19.

The colloids used in this study were separated from sediments by the centrifugation and coagulation techniques and characterized for the elemental content and mineralogy by SEM combined with EDS and XRD respectively. The effect of initial concentration, pH and adsorbent mass on the adsorption of dyes was studied in batch experiments.

The X ray diffraction spectra of colloids used in adsorption experiments is given in Figure 3.20. The primary minerals found in the colloids are Quartz, calcite and kaolinite with the 2θ values of 27, 30 and 28 reported in literature. The EDX spectrum of colloids is given in Figure 3.21 and the elemental content of colloids is given in Table 3.15. It is evident that the percentage of indicator elements of colloids such as Si and Al is high in the sample. Scanning electron microscopy images are shown in Figure 3.22 and it shows that the colloidal particles are highly irregular in shape.

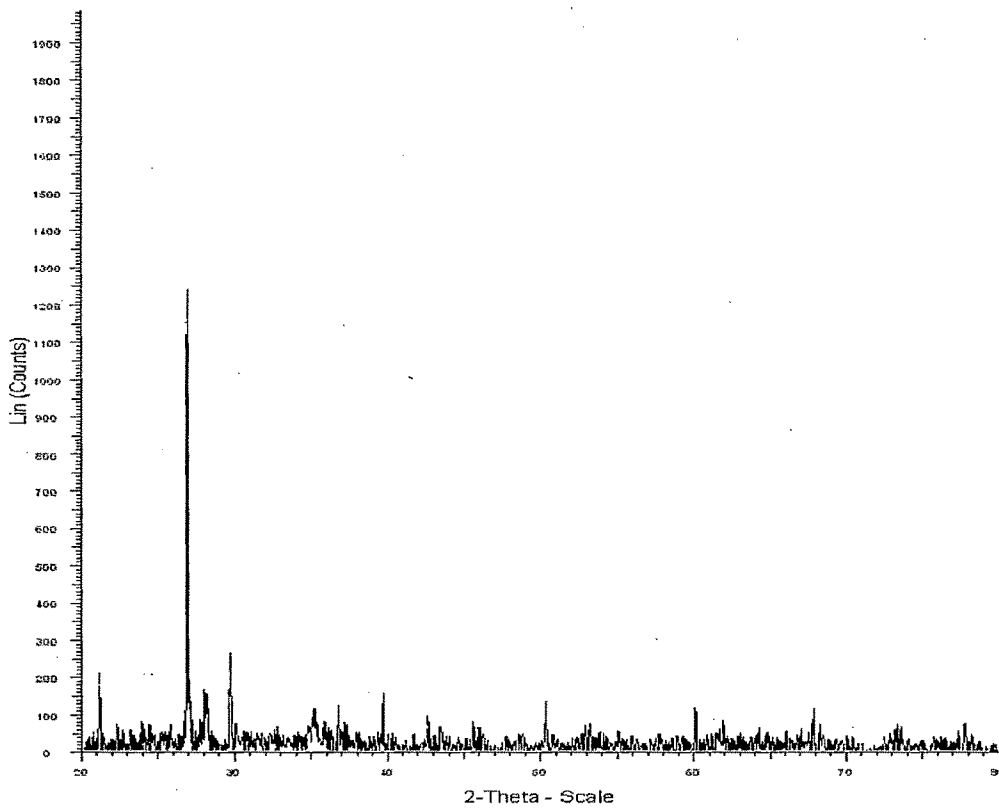


Figure 3.20. X ray diffraction spectra of colloids

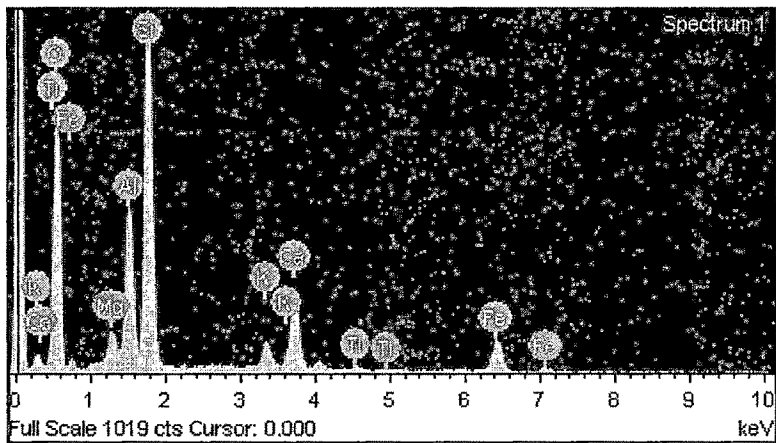


Figure 3.21. Energy dispersive X-ray analysis (EDS) spectra of colloids

Table 3.15. Elemental content of colloids used in the adsorption experiments

Element	Weight (%)	Atomic (%)	Compound (%)
Mg	2.38	2.14	3.95
Al	9.31	7.55	17.60
Si	26.16	20.38	55.97
K	2.19	1.23	2.64
Ca	6.53	3.56	9.13
Ti	0.57	0.26	0.95
Fe	7.59	2.97	9.76
O	45.27	61.90	

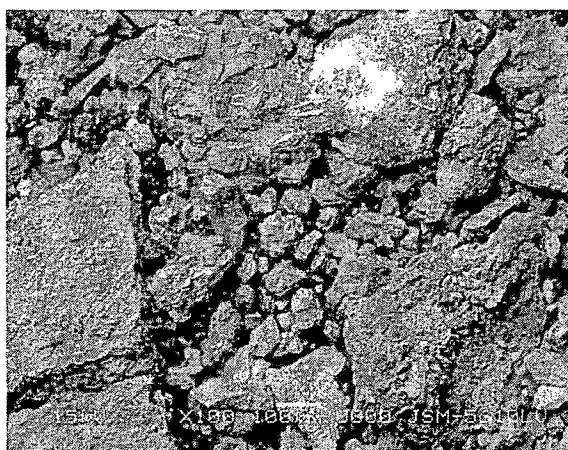
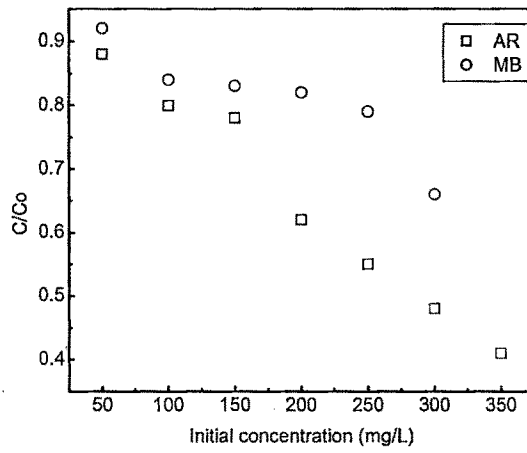


Figure 3.22. Scanning electron microscopy image of aggregated soil colloids

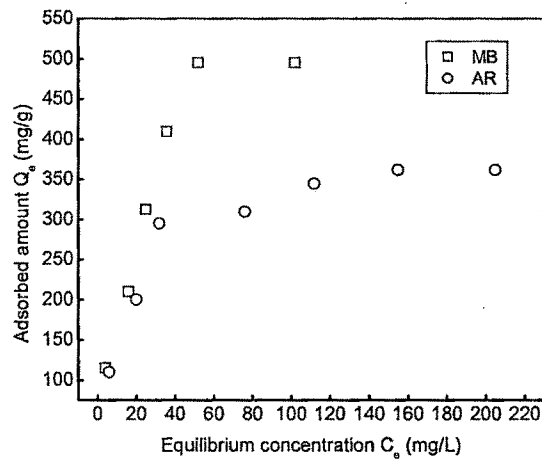
3.8.1. Effect of initial concentration

The effect of initial solution concentration was investigated at ambient conditions with measurements made after an equilibrium time of 6 hr. The adsorption experiments were conducted by varying the initial solution concentration of dye 50-350 mg/L at ambient conditions at temperature of $30\pm 2^\circ\text{C}$ and the relative concentration data (C/C_0) were plotted against initial concentration, where C_0 is the initial concentration and C is the adsorbed amount and is given in Figure 3.23a. It can be seen that the relative adsorption of dyes shows a decreasing trend with increase in initial concentration, indicating the importance of concentration in solution. But, as shown in Figure 3.23b the actual amount of dye adsorbed on colloid increases with increase in concentration of dye in solution and attains equilibrium.

At lower concentrations, all the dye molecules present in the aqueous media are able to interact with the adsorption sites on the colloids and this yields the higher adsorption percentage. But the surface adsorption sites are saturated with increasing concentration of dye solution and this reduces adsorption efficiency of colloids. However, significant variation in the amount of adsorption of AR and MB on colloids was observed at different initial concentrations. The amount of adsorption of alizarin red on colloid is lower than that of methylene blue.



(a)



(b)

Figure 3.23. Effect of initial concentration on adsorption of dye

3.8.2. Adsorption isotherm

Freundlich adsorption isotherm

The experimental data were fitted to the logarithmic form of the Freundlich equation

$$\text{Log A} = \text{Log } K_F + N \text{ Log C}$$

Where A is the solid phase concentration (mg/g) and C is the liquid phase concentration (mg/L). The parameters K_F indicates maximum adsorption capacity [(mg/g)/(L/mg)] and N (dimensionless) indicating isotherm nonlinearity were determined by linear regression of the log transformed data. The slope of the linear plot gives the value of N and the intercept gives the value of Log K_F from where the value of K_F is calculated. If the K_F value increases adsorption capacity also increases. If N is close to 1, the surface heterogeneity becomes less significant. N is a measure of a deviation from the linearity of adsorption.

Langmuir isotherm

Langmuir isotherm can be represented by the equation given below

$$C_e/Q_e = 1/Q_0 b + C_e/Q_0$$

Where C_e is the equilibrium concentration (mg/L), Q_e is the amount adsorbed at equilibrium (mg/g). b is a constant related to the intensity of the adsorption process or related to the energy of adsorption, Q_0 is a constant related to the area occupied by the monolayer of adsorbate, shows the adsorption efficiency (mg/g). The linear plots of C_e/Q_e against C_e suggest the applicability of langmuir adsorption isotherm. The values of Q_0 and b were determined from the slope and intercept of the plots.

Freundlich and Langmuir isotherm parameters for the adsorption of organic dyes by colloids are given in Table 3.16. From this table it is observed that the adsorption capacity (K_F) of colloids for the methylene blue is some what higher than that of alizarin red with the correlation coefficient being 0.9650 and 0.9701 for alizarin red and methylene blue respectively. A better fit with Langmuir model is obtained than the Freundlich model as reflected in the correlation coefficient values of 0.9983 and 0.9860 for alizarin red and methylene blue respectively.

Table 3.16. Freundlich isotherm parameters for the effect of initial concentration

Dye	Freundlich isotherm			Langmuir isotherm		
	K_F (mg/g)/(L/mg)	N	R^2	Q_0 (mg/g)	b (L/mg)	R^2
Alizarin red	50.1	0.46	0.9650	400	0.069	0.9983
Methylene blue	58.8	0.49	0.9701	625	0.053	0.9860

3.8.3. Effect of adsorbent mass

The experimental investigations involving the effect of adsorbent mass on the adsorption of organic dyes was studied by varying the quantity of colloids 3-15 mg. The volume of dye solution and concentration used were 50 mL and 100 mg/L respectively. It is observed from Figure 3.24 that the amount of dye adsorbed on colloid increases with respect to adsorbent mass. With increasing adsorbent mass, more surface area and hence more adsorption sites are available for the adsorption of dyes in the aqueous media. Thus the amount of adsorption of dye on colloid increases with increasing colloid mass.

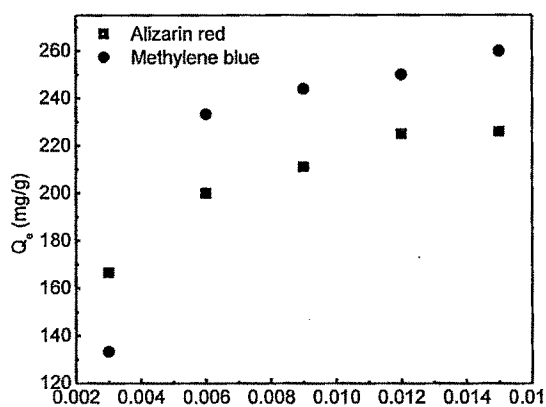


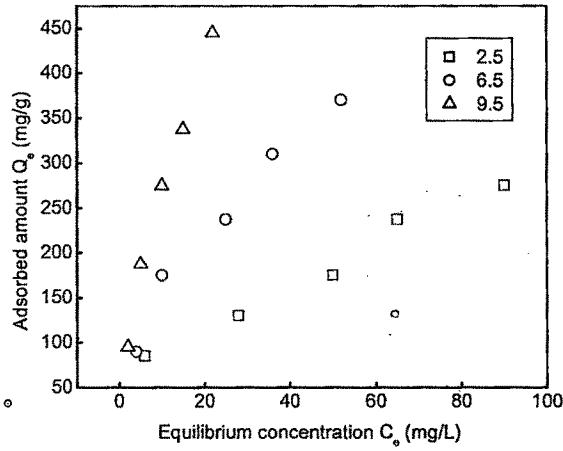
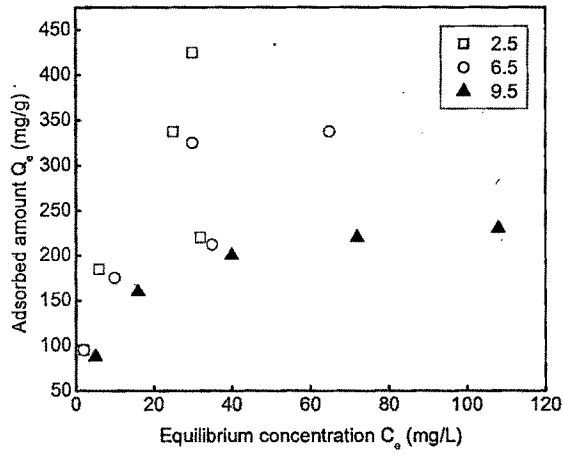
Figure 3.24. Effect of adsorbent mass on adsorption of dye

3.8.4. Effect of pH

The effect of pH on the adsorption of dye was investigated by varying the solution pH over the range of 2.5 to 9.5 with 0.1 N NaOH/HNO₃ and the results are shown in Figure 3.25. It is evident from this Figure that the adsorption capacity of colloids for the alizarin red is found to be high at pH 2.5 than at pH 6.5 and 9.5.

The colloids used in this adsorption experiments consists of quartz and kaolinite minerals and it has been reported that isoelectric point for quartz is approximately 3 and for kaolinite it is between 3.3 to 5, below which the colloidal particles becomes positively charged (23, 152). Thus the higher amount of anionic alizarin red dye gets adsorbed on the positively charged colloidal particles at a pH of 2.5. But, as the pH increases the colloidal particles get negative charge that leads to the decrease in the adsorption of alizarin red. The change in zeta potential with respect to pH is shown in Figure 3.26. The zeta potential is positive at pH 3.5, with approximate neutralization (point of zero charge, pH_{pzc}) at pH of 4.5 and became more negative as pH increased from 7.5 to 11.5. The repulsion between the negatively charged sites on colloidal surface and the dye causes this low adsorption at high pH. It has also been reported that surface charge of colloids becomes more negative with increasing pH (83). Therefore the adsorption of the alizarin red on the colloidal particles is likely to be less.

However, the adsorption of methylene blue shows a different trend in contrast to the alizarin red. It is observed from Figure 3.25 that the maximum amount of adsorption of methylene blue occurs at pH of 9.5. The mutual attraction between the negatively charged colloidal surface and the cationic methylene blue dye causes the enhanced adsorption at high pH.



(a)

(b)

Figure 3.25. Effect of pH on the adsorption of (a) Alizarin red (b) Methylene blue on colloid

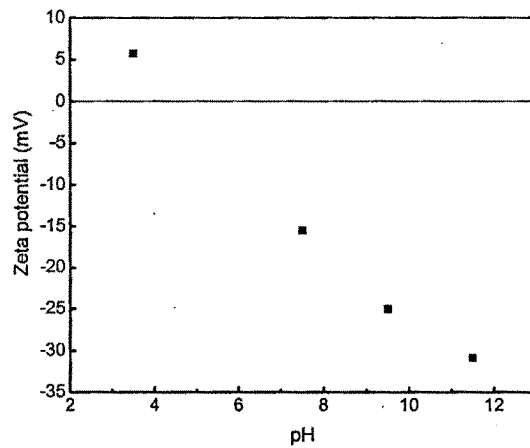
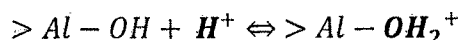
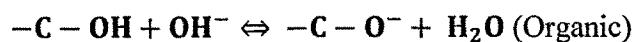
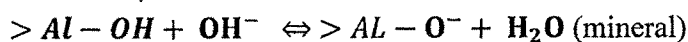


Figure 3.26. Zeta potential of colloidal suspensions at different pH

The surface charge of the colloids is attributed to the pH of the dye solution in which it is added. It gets negative charge in alkaline medium and positive charge in acidic medium as shown below



At low pH values of dye solution, the positive charge on the surface of colloid increases and this causes repulsion between the cationic methylene blue molecules and the colloidal surface, leads to the decrease in adsorption.

It was found that the Freundlich adsorption isotherm represented the adsorption behavior of dye on colloids and it is given in Table 3.17a. The adsorption capacity (K_F) and slope N of colloids for alizarin red decreases with respect to the increase in solution pH. In the case of methylene blue, maximum adsorption capacity (K_F) of colloids increased with increasing pH of dye solution. In this case the N value shows the increasing trend. The increase in the correlation coefficient value for the adsorption of alizarin red from 0.89 to 0.96 shows the linear relationship exist between the concentration and adsorbed amount of dye.

A favorable Langmuir adsorption isotherm is obtained as reflected in the correlation coefficient (R^2) values for alizarin red at pH 9.5 and for methylene blue at pH 6.5. While the monolayer adsorption capacity (Q_0) is decreased with the increase in solution pH for alizarin red, the methylene blue showed increasing trend with increase in pH.

A comparison of the adsorption capacity of the soil colloids with other adsorbents is given in Table 3.18. The results prove the adsorption capacity of soil colloids over other adsorbents reported in literature.

Table 3.17. (a) Freundlich isotherm parameters for the effect of pH

Dye	(mg/g)/(L/mg)			N			R ²		
	2.5	6.5	9.5	2.5	6.5	9.5	2.5	6.5	9.5
pH	2.5	6.5	9.5	2.5	6.5	9.5	2.5	6.5	9.5
Methylene blue	35.4	44.6	69.1	0.42	0.53	0.54	0.9709	0.9911	0.9693
Alizarin red	75.8	74.1	58.8	0.42	0.35	0.30	0.8931	0.9412	0.9657

(b) Langmuir isotherm parameters for the effect of pH

Dye	Q ₀ (mg/g)			b (L/mg)			R ²		
	2.5	6.5	9.5	2.5	6.5	9.5	2.5	6.5	9.5
pH	2.5	6.5	9.5	2.5	6.5	9.5	2.5	6.5	9.5
Methylene blue	370.3	476.1	555.5	0.027	0.063	0.150	0.9198	0.9843	0.9025
Alizarin red	344.8	370.3	256.4	0.290	0.117	0.111	0.8621	0.9477	0.9996

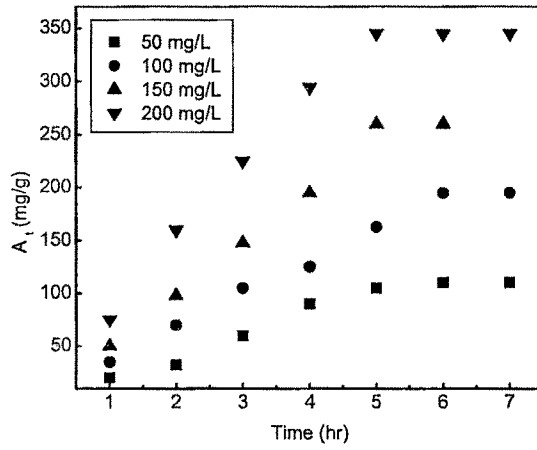
3.8.5. Adsorption kinetics

In the case of kinetic experiments the same procedure described earlier was performed with initial concentrations ranging from 50- 200 mg/L. The volume of dye solution and the quantity of adsorbent taken was 50 mL and 20 mg respectively. The samples were withdrawn from the beaker at definite time intervals and analyzed for dye concentration with UV-Visible spectrophotometer. The amount of dye adsorbed at definite time intervals was determined by using the formula given below

$$Q_t = (C_0 - C_t)V/W$$

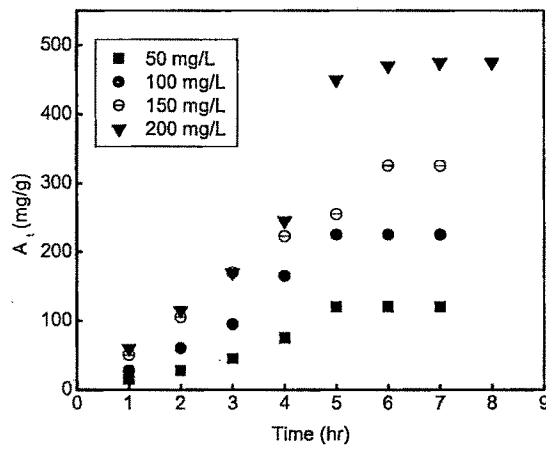
where C_0 and C_t are the initial concentration of dye and concentration of dye in the liquid phase at time t (mg/L) respectively. V is the volume of the dye solution (in liters) and W mass of the colloid adsorbent (g).

The effect of initial dye concentration on the rate and extent of adsorption of colloids were studied in a range of 50-200 mg/L with 20 mg of colloids at room temperature ($30\pm 2^\circ\text{C}$) and the experimental data is shown in Figure 3.27. It can be seen that the rate of adsorption increased with time and attains a plateau after 5 hr. The kinetic data have been analyzed using the pseudo first and second order model.



Alizarin red

3



Methylene blue

Figure 3.27. The adsorbed amount of dye at different initial concentration vs time

3.8.6. Pseudo first order equation

The adsorbed amount of dye at different time intervals on colloids were calculated with the Equation as reported earlier. The kinetics of dye adsorption on colloid was studied using the pseudo first order equation given below

$$dq/dt = K_1(q_e - q_t)$$

Where q_e is the amount of dye adsorbed at equilibrium per unit weight of adsorbent (mg/g), q_t is the amount of dye adsorbed at time t (mg/g) and K_1 is the adsorption constant. The linearized form of the above equation as a function of time is

$$\log (q_e - q_t) = \log q_e - K_1 t / 2.303$$

where k_1 is the first-order rate constant

Plots of the linearized equation were constructed and the constants were calculated from the slopes and intercepts of the plots of $\log (q_e - q_t)$ vs time. The correlation coefficient values were found to be low and the calculated q_e values did not agree with the experimental q_e values. Thus the adsorption of alizarin red and methylene blue does not follow pseudo first order kinetics.

3.8.7. Pseudo second order equation

The kinetics of adsorption of dye on colloid was studied using the pseudo second order equation given below

$$dq_t/dt = K(q_e - q_t)^2$$

where K is the pseudo second order rate constant (g/mg/h), q_e is the adsorbed amount of dye at equilibrium (mg/g) and q_t is the adsorbed amount of dye at time t (mg/g). Integrating the above equation for the boundary conditions $t=0$ to $t=t$ and $q_t=0$ to $q_t=q_t$, gives

$$1/(q_e - q_t) = 1/q_e + Kt$$

The linear form of the above equation after integration is

$$t/q_t = 1/(Kq_e^2) + (1/q_e)t$$

The intercept and slope of the plot of t/q_t vs t gives the value of K and q_e respectively.

The correlation coefficient values of the pseudo second order model were low and in this case too the calculated q_e values did not match the experimental q_e values. It suggests that the adsorption of dye does not follow second order kinetics.

3.8.8. Intra-particle diffusion studies

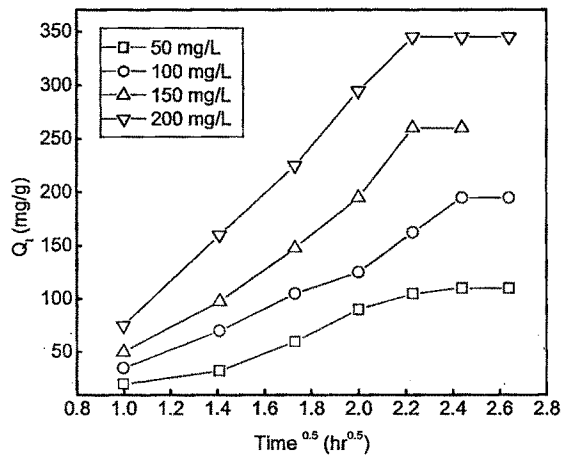
Weber and Morris stated that if intra-particle diffusion is a rate controlling factor, uptake of adsorbate varies with square root of time. It is given by the formula

$$Q_t = K_p t^{0.5}$$

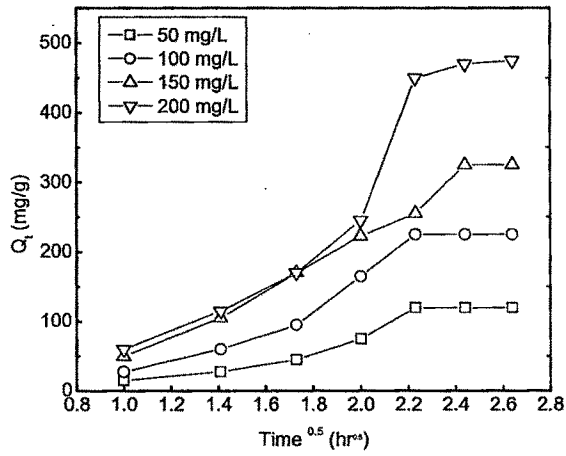
where k_p intra particle diffusion rate parameter.

The possibility of intra particle diffusion was investigated by plotting amount of dye adsorbed (Q_t) vs $t^{0.5}$ at different initial concentration of dye in solution. It is observed from Figure 3.28 that the amount of dye adsorbed on colloid increases gradually and attains a equilibrium. The initial curve portion is attributed to the surface adsorption where as the linear equilibrium portion shows the intra-particle diffusion effect.

The linear plot of $t^{0.5}$ and Q_t indicates the intra-particle diffusion effect of dyes on colloid and this would be a rate controlling step if this line passed through the origin. However, the line do not pass through the origin shows the intraparticle diffusion occurs in the process and it is not the only rate controlling step but other processes such as surface adsorption also involved. The rate constant for intra particle diffusion coefficient $K_p(\text{mg/g/hr}^{0.5})$ was determined from the slope of the linear plot of Figure 3.28 and the values of K_p over the concentration range 50-200 mg/L are 63.43, 104.75, 158.69 and 178.20 for alizarin red 76.14, 140.88, 179.91 and 293.28 for methylene blue. The correlation coefficient values were found to be greater than 0.98 suggesting the intraparticle diffusion. As the colloidal material is crystalline as is evident from the sharp peak in X ray diffraction, intra particle diffusion occurs through the space between the lattice layers.



Alizarin red



Methylene blue

Figure 3.28. Intra-particle diffusion plot for the adsorption of dye on colloid

Table 3.18. Comparison of adsorption capacities of various adsorbents

Adsorbent	Dye	Adsorption (mg/g)	Reference
Solid waste from leather industry	Methylene blue	80.00	153
Solid waste from leather industry	Reactive red	163.00	153
Natural Tripoli	Methylene blue	16.60	154
Sludge ash	Methylene blue	1.60	155
Activated carbon	Congo red	21.10	156
Activated carbon	Rhodamine B	8.50	156
Burnt clay	Congo red	22.80	157
Soil colloids	Alizarin red	400.00	Present study
Soil colloids	Methylene blue	625.00	Present study

3.9. Alizarin red dye adsorption and transport experiments

The effect of colloids isolated from sediment (MR 49) on the transport of alizarin red dye was studied in sediment packed glass chromatographic columns at two different ionic strength conditions and three different pH values at the constant flow rate of 0.3 mL/min. The mass balance of colloids and dye were calculated using effluent concentration data for the flow rate of 0.3 mL/min.

3.9.1. Colloid characterization

The X-ray diffraction analysis (Figure 3.29) confirmed that the colloidal particles isolated from sample MR 49 were highly heterogeneous in their mineralogical composition. The primary minerals identified were quartz, calcite, kaolinite and manganite from the 2θ values of these minerals reported in literature. The elemental content of aggregated colloids is given in Table 3.19 and its spectra is shown in Figure 3.30.

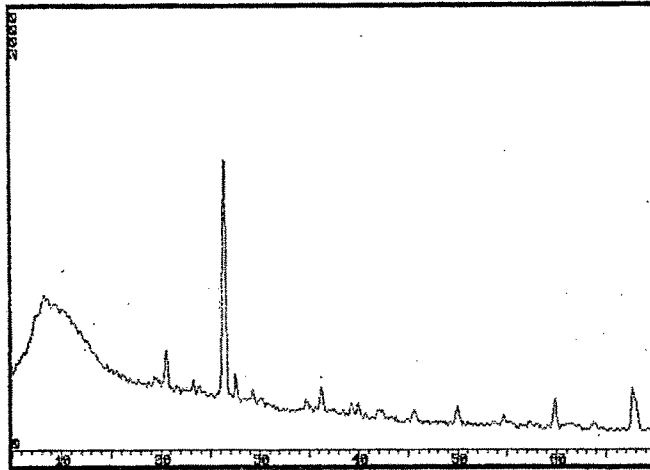


Figure 3.29. X-ray diffractogram of aggregated colloidal particles

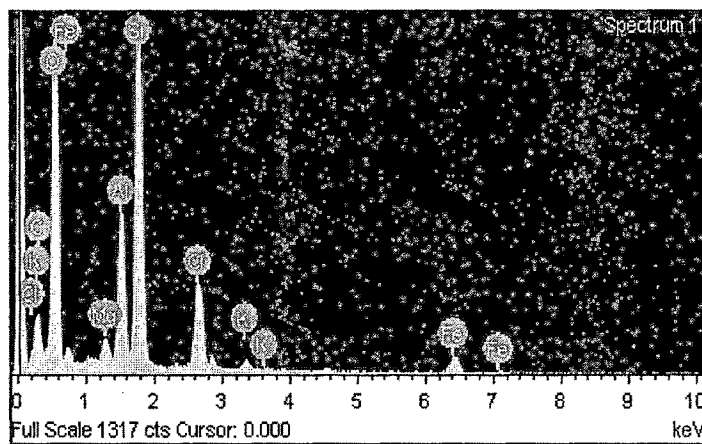


Figure 3.30. EDX spectra of aggregated colloidal particles

Table 3.19. Elemental content of native colloidal particles

Element	Weight %	Atomic %
C	14.99	23.01
O	47.79	55.07
Mg	01.08	00.82
Al	06.29	04.30
Si	17.20	11.29
Cl	06.45	03.35
K	00.81	00.38
Fe	05.39	01.78

3.9.2. Dye adsorption experiments

Adsorption of the dye on the colloids was carried out by varying the initial concentration of dye from 10-100 mg/L. Solid/liquid ratio was maintained at 12 mg/30mL at room temperature. The amount of the dye adsorbed with change in concentration is shown in Figure 3.31. A linear regression of the data (Correlation coefficient $R= 0.99$) gives the distribution coefficient (K_d) of 1.97 mL/mg. The adsorption of dye on colloid increases with increasing dye concentration. This is clearly an indication of intraparticle diffusion, considering a little quantity of colloid taken for experiments (12 mg). These dye adsorption experiments indicate that at low concentrations adsorption on the external surface of colloids occurs, that is followed by the slow intraparticle diffusion into the interior of the particles at higher concentrations. As the colloid is crystalline material intraparticle diffusion occurs through the space between the lattice layers.

3.9.3. Mass balance calculations

Mass balance of contaminants at the outflow was calculated by applying the principles of law of conservation of mass. According to this law, the total mass of the substance entering the system is equal to the total mass of substance leaving plus mass of any material accumulating or left in the process. So

$$\text{Input} = \text{Output} + \text{Accumulation}$$

$$\text{Output} - \text{Input} + \text{Accumulation} = 0 \text{ (mass generation)}$$

The mass balance of the contaminants at the outlet was calculated at the inlet flow rate of 0.3 mL/min at five minutes time interval.

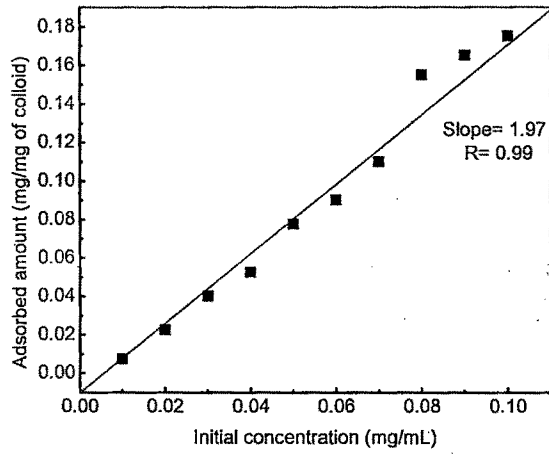


Figure 3.31. Adsorption of alizarin red dye on native colloids

3.9.4. Colloid mobilization

The experimental investigations involving the mobilization of colloidal particles from sediments have been carried out with distilled water. The concentration of colloids in the effluent and the mass balance of the colloids are given in Figure 3.32. A significant amount of colloidal particles were found in the effluent after leaching the sediment packed column with water at 5 pore volumes. The breakthrough curves show that the maxima of colloidal concentration appears at 15 pore volumes, and colloids kept eluting from the column for about 40 pore volumes to a low concentration. During the course of this colloid release experiment, a secondary maximum was observed at about 25 pore volumes. The appeared secondary maximum could be due to the sudden release of trapped colloidal particles from the sediment column. The primary mechanism behind the release of colloidal particles is the dissolution of binding agents such as silica, iron oxides and carbonate that bind colloidal sized material to larger mineral grains. After reaching maxima, the concentration of the colloids gradually decreases.

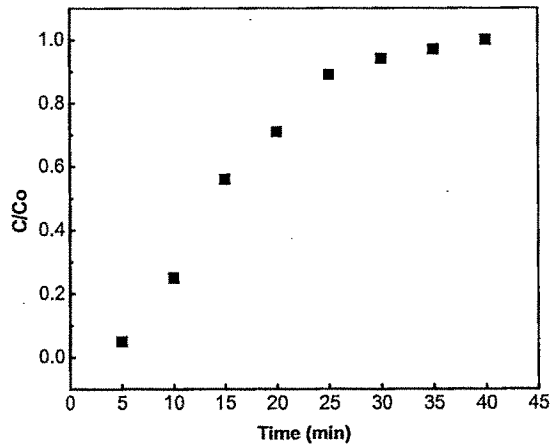
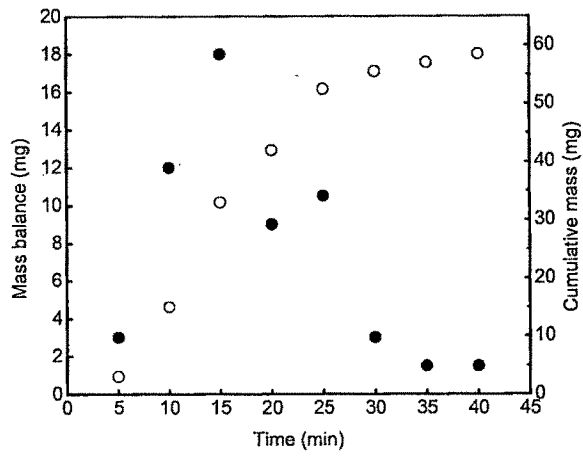
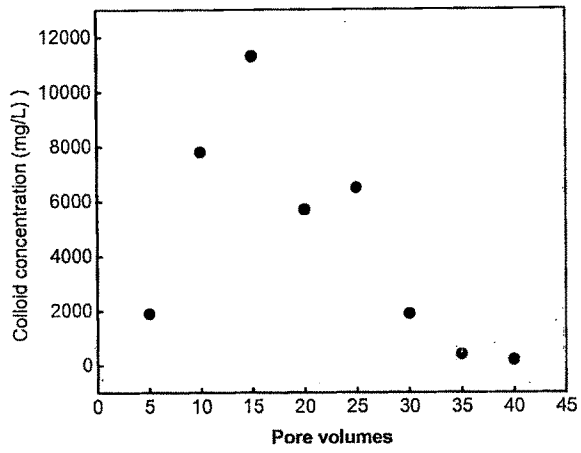


Figure 3.32. Leaching of colloidal particles from soil column

Table 3.20. Mass balance calculations for the leaching of colloidal particles from soil column

Pore volume	Colloid concentration (mg/L)	Time (min)	Mass balance (mg)	Cumulative mass (mg)	C/Co
5	2000	5	03.0	03.0	0.05
10	8000	10	12.0	15.0	0.25
15	12000	15	18.0	33.0	0.56
20	6000	20	09.0	42.0	0.71
25	7000	25	10.5	52.5	0.89
30	2000	30	03.0	55.5	0.94
35	1500	35	01.5	57.0	0.97
40	1500	40	01.5	58.5	1.00

The mass balance calculations are given in Table 3.20. The cumulative mass of colloids in the effluent is turned out to be 58.5 mg at 40 pore volumes and the relative concentration C/C_0 was calculated from this cumulative mass of colloids. It can be seen from Figure 3.32 that, the cumulative mass curve of colloids exhibits a non-linear pattern. It has been previously reported that the cumulative mass of colloidal particles is flow rate dependent and shows linearity at low flow rate while at high flow rate it shows non-linearity [51]. Our observations indicate non-linearity similar to that at high flow rate though our flow rate was not as high. Diffusion limited colloid mobilization was explained to be the cause of linearity of cumulative mass at low flow rate. In contrast, the non linear trend in our experiments may be due to the non-equilibrium processes and physiochemical characteristics of the soil on colloid mobilization. One of the reasons for the non-equilibrium process could also be due to the size variation of the colloidal particles leading to different adsorption capacity of the colloid.

3.9.5. Particle release rate calculations

Assuming a first order colloid release from column, we have

$$C_t = C_{\max} e^{-K_{\text{rel}}t}$$

Where C_{\max} is the maximum colloid concentration in breakthrough curve. K_{rel} is the First order release rate coefficient.

A first order colloid release rate coefficient (K_{rel}) was determined by fitting the decrease in the colloid concentration of breakthrough curve ie from maximum to minimum colloid concentration for 15 min time interval to the above Equation and estimated to be 0.0451 min^{-1} .

3.9.6. Particle size distribution

The size distribution of colloidal particles eluted from the sediments is given in Figure 3.33. While the first sample has the particles of very small size range, the particle size of colloids after 25 pore volumes is high. Thereafter, the size of the colloids shows the decreasing trend and then again increases after 55 porevolumes. Such zig-zag trend observed in the size distribution colloids implies that the sediment contain particles of varying size and get detached and eluted out in a mixed manner. In contrast to this,

the samples 10, 13 and 15 shows monodispersity, which means that the samples possess particles of same size.

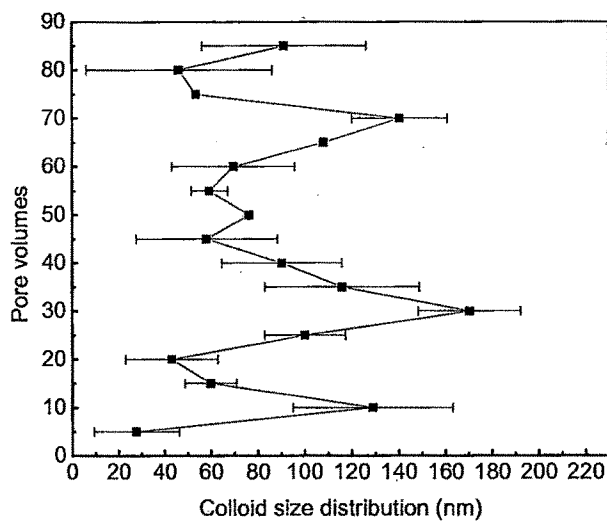


Figure 3.33. Particle size distribution of colloids eluted from sediments

3.9.7. Effect of ionic strength

The breakthrough curves for the column experiments at the ionic strength of 0.01M and 0.001M NaCl and the mass balance for the dye transport are shown in Figure 3.34. The influent solution flow rate of 0.3 mL/min was maintained throughout the transport experiments. It can be seen from Figure that the total dye concentration in the effluent is low for the experiments performed with influent solution of 0.01M NaCl. The reason behind the reduced concentration of dye is that the surface charges of the colloidal particles get neutralized and the strongly sorbing species destabilizes the colloidal particles at low concentrations. High ionic strength influent solution reduces the excluded area of colloidal particles through the compression of diffuse double layers and this causes the decrease in particle mobility (16).

However, the column experiments performed with 0.001 M NaCl showed a different behavior. Initially the concentration of the dye increases marginally to a maxima and then decreases gradually. When the preconditioned column is infiltrated with the low ionic strength solution of NaCl, normality front develops and the colloid facilitated transport of dye starts. This effect is clearly seen in our experiments with abrupt increase in dye concentration of 46 mg/L at 10 pore volumes for 0.001 M NaCl. Adsorption of dye on colloid would be less when it is attached with solid matrix, but after its release from sediment matrix, the adsorption would be more. The release of colloids occurs at normality front contribute to the transport of dye in our column experiments.

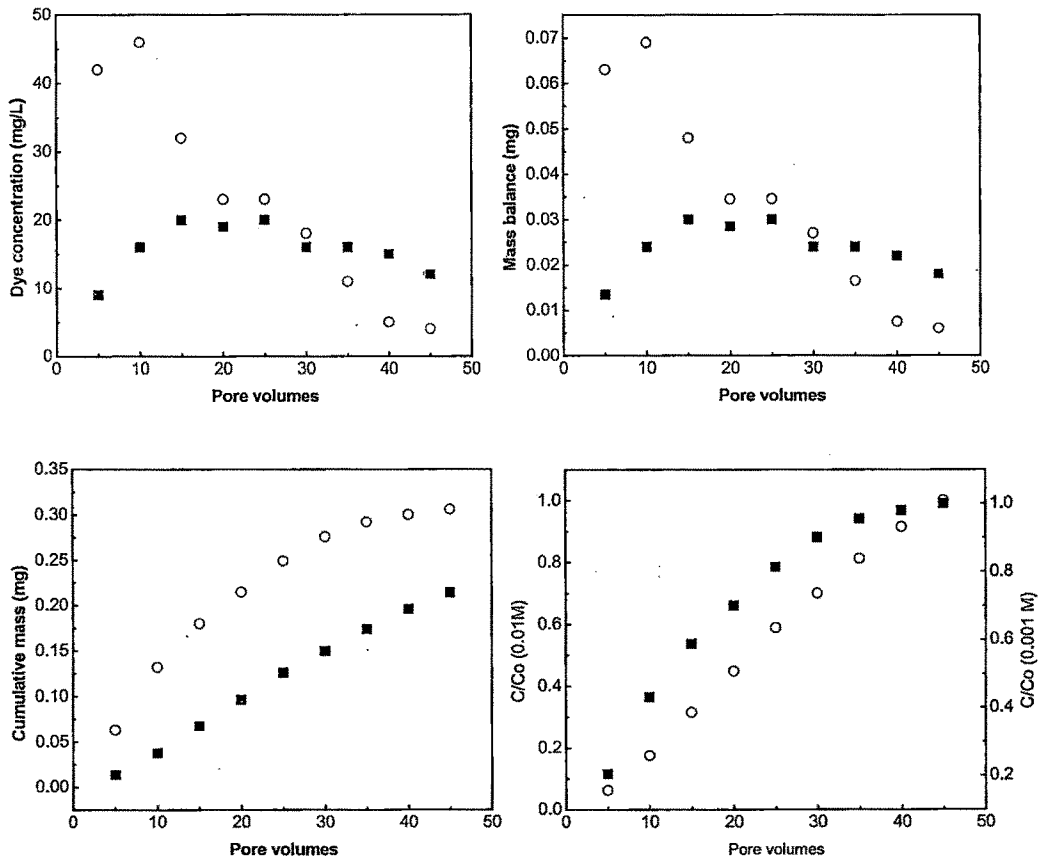


Figure 3.34. Transport of the alizarin red dye through the soil column at (■) 0.01M NaCl, (○) 0.001M NaCl

Table 3.21. Mass balance calculations for the alizarin red dye transport experiments at 0.01 M NaCl and 0.001 M NaCl

Pore volume	Inlet mass (mg)	Out less mass (mg)		Dye Concentration (mg/L)		Mass Balance (mg)		Cumulative mass (mg)		C/Co	
		0.01 M	0.001 M	0.01 M	0.001 M	0.01 M	0.001 M	0.01 M	0.001 M	0.01 M	0.001 M
5	1.0	0.04	0.21	9	42	0.013	0.063	0.013	0.063	0.063	0.205
10		0.08	0.04	16	46	0.024	0.069	0.037	0.132	0.175	0.431
15		0.10	0.16	20	32	0.030	0.048	0.067	0.180	0.315	0.588
20		0.09	0.11	19	23	0.028	0.034	0.096	0.214	0.448	0.700
25		0.10	0.11	20	23	0.030	0.034	0.126	0.249	0.588	0.813
30		0.08	0.09	16	18	0.024	0.027	0.150	0.276	0.700	0.901
35		0.08	0.05	16	11	0.024	0.016	0.174	0.292	0.813	0.955
40		0.07	0.02	15	5	0.022	0.007	0.196	0.300	0.915	0.980
45		0.06	0.02	12	4	0.018	0.006	0.214	0.306	1.000	1.000
Total		0.70	1.00								

At the ionic strength of 0.001 M, the stability of the colloidal particles is more and this occurs due to the expansion of the double layer of the colloids. This double layer expansion causes the colloidal particles get easily released from the column along with the dye. The reason for this expansion is the decrease in the electrolyte concentration and ionic strength. At low ionic strengths, the repulsion between the colloidal particles and soil grains increases and so the colloidal particles get easily released from the column and there is a uniform decrease with pore volume.

When we compare the alizarin red dye transport experiments at 0.01 M and 0.001 M NaCl, it is evident that the contaminant transport at column outlet is inversely proportional to the electrolyte concentration. Under such low ionic strength conditions nearly all colloidal particles are released with the contaminant.

For the experiments performed with 0.01M NaCl, the maxima occurs at around 15 pore volumes with low dye concentration in the effluent whereas with 0.001 M NaCl, the observed trend is quite different with maxima of dye concentration occurs at about 10 pore volumes with dye concentration at the outlet approached the inlet dye concentration. The observed trend in the breakthrough curves of dye transport experiments clearly shows that low ionic strength conditions facilitates the transport of dye more and quicker than high strength conditions. These results on native colloids using a model dye reported for the first time are in agreement with the previous data on simulated column experiments (81) and thus can be used to study the transport of other organic contaminants.

The mass balance calculations for the alizarin red dye transport is given in Table 3.21. For the two types of column transport experiments performed, total mass of the dye at the inlet (inside the column) is 1 mg. As the columns are leached with low ionic strength solutions of 0.01M and 0.001M NaCl, total mass of the dye in the outlet increased to a maxima and then attains a low level. Total mass of the dye at the outlet was found to be 0.7 mg and 1.0 mg for the columns leached with 0.01M and 0.001M ionic strength influent solutions respectively. So that it becomes clear that the ionic strength influences the mass transport of dye through sediment packed column and the mass of the dye retained within the column decreases as the ionic strength of the influent solution decreases. Significant difference in dye mass at the outlet of two dye contaminant transport experiments at different ionic strength conditions shows that

the colloid facilitated transport has a stronger effect on dye transport rather than advection-dispersion transport. The release rate coefficient of dye at the ionic strength of 0.01 M and 0.001 M are 0.0048 min^{-1} and 0.0387 min^{-1} respectively. The higher release rate at 0.001 M suggests the high mobilization of colloids from the sediment column.

3.9.8. Effect of pH

The effect of pH on the transport of dye in the column and its mass balance calculations are given in Figure 3.35. The amount of dye that transports through the column increases significantly with increase in the pH of the influent solution. While the concentration of dye in the effluent is less for pH 7.5 and 9.5, dye concentration is found to be higher at pH 11.5 and is shown in the Figure 3.35a & 3.35b.

Table 3.22. Mass balance calculations for the alizarin red dye transport experiments at three pH values

Pore volume	Inlet mass (mg)	Out let mass (mg)			Mass balance (mg)			Cumulative mass (mg)			C/Co		
		pH 7.5	pH 9.5	pH 11.5	pH 7.5	pH 9.5	pH 11.5	pH 7.5	pH 9.5	pH 11.5	pH 7.5	pH 9.5	pH 11.5
5	1.0	0.040	0.045	0.125	0.012	0.013	0.037	0.012	0.013	0.037	0.166	0.166	0.138
10		0.045	0.050	0.130	0.013	0.015	0.039	0.025	0.028	0.076	0.347	0.351	0.283
15		0.030	0.030	0.110	0.009	0.009	0.033	0.034	0.037	0.109	0.479	0.462	0.405
20		0.030	0.025	0.090	0.009	0.007	0.027	0.043	0.045	0.136	0.604	0.555	0.505
25		0.025	0.025	0.090	0.007	0.007	0.027	0.051	0.052	0.163	0.708	0.648	0.605
30		0.025	0.030	0.095	0.007	0.009	0.028	0.058	0.061	0.192	0.812	0.759	0.711
35		0.025	0.025	0.090	0.007	0.007	0.027	0.066	0.069	0.219	0.916	0.851	0.811
40		0.010	0.020	0.085	0.003	0.006	0.025	0.069	0.075	0.244	0.950	0.925	0.903
45		0.010	0.020	0.085	0.003	0.006	0.025	0.072	0.081	0.270	1.000	1.000	1.000
Total		0.240	0.270	0.900									

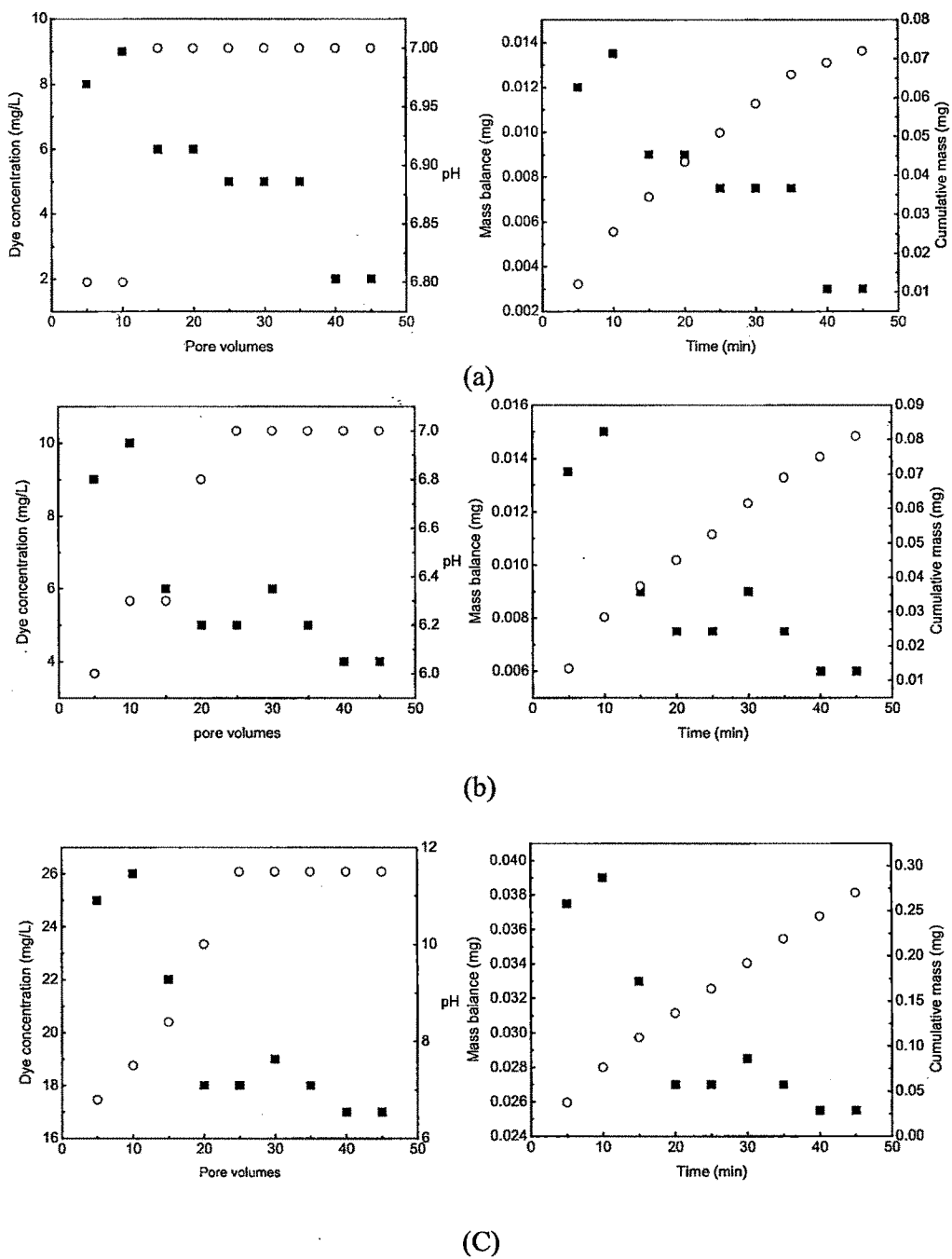


Figure 3.35. Transport of the dye contaminant at elevated pH values (a) pH 7.5 (b) pH 9.5 (c) pH 11.5, (■) Dye concentration, Mass balance (○) pH, Cumulative mass

This increase in dye concentration with respect to pH can be attributed to favorable change in surface charge of the colloidal particles. Bunn et al. (48) have observed that the pH of the influent solution would have to significantly exceed the pH of the grain coatings to cause colloid release and the amount of colloid release increased with increasing pH of the influent solution. Hendershot and Lavkulich (152) has observed that the surface coating of iron oxide on the quartz based colloids shifts the point of zero charge from a pH below 3 to approximately pH 8.1 and to a less extent for kaolinite. Thus the influent solution with the pH of above 8.1 causes the significant colloid release and dye transport. Though the effluent concentration of dye observed at pH 9.5 which is above the point of zero charge value of 8.1 is slightly higher than at pH 7.5, a large increase in dye concentration was observed for the pH of 11.5. And, this result establishes the effect of pH on the colloid facilitated transport dye in our experiments. Swartz and Gschwend (68) suggested that the chemical and electrostatic bonds have to be broken in order to cause significant colloid release because of their ability to hold the coatings.

From the breakthrough curves of these column experiments, it is observed that maxima of dye concentration occurs at about 10 pore volumes for all the experiments performed at different pH conditions and then dye concentration decreased gradually to a low level. For the experiments performed at pH 9.5 and 11.5, the secondary maximum in the breakthrough curves of dye concentration was observed at about 30 pore volumes. This could be due to the release of trapped colloidal particles with dye in the soil pores, during the continuous leaching with an influent solution. So that the increased colloidal concentration carrying the dye tends to give secondary maximum at 30 pore volumes. The mass balance calculations for the transport of the dye at elevated pH values are given in Table 3.22. The total mass dye inside the column (inlet mass) is 1 mg as the column is saturated with 20 mL of the dye solution with a concentration of 50 mg/L. While the sediment packed column is leached with a influent solution of pH 7.5, contaminant mass at the outlet was found to be 0.24 mg as against the inlet mass of 1mg. For the columns flushed with influent solutions of pH 9.5 and pH 11.5, the dye contaminant mass at the outlet was 0.27 mg and 0.9 mg respectively. The observed difference in mass of dye at the outlet between the experiments performed with the influent solutions of pH 7.5 and pH 9.5 is very less.

But at pH 11.5, the mass of the dye at the outlet was found to be higher as compared to that obtained with influent solutions of low pH. These mass balance calculations show that the mass of the dye retained within the column decreases as the column is leached with influent solutions of increased pH. From these mass balance calculations, it is observed that at higher pH conditions colloidal particles facilitates the transport of dye more because of increased colloid release.

As shown in the Figure 3.35, there is a step wise variation of pH of the effluent solution. At the pH 7.5, the effluent solution pH was found to be low after which the pH increases to 7. In the case where the pH was 9.5 and 11.5 the pH of the effluent was found to start at three to four pH units less than that of the influent solution. When the experiments were stopped, the effluent decreased to pH 7 for the influent solution pH of 9.5, but the effluent pH remained the same for pH 11.5. Ion exchange is one of the possible factors for the observed decrease in pH of the effluent solution of transport experiments. The exchange of Ca^{2+} for Al in the kaolinite during the preconditioning step and subsequent hydrolysis of exchanged Al with the influent solution of different pH values causes the release of proton leading to the decrease in pH of effluent solution.

3.10. Methylene blue transport experiments

The methylene blue transport experiments were carried out with Jaspur sediment (MJ 52) and the colloids isolated from this sediment were used in the adsorption experiments. The properties of this sediment are given in Table 3.23.

3.10.1. Contaminant

Methylene blue is a cationic dye widely used in textile dyeing industries. It was selected as the model contaminant. Solution of methylene blue was prepared and used in the experiments. The concentration of methylene blue was measured by UV-Visible spectrophotometer (UV 2450, Shimadzu) at a wavelength of 665 nm.

Table 3.23. Properties of sediment (MJ 52) used in the experiments

	Properties	MJ 52
1	pH	6.92
2	Electrical conductivity (mS/cm)	0.352
3	Organic carbon (g/kg)	5.3
4	Cation Exchange capacity (mmol/kg)	40
5	Clay	21
6	Silt	54
7	Sand	25

3.10.2. Characterization of colloids

The elemental content of separated native colloidal aggregates is given in Table 3.24 and its spectra are shown in Figure 3.36. The percentage of major indicator elements of colloids Si, Al and Fe are found to be high.

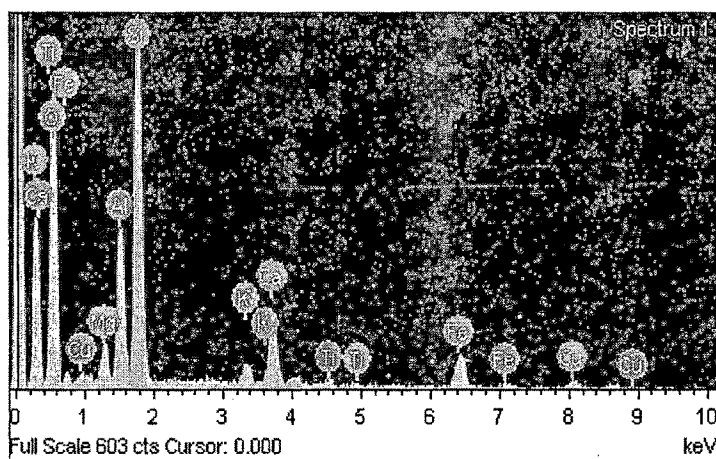


Figure 3.36. SEM combined EDS spectra of colloids

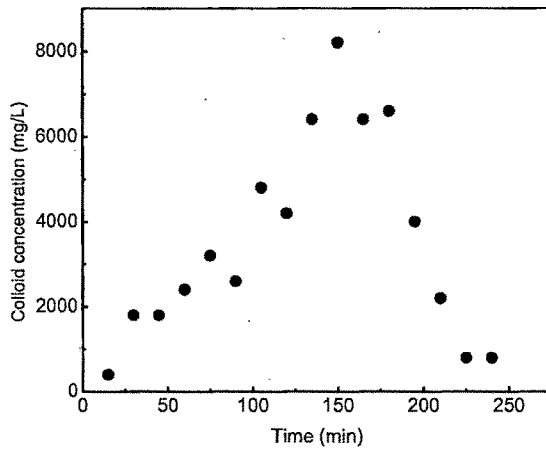
Table 3.24. Elemental content of colloids of MJ 52 sediment

Element	Weight (%)	Atomic (%)	Compound (%)
Mg	2.80	2.54	4.64
Al	9.48	7.76	17.92
Si	25.10	19.73	53.70
K	1.77	1.00	2.14
Ca	6.04	3.33	8.45
Ti	0.66	0.31	1.10
Fe	7.37	2.91	9.48
Cu	2.05	0.71	2.57
O	44.72	61.71	

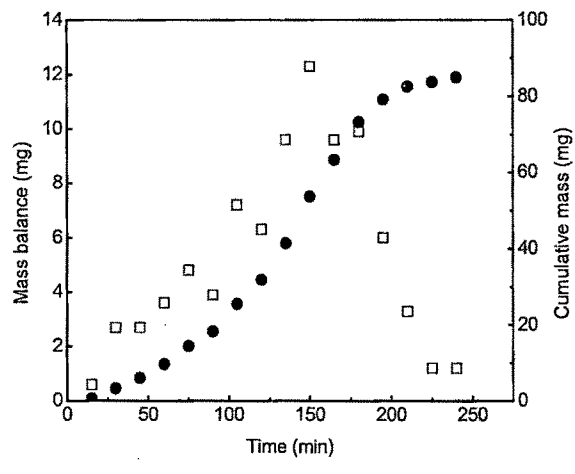
3.10.3. Mobilization of colloidal particles from the soil column

The colloid mobilization experiments were conducted through a 4 cm diameter column packed up to a height of 20 cm with 354g of sediments. The bulk density of the soil column was found to be 1.41 g/cm^3 . The concentration of colloidal particles in the effluent was plotted against time and it is shown in Figure 3.37a. It can be seen that the colloid concentration is low at the initial stage of the experiments. Thereafter the colloid concentration peaks at 150 min corresponding to 45 mL of distilled water and then decreases. After which there is a sudden increase in colloid concentration at 180 min is seen followed by sharp decline in colloid concentration to a low level and after 240 min duration the measurements were stopped. Further it is seen that the colloid concentration decrease at 90 and 120 minutes and this is due to the blocking of colloids in the pores of the soil column.

The mass balance of colloids was calculated at 5 min interval for the flow rate of 0.3 mL/min and is shown in Figure 3.37b. The colloid mass of 13 mg was obtained at 150 min. As shown in the Figure 3.37b, the plot of cumulative mass of colloidal particles vs time exhibit a non-linearity with a mass of 85 mg for the whole duration of the experiment and levels off at the final stage of experiment. In this case also the cumulative mass of colloidal particles shows a non linearity as observed earlier. This can be explained that in addition to the diffusion of released colloids with fluid flow, the physical and chemical characteristics of the soil also influence the mobilization of colloids from sediment matrix.



(a)



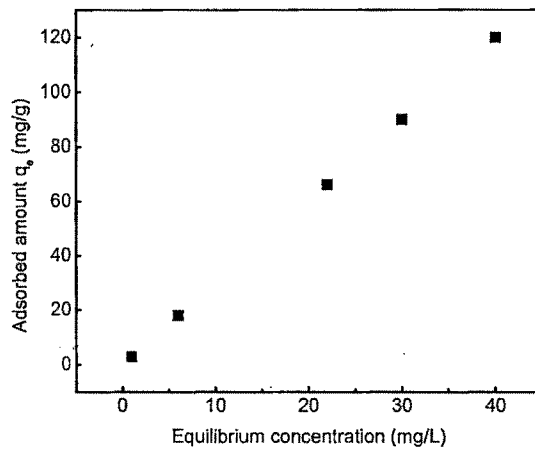
(b)

Figure 3.37. Mobilization of colloids from sediments

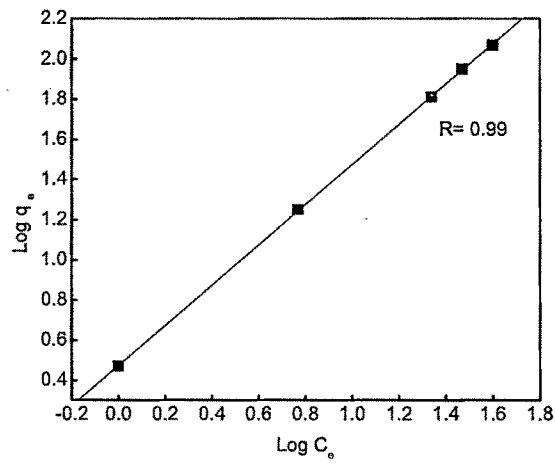
3.10.4. Adsorption of methylene blue on colloids

The dye adsorption experiments were conducted at the concentration range of 20-100 mg/L at ambient conditions at temperature of $30\pm 2^\circ\text{C}$. The amount of dye adsorbed with the change in concentration is shown in Figure 3.38a. From this experiment it is observed that the adsorption of dye on colloid increases with increasing concentration. As the colloidal particles possess large surface area it shows a good adsorption capacity for the dye in aqueous solution.

The adsorption data were fitted to the logarithmic form of the Freundlich equation as given earlier. It was found that the Freundlich adsorption isotherm represented the adsorption behavior of methylene blue on the colloids as shown in the Figure 3.38b. The maximum adsorption capacity(K_F) was found to be 2.97.



(a)



(b)

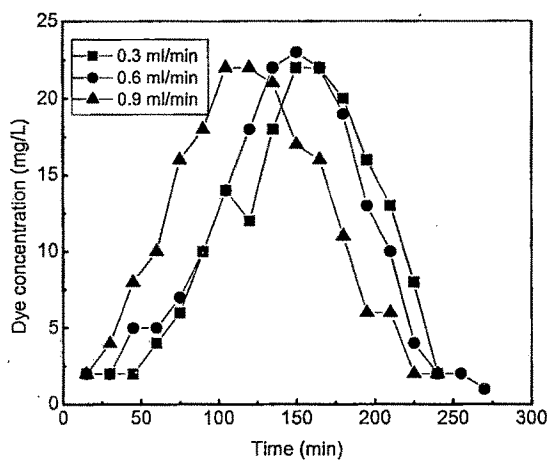
Figure 3.38. (a) Adsorption of dye on colloid (b) Freundlich adsorption isotherm

3.10.5. Methylene blue transport experiments

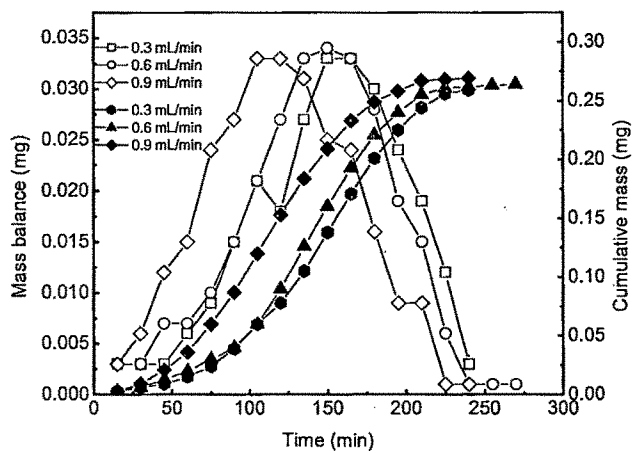
The transport experiments were conducted through a 4 cm diameter column packed up to a height of 20 cm with 348 g of sediments. The bulk density of the soil column was found to be 1.38 g/cm^3 . The dye was displaced from the column by introducing 0.001 M NaCl solution at the flow rate of 0.3, 0.6 and 0.9 mL/min. In order to maximize the colloid release from the sediments, the low ionic strength solution of 0.001M NaCl was used. At this low ionic strength the repulsion between the colloidal particles and soil grains increases, so the colloidal particles get easily released from the column. The stability of colloids at this low ionic strength condition is also more due to the expansion of double layer.

The breakthrough curves for the transport of methylene blue dye through the soil column at the influent flow rate of 0.3, 0.6 and 0.9 mL/min are shown in the Figure 3.39a. As shown in the Figure 3.39a at the flow rate of 0.3 mL/min, the concentration of the dye in the effluent is 2 mg/L upto 45 min, thereafter the dye concentration peaks at 150 min corresponding to 45 mL of 0.001 M NaCl solution passed through the sediment matrix and remains unchanged up to 165 min. Then the dye concentration decreases to a low level after 165 min and after 240 min the experiment was stopped. The results are in agreement with the advection- dispersion phenomena of contaminant transport.

The corresponding mass balance of dye calculated at 5 min interval attains a maxima and then shows a decreasing trend as observed in the dye transport. The corresponding cumulative mass of dye rises gradually to 0.25 mg for the whole experimental duration of 240 min. The experimental investigations carried out using similar set of column and influent solution flow rate of 0.3 mL/min for both the colloid mobilization and dye transport experiments showed a maxima at 150 min and this confirms the colloid facilitated transport occurring in the soil column.



(a)



(b)

Figure 3.39. Transport of methylene blue through the column

For the experiments performed with the flow rate of 0.6 mL/min, it is seen that there is no shift in the peak value of the dye concentration and the time taken to attain the peak concentration.

For the experiments performed with the inlet flow rate of 0.9 mL/min which is three times more than that of the previous studies, the dye eluted more rapidly and the dye concentration attains the peak at 105 min which is earlier than at 150 min.

The total mass of the dye eluted out from the column is similar for the flow rate of 0.3 and 0.6 mL/min. The 86% of the initial dye added was eluted out from the column for the flow rate of 0.3 and 0.6 mL/min but for the flow rate of 0.9 mL/min almost 91% dye was eluted out. As the flow rate increases the total mass of the dye eluted out from the column increases considerably. This result shows the effect of flow rate on the transport of dye in the soil column. The cumulative mass of colloids (Figure 3.39b) shows a non linearity with respect to time and then the curve flattened.

3.11. Adsorption of Chromium on colloids

3.11.1. Effect of pH

The effect of pH on the adsorption of chromium was investigated at initial solution pH of 2.75 to 9.75 and the concentration ratio (C/C_0) was plotted against time, where C is the adsorbed amount of Cr(VI) on colloid and C_0 is the initial concentration of Cr(VI) in solution. It is observed from Figure 3.40 that there is hardly any adsorption of Cr on colloid at pH of 7.5 and 9.75. As the pH decreased to 5.2 about 16% of Cr got adsorbed in the first 30 minutes and there after the concentration remained constant.

Further reducing the pH to 2.75 almost 84% solute got adsorbed. In this case too after 60 minutes there was hardly any further increase of the amount of chromium adsorbed indicating that chromium adsorption was sensitive to solution pH and equilibrium condition was rapidly attained.

It has been reported that isoelectric point for quartz is 3 and for kalonite it is between 3.3 to 5, below which the colloidal particles becomes positively charged (23, 152). Thus at pH 2.75, the anionic species of chromium, HCrO_4^- gets adsorbed strongly on the colloids. As the pH increases the colloidal particles get negative charge that leads to the decrease in the adsorption rate.

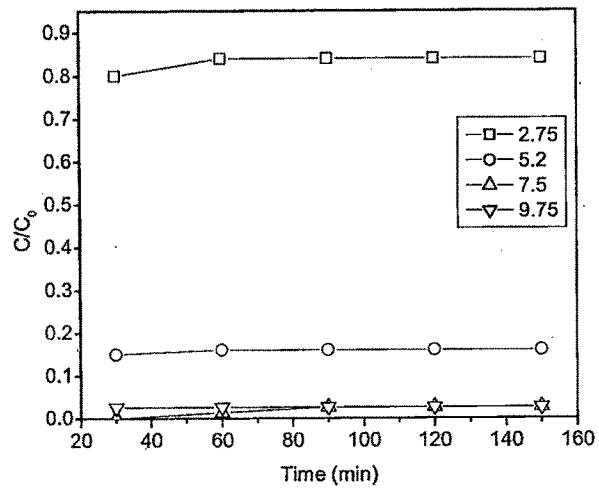


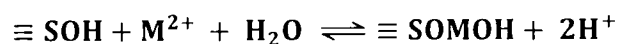
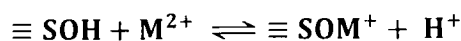
Figure 3.40. Effect of pH on the adsorption of Cr(VI) on colloid



3.11.2. Cr(VI), Pb(II), Ni(II) and Cu(II) adsorption on colloids

The adsorption of Cr(VI), Pb(II), Ni(II) and Cu(II) on colloids was investigated at room temperature ($30 \pm 3^\circ\text{C}$) with measurements made after an equilibration time of 24 hr. Freundlich and Langmuir isotherm parameters for the adsorption of toxic metals are given in Table 3.25 and the data are shown in Figure 3.41. The adsorbed amount of Pb(II) on colloid was higher and decreased in the sequence Ni(II), Cu(II) and Cr(VI).

The adsorption at a colloid surface is mainly a result of electrostatic binding forces that exist between ions of toxic metals to the adsorbent surface as natural colloids are negatively charged [1] and also due to the cation exchange of divalent metals to the H^+ ions. The divalent cations can interact with the available surface sites on colloids, $\equiv\text{SOH}$, where S represents Si and Al which are the main constituent of colloids and are shown in Equation below.



In the case of Cr(VI) adsorption, where the pH of the system is 2.75, the adsorbent surface contains a large number of protonated aluminol (AlOH_2^+) and silanol (SiOH_2^+) groups that bind electrostatically with the $\text{Cr}_2\text{O}_7^{2-}$ to cause the adsorption.

The adsorption of toxic metals is found to be relatively higher on soil colloids than other adsorbents reported in literature and it is given in Table 3.26.

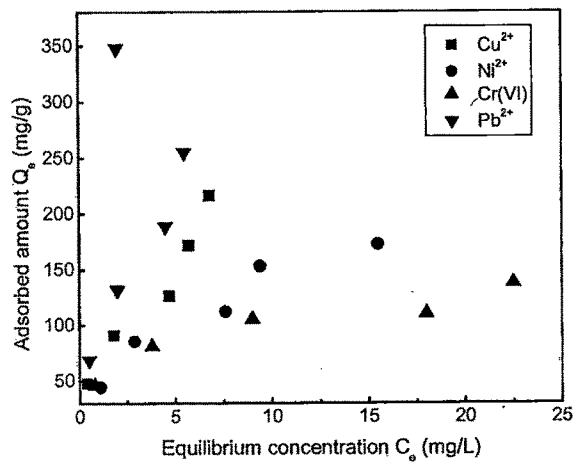


Figure 3.41. Effect of initial solution concentration on the adsorption of Pb(II), Cr(VI), Cu(II) and Ni(II) on soil colloids

Table 3.25. Freundlich and Langmuir adsorption isotherms for toxic metals

Contaminant	Freundlich isotherm			Langmuir isotherm		
	K_F (mg/g)/(L/mg)	N	R^2	Q_0 (mg/g)	b (L/mg)	R^2
Cr(VI)	50.4	0.30	0.9858	140.8	0.0178	0.9839
Pb(II)	117.6	0.48	0.7368	294.1	0.0045	0.8691
Ni(II)	71.6	0.48	0.9752	263.1	0.0108	0.8872
Cu(II)	44.8	0.50	0.9839	222.2	0.0226	0.9724

Table 3.26. Comparison of adsorption capacities of various adsorbents

Adsorbent	Contaminant	Adsorption capacity (mg/g)	Reference
Granular Ferric hydroxide	Cr(VI)	0.78	158
Goethite	Pb(II)	120.4	159
	Cu(II)	63.6	159
Sawdust activated carbon	Cr(VI)	44.0	160
Soil colloids	Pb(II)	294.1	This study

3.11.3. Cr(VI), Pb(II), Ni(II) and Cu(II) transport experiments

The characterization data of the sediment (MD 34) used in the transport experiments is given in Table 3.27. Elemental content of colloids isolated from this soil sample is given in Table 3.28.

Table 3.27. Characterization of sediment (MD 34)

	Properties	Values
1	Organic carbon (g/kg)	5.2
2	Cation exchange capacity (mmol/kg)	40
3	Clay (%)	14
4	Silt (%)	51
5	Sand (%)	35

Table 3.28. Elemental content of aggregated colloids of sediment (MD 34)

Element	Weight (%)	Atomic (%)
C	12.05	18.00
O	57.34	64.32
Mg	1.38	1.02
Al	6.46	4.30
Si	14.18	9.06
S	0.25	0.14
K	0.67	0.31
Ca	2.98	1.34
Ti	0.31	0.11
Cr	0.01	0.0
Fe	4.38	1.41

The transport experiments were conducted in a 4 cm diameter column packed up to a height of 30 cm with 524 gm of sediments. Initially NaCl solution (0.5M) was introduced through the column at a rate of 0.3 mL/min for 2 hr. This led to dense packing of the sediments in the column and filling of the void space. Thereafter the column was loaded with hexavalent chromium solution by introducing 50 mL chromium solution having concentration of 15 mg/L (7.8×10^{-5} M). Subsequently the chromium was displaced from the column by introducing 0.001 M NaCl at the flow rate of 0.3 mL/min. The effluent concentration of chromium was recorded with time as a plot of C/C_0 vs time as shown in Figure 3.42 where C is the concentration of Cr(VI) in the effluent and C_0 is the initial concentration of Cr(VI) in solution. The effluent chromium concentration peaks at 120 min corresponding to 40 mL of salt solution percolating through the bed. After 160 min there is a sharp decline in the chromium concentration and after 200 minutes the measurements were stopped, by this time 89.73% of the chromium added had eluted out from the column.

The investigations involving the transport of Ni(II), Cu(II) and Pb(II) through the sediment packed column show that the Ni(II) concentration attains maxima at around 135 min, while the Cu(II) and Pb(II) peaked at 105 min corresponding to 45 mL and 35 mL of salt solution passing through the bed respectively. By the time the effluent concentration decreased to a low level, almost 89% of Cu(II), 86% of Ni(II) and 57% of Pb(II) had eluted out from the column. The higher adsorption of Pb(II) on colloids present in the sediment column retain them which leads to the decrease in effluent mass. The correlation between release rate of toxic metals and their adsorption on colloids was observed and the release rate is shown in Table 3.29. The maximum adsorption of Pb(II) on colloids present inside the column than other metals, as evident from batch experiments (Table 3.25), contribute to their high release rate and transport. The release rate decreases in the sequence Ni(II), Cu(II) and Cr(VI) so as their adsorption on colloid.

The mass balance of contaminants was calculated for the flow rate of 0.3 mL/min for the time interval of 5 min and the data are given in Figure 3.42.

Table 3.29. Release rate coefficient of Cr(VI), Pb(II), Ni(II) and Cu(II)

Experiment	Contaminant	Ionic strength	Flow rate (mL/min)	Release rate coefficient (min ⁻¹)
1	Cr(VI)	0.001 M	0.3	0.0046
2	Pb(II)	0.001 M	0.3	0.0463
3	Ni(II)	0.001 M	0.3	0.0134
4	Cu(II)	0.001 M	0.3	0.0113

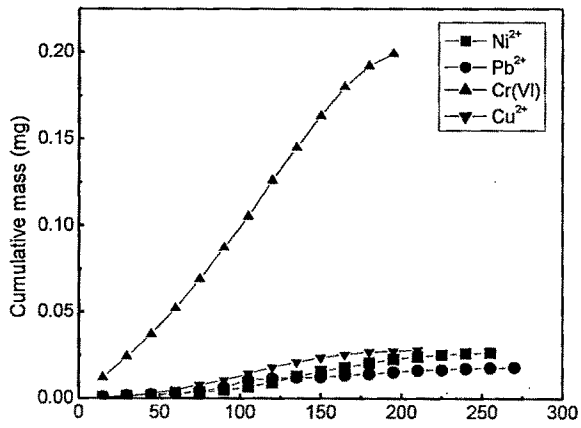
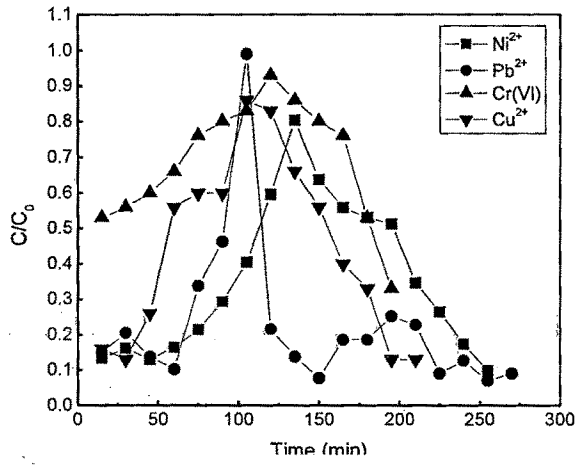


Figure 3.42. Transport of Ni(II), Pb(II), Cr(VI) and Cu(II) through the soil column

Most studies concerning contaminant transport in subsurface environment have considered soil or ground water as essentially a two phase system where contaminants partition between the mobile phase and the immobile solid phase. However, the unexpected appearance of relatively low solubility contaminants some distance away from their known source or sooner than expected from their solubility is a pointer to the possible involvement of mobile colloids in contaminant transport. There exist in literature a few field studies that provide evidence for colloid-facilitated transport of contaminants (4).

The idea of colloids being involved in contaminant transport gave rise to the three-phase model of contaminant transport i.e. mobile liquid phase, mobile colloidal phase and the immobile solid phase. Sen et al (87) have noted that most of the three phase models that have been reported so far have assumed equilibrium interactions between the colloid particles and the contaminant in the dissolved phase. These models predict a reduction of the effective retardation arising out of sorption onto the solid matrix depending on the concentration of the colloidal fines and the partition coefficient for contaminant sorption on the colloidal fines.

In this study the contaminant Cr(VI) is water soluble, hence it is difficult to differentiate the extent of transport taking place with the mobile aqueous phase vis-à-vis the transport by adsorption on colloids. The relatively high concentration in the effluent stream during the initial period of the experiments as seen in Figure 3.42 indicates that the chromium present in the aqueous phase within the pores of the bed is initially eluted out and subsequently the chromium adsorbed on the solid phase gets desorbed in the mobile phase. The net effluent concentration is a sum of the chromium transported by mobile phase and the chromium transported by the colloids. The decline in concentration at long time intervals is attributed to equilibrium considerations due to the depletion of the chromium adsorbed in the bed.

3.11.4. Transport of chromium in mixed bed

The effect of the uncontaminated zone on the effluent concentration is shown in Figure 3.43 and the mass balance calculations are given in Table 3.30. Also incorporated in the figure is the rate of stripping of chromium from 10 cm contaminated soil without a layer of sediment below it. The high initial chromium concentration in the effluent and its rapid increase in this particular case is evidence of the chromium in the mobile phase within the pores eluting out quickly with the NaCl solution. In the presence of layer of uncontaminated soil there is a marked difference

in the nature of the plots. The chromium concentration in the effluent slowly builds up and the detection of chromium in the effluent gets delayed with an increase in the layer of uncontaminated soil providing evidence to adsorption-desorption phenomena occurring in the uncontaminated zone.

It is likely that the Chromium ions eluting through the uncontaminated soil get adsorbed mildly in the sediment layer causing a widening of the curves. Adsorption of chromium on sediment was also studied and it was found that linear adsorption isotherm represented the adsorption behavior with distribution coefficient (K_D) of 0.0068 g/L as seen in Figure 3.44. Increase in the thickness of the uncontaminated zone results in the removal of the skewed nature of the effluent concentration – time plots. The nature of these plots obtained for 10 cm and 15 cm thick uncontaminated soil layers tend to become Gaussian as observed in Figure 3.43, such pattern of concentration profiles is often obtained in chromatographic data.

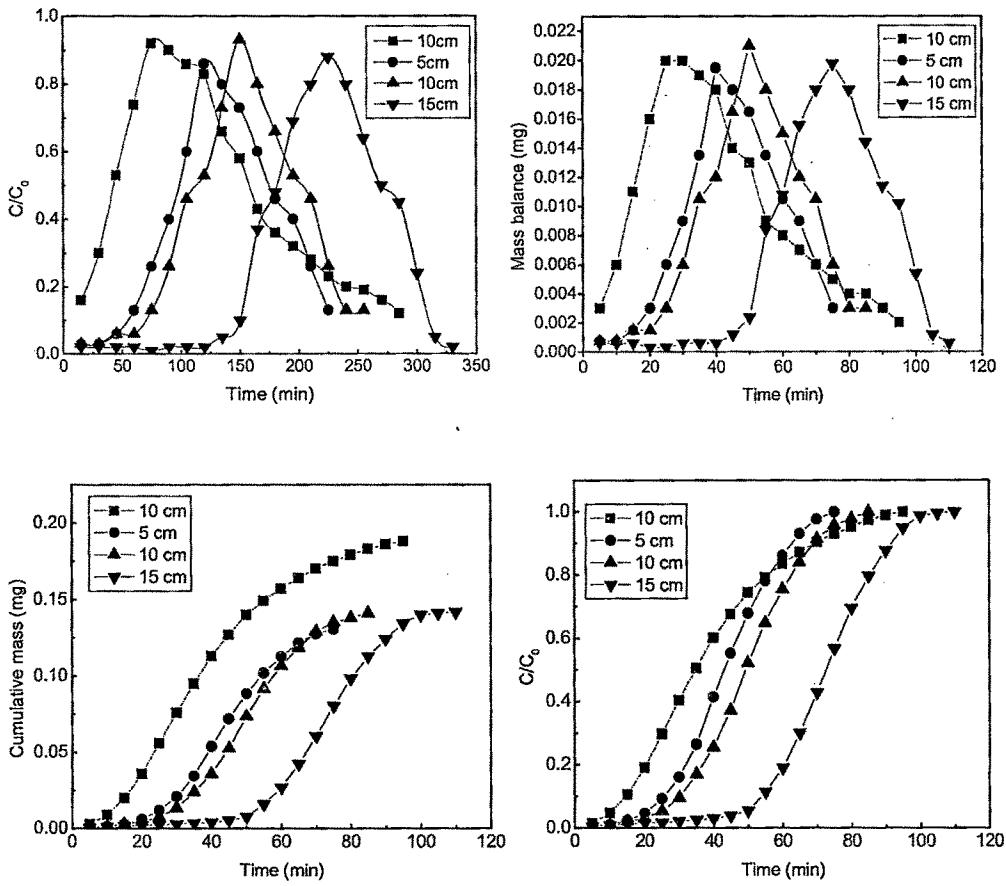


Figure 3.43. Transport of chromium through (■) contaminated sediment (10 cm) and (●▲▼) contaminated zone supported on uncontaminated zone

The concentration profiles were modeled by the equation given below.

$$\frac{y}{y_0} = \exp \left[- \frac{\left(\frac{t}{t_0} - 1 \right)^2}{2\sigma^2} \right]$$

Where y_0 is the maximum concentration, t_0 is the time at which the maximum concentration exists and σ is the standard deviation of the peak. The key parameters of the plot ie the standard deviation of the curves, were obtained as 0.296 and 0.15 for uncontaminated soil layer height of 10 cm and 15 cm respectively, which could be used conveniently to model the concentration distribution in shallow depths.

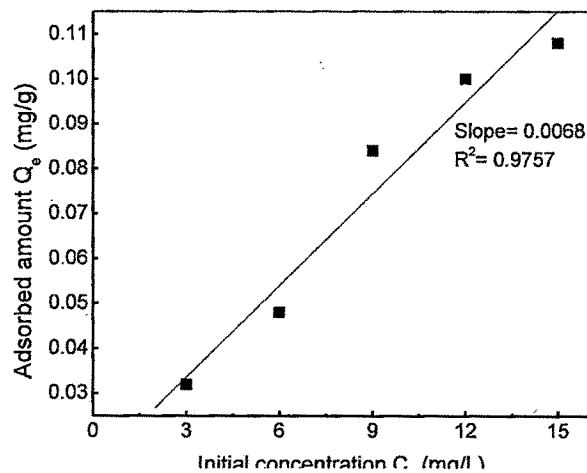


Figure 3.44. Adsorption of chromium on sediment

Table 3.30. Mass balance and cumulative mass of Cr(VI) through mixed bed**5 cm**

Pore volume	Mass balance	Cumulative mass	C/Co
5	0.00075	0.00075	0.0057
10	0.00075	0.0015	0.0114
15	0.0015	0.003	0.0229
20	0.003	0.006	0.0459
25	0.006	0.012	0.0919
30	0.009	0.021	0.1609
35	0.0135	0.0345	0.2643
40	0.0195	0.054	0.4137
45	0.018	0.072	0.5517
50	0.0165	0.0885	0.6781
55	0.0135	0.102	0.781
60	0.0105	0.1125	0.862
65	0.009	0.1215	0.9310
70	0.006	0.1275	0.977
75	0.003	0.1305	1.000

10 cm

Pore volume	Mass balance	Cumulative mass	C/Co
5	0.00075	0.00075	0.0053
10	0.00075	0.0015	0.0106
15	0.0015	0.003	0.021
20	0.0015	0.0045	0.031
25	0.003	0.0075	0.053
30	0.006	0.0135	0.095
35	0.0105	0.024	0.170
40	0.012	0.036	0.255
45	0.0165	0.0525	0.372
50	0.021	0.0735	0.521
55	0.018	0.0915	0.648
60	0.015	0.1065	0.755
65	0.012	0.1185	0.840
70	0.0105	0.129	0.914
75	0.006	0.135	0.957
80	0.003	0.138	0.978
85	0.003	0.141	1.000

15 cm

Pore volume	Mass balance	Cumulative mass	C/Co
5	0.0006	0.0006	0.0042
10	0.0006	0.0012	0.0084
15	0.0006	0.0018	0.0127
20	0.0003	0.0021	0.0148
25	0.0003	0.0024	0.0169
30	0.0006	0.003	0.0211
35	0.0006	0.0036	0.0254
40	0.0006	0.0042	0.0296
45	0.0012	0.0054	0.0381
50	0.0024	0.0078	0.0550
55	0.0084	0.0162	0.1144
60	0.0108	0.027	0.1906
65	0.0156	0.0426	0.3008
70	0.018	0.0606	0.4279
75	0.0198	0.0804	0.5677
80	0.018	0.0984	0.6949
85	0.0144	0.1128	0.7966
90	0.0114	0.1242	0.8771
95	0.0102	0.1344	0.9491
100	0.0054	0.1398	0.9872
105	0.0012	0.141	0.995
110	0.0006	0.1416	1.000

10 cm

Pore volume	Mass balance	Cumulative mass	C/Co
5	0.003	0.003	0.015
10	0.006	0.009	0.047
15	0.011	0.020	0.106
20	0.016	0.036	0.191
25	0.020	0.056	0.297
30	0.020	0.076	0.404
35	0.019	0.095	0.505
40	0.018	0.113	0.601
45	0.014	0.127	0.675
50	0.013	0.140	0.744
55	0.009	0.149	0.792
60	0.008	0.157	0.835
65	0.007	0.164	0.872
70	0.006	0.17	0.904
75	0.005	0.175	0.930
80	0.004	0.179	0.952
85	0.004	0.183	0.973
90	0.003	0.186	0.989
95	0.002	0.188	1.000

3.12. Heavy metal analysis of sediments and water

3.12.1. Sample collection

Sediment samples were collected from two different stations (Angad and Amrapura) along the mini river, flowing through the Nandesari industrial area. Samples were collected at 30 cm intervals from the cliffs of river bed. The collected samples were dried and thoroughly mixed to generate a homogenous mixture and sieved through a 2 mm sieve in order to collect granulometric fraction. The soil samples were also collected from the upstream area which is less contaminated to determine the background concentration of heavy metals.

3.12.2. Water samples

The water samples were collected at five different locations from the river channel namely Chamunda Nagar (RS1 & RS 2), Angad (RS 3), Amrapura (RS 4) & Singrot (RS 5) carrying industrial effluents. Thick quality polyethylene bottles rinsed with 10% nitric acid and then with double distilled water were used to collect samples. These water samples were collected from 30 cm below the water surface at five different locations.

Water samples were also collected from wells located <500m from the mini river at three different locations namely Chamunda Nagar (GW1), Rampura(GW2) and Angad(GW3). Though number of tube wells are available in this area, the open wells located near the river was selected for the sampling to study the possible contamination by heavy metals.

3.12.3. Analytical methods

The organic carbon content of the sediment samples were determined by walkely-Black method (146). Sediment texture (sand,silt and clay) was determined by pipette method (3). The pH of the sediments was measured by using a glass electrode in 1:8 sediment-water suspension. The electrical conductivity was measured by using conductivity meter.

The total heavy metal concentration was determined by digestion of <63 μ m sediment fraction (1 ± 0.05 g) with 1M HNO₃ at 90°C for 1 hr, making final volume to 10 mL and the samples were centrifuged at 1500 RPM for 15 minutes and the dissolved metals in the supernatant were analyzed by atomic absorption spectrophotometer.

The following procedure was adopted for the pretreatment of water samples before the heavy metal analysis (161). The collected water samples were adjusted to pH 4 with concentrated nitric acid. Then 100 mL of this water sample was transferred to 250 mL conical flask. About 5 mL of conc HCl was added followed by heating on a hot plate for 20 min. Further, this sample was filtered through the sintered-glass crucible after cooling at room temperature. This filtered sample was made upto 100 mL with double distilled water used for rinsing filter flask. These samples were used for the heavy metal analysis by atomic absorption spectroscopy.

The basic statistics of the variables data set of the Mini river sediments are given in Table 3.31. The pH of the Angad sediments varied from 7.48 to 7.98, while the pH for the Amrapura sediments varied from 7.68 to 7.87. The electrical conductivity values of the sediments ranged from 0.22 to 3.12 for Angad and 0.29 to 0.45 for Amrapura area. The mean electrical conductivity of Angad samples is higher than the Amrapura. Results of the sediment fraction analysis by pipette method shows that samples of both study sites are composed of predominantly silt fraction followed by sand and clay fraction.

The concentration of heavy metals (Pb, Fe, Ni) present in the sediments collected from Angad and Amrapura are shown in Figure 3.45 and 3.46 respectively. It is seen from this Figure that the concentration of heavy metals found in the sediments is higher than the maximum permissible limit stipulated by a WHO and ISO. While the concentration (ppm) of heavy metals in sediments of the Angad ranged between 0.023 to 0.062 for Pb, 164.35 to 388 for Fe and 1.776 to 20.45 for Ni, the heavy metal concentration in sediments of Amrapura ranged from 0.039 to 0.085 for Pb, 208.05 to 230.15 for Fe and 1.642 to 2.149 for Ni. The concentration of Cd was found to be below the detection limit in all the sediment samples.

The sediment contamination of heavy metals is found to be higher in Amrapura area than the Angad location. Such increased concentration of heavy metals in Amrapura area is due to the effluent discharged from the number of industries operating in the nearby area into the river. Over the period of time, such heavy metals present in the untreated effluents get accumulated in the sediments.

Table 3.31. Characterization of Mini river sediments

Variable	Unit	Minimum		Maximum		Mean		Standard Deviation	
		AN	AM	AN	AM	AN	AM	AN	AM
pH	----	7.48	7.68	7.98	7.87	7.77	7.78	0.15	0.06
Electrical Conductivity	mS/cm	0.22	0.29	3.12	0.45	0.84	0.38	1.01	0.07
TOC	%	0.11	0.15	0.70	0.22	0.25	0.18	0.18	0.02
Sand	%	27	29	54	45	39.5	34.8	8.32	6.09
Silt	%	30	34	55	50	43.3	45.6	7.83	6.80
Clay	%	13	15	21	23	17.2	19.6	3.29	3.43

AN- Angad, AM- Amrapura

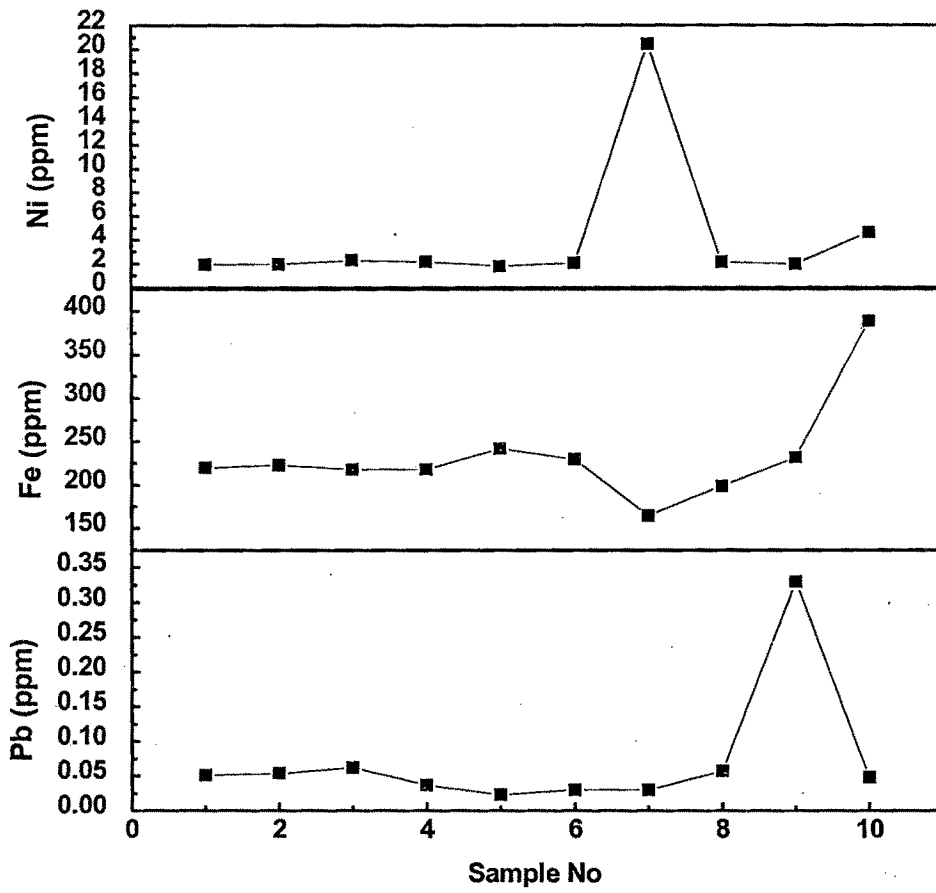


Figure 3.45. Heavy metal content in Angad sediments

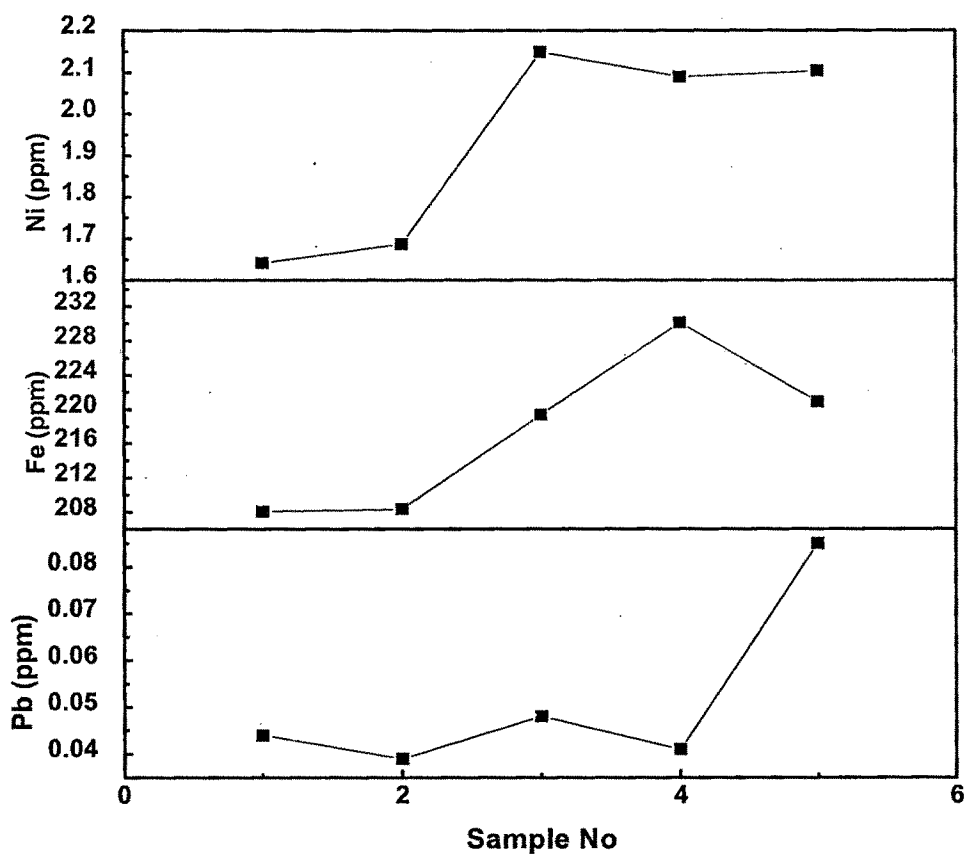


Figure 3.46. Heavy metal content in Amrapura sediments

3.12.4. Enrichment factor

The values of the enrichment factor (EF) are given in Table 3.32. The values of the enrichment factor show that the Pb is enriched by the factor of 1.1 to 16 in Angad, 3.2 to 7 in Amrapura, Iron varies from 1.4 to 3.5 in Angad, 1.7 to 1.9 in Amrapura and Nickel varies by the factor of 7.4 to 85.2 in Angad, 9.1 to 11.9 in Amrapura. While the enrichment factor value for Pb is high in sample no 9 in Angad, sample No 7 shows very high value for Ni. This reveals that at the particular depth, sediment profile is highly contaminated with Pb and Ni. Thus, with respect to background concentration values, the sediment profile is highly contaminated with heavy metal in the order of Ni > Pb > Fe.

I_{geo} classes for the heavy metals determined are given in Table 3.33. I_{geo} class values for Pb indicate that the sediment profile are unpolluted to moderately polluted in both the study sites, except sample No 9 in Angad which is highly contaminated.

While the Angad sediments are moderately polluted with respect to Ni except sample no 10 which is highly polluted, the level of pollution in Amrapura are moderately polluted with few sample showing moderate to high pollution. The stainless steel production units, welding products, pigments and electroplating industries are the main source of Nickel contamination in sediments and water bodies.

I_{geo} class value for Fe indicates that the sediments are unpolluted to moderately polluted. Thus with respect to background concentration values there is hardly any possible contamination by iron is found in sediments.

Table 3.32. Enrichment factor (EF) for Pb, Fe and Ni in river sediments

Sample No	Lead		Iron		Nickel	
	Angad	Amrapura	Angad	Amrapura	Angad	Amrapura
1	2.5	3.6	1.9	1.7	8.0	9.1
2	2.7	3.2	2.0	1.7	8.1	9.3
3	3.1	4.0	1.9	1.8	9.5	11.9
4	1.8	3.4	1.9	1.9	8.9	11.6
5	1.1	7.0	2.1	1.8	7.4	11.6
6	1.5	-	2.0		8.5	
7	1.5		1.4		85.2	
8	2.8		1.7		8.8	
9	16		2.0		8.2	
10	2.4		3.5		19.3	

Table 3.33. I_{geo} classes for Pb, Fe and Ni in river sediments

Sample No	Lead		Iron		Nickel	
	Angad	Amrapura	Angad	Amrapura	Angad	Amrapura
1	1	1	1	1	2	2
2	1	1	1	1	2	2
3	1	1	1	1	2	3
4	1	1	1	1	2	3
5	1	2	1	1	2	3
6	1		1		2	
7	1		1		2	
8	1		1		2	
9	4		1		2	
10	1		1		4	

The natural background concentration of heavy metals (Pb, Ni and Fe) was compared with the concentrations of heavy metals in mini river sediments to find the cause of pollution. The enrichment of heavy metals in river sediments than the background samples shows the anthropogenic source of pollution.

The pH and electrical conductivity (mS/cm) of river water samples were 6.64, 6.89, 6.90, 6.79, 6.81 and 14.48, 4.23, 4.40, 4.34, 5.12 respectively (sample 1-5). The pH and electrical conductivity of ground water samples were 7.18, 7.23, 7.35 and 3.98, 4.95, 3.87 respectively (sample 1-3). The electrical conductivity of RS 1, the site which receives the effluents, is considerably higher than those of other samples. The high electrical conductivity of ground water depends on the mineralization of water and indicates the impact of anthropogenic pollution (162).

The concentration of heavy metals (Pb, Fe and Ni) found in river water samples are given in Figure 3.47. The concentration of Fe in mini river water is higher followed by nickel and lead. The concentration of Cr(VI) in river water sample 1 was found to be 0.66 ppm, while in other samples the presence of Cr(VI) was found to be below the detection level. The concentration of cobalt was below the detection level in all the samples. The presence of Cr(VI) in RS1 is attributed to the dyeing industries functioning in that area.

The concentration of heavy metals in ground water samples are shown in Figure 3.48. In this case also, the concentration of Fe is higher in water sample followed by Ni and Pb. The concentration of Cr(VI) and Co was found to be below the detection level in all three ground water samples. The concentration of Fe and Ni in ground water is higher than the EPA permissible limit of 0.3 ppm and 0.1 ppm respectively (163). The permissible limit of contaminants according to Environmental protection agency (EPA 2002) is given in Table 3.34. This results corroborate well with the concentration of heavy metals found in river water and sediments as both showed the concentration of heavy metals in the following order $Fe > Ni > Pb$.

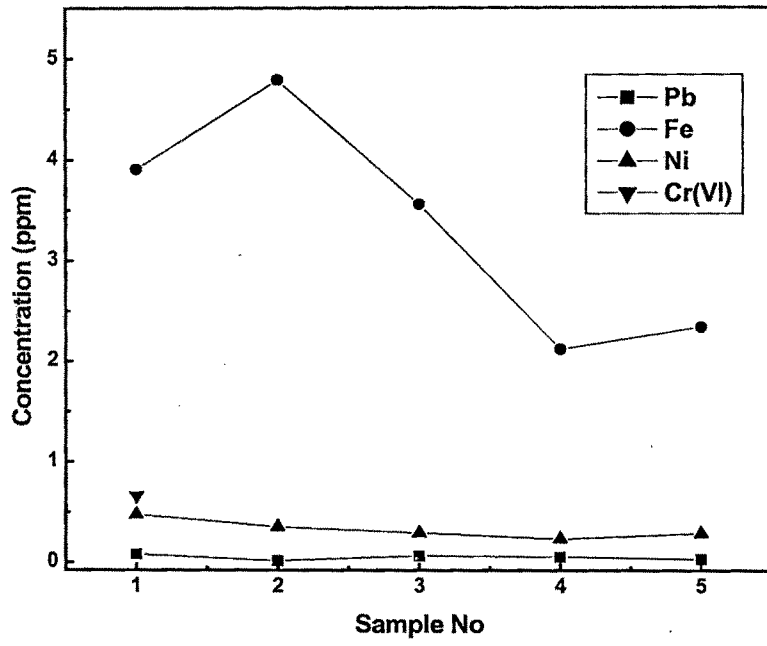


Figure 3.47. Concentration of heavy metals in River water

Table 3.34. Permissible limit of contaminants as per EPA

Heavy metals	Permissible limit (ppm)	Reference
Pb	0.01	163
Cr	1.0	163
Fe	0.3	163
Ni	0.1	163
Cu	1.3	163

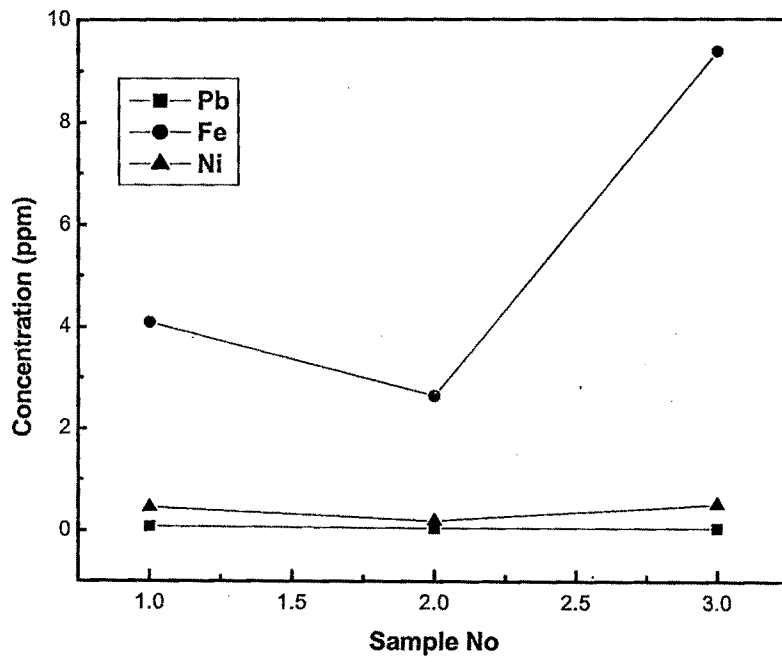


Figure 3.48. Concentration of heavy metals in ground water

The concentration of heavy metals found in ground water, collected from the open wells of area along which the river passes through, indicate the possible movement of contaminants through the soil layer. The heavy metals present in the untreated industrial effluents find their way into ground water through the soil pores by various mechanisms. While the movement of dissolved contaminants occurs during the rainy season, colloidal particles present in the sediments transport these contaminants to greater depths by surface adsorption.

3.12.5. Water analysis

The experiments were carried out to determine the ground and river water quality and the results are given in Table 3.35 and 3.36. Being the primary parameter to determine the water quality, colour of the water samples were determined and found to be brownish except samples 4 and 5. The pH of all the ground water samples was higher than the permissible limit stipulated by ISI and WHO, indicating the alkaline nature of water. Despite the low concentration of total dissolved solids, the electrical conductivity of all the samples was higher. COD level, chloride and sulphate were found to be less than the permissible limit in all the ground water samples. The low COD values indicate the absence of organic contaminants in the water samples.

Table 3.35. Results of ground water analysis

SNo	Parameter	Standard		Ground water				
		ISI (mg/L)	WHO (mg/L)	GW1	GW2	GW3	GW4	GW5
1	Colour	Colourless	Colourless	Brownish Yellow	Brown	Brownish Yellow	Colourless	Colourless
2	pH	6.9	6.9	7.35	7.10	7.18	7.23	7.30
3	EC (mS/cm)	---	---	3.87	5.12	3.98	4.95	4.32
4	TDS	---	1500	540	430	425	40	45
5	DO	---	---	5.21	4.87	4.89	5.21	5.31
6	COD	200	---	120	135	124	25	20
7	Chloride	600	250	252	243	198	234	225
8	Sulphate	1000	400	105	125	40	45	32
9	NO ₃ - N	---	10	0.74	0.72	0.61	0.22	0.32
10	Fluoride	3.0	1.5	0.62	0.45	0.60	0.75	0.44
11	Phosphate	---	---	0.38	0.45	0.40	0.28	0.23

Table 3.36. Results of river water analysis

SNo	Parameter	Standard		River water			
		ISI (mg/L)	WHO (mg/L)	RW1	RW 3	RW4	RW 5
1	Colour	Colourless	Colourless	Red	Red	Red	Red
2	pH	6.9	6.9	6.90	6.89	6.64	6.70
3	EC (mS/cm)	-	-	4.40	4.23	14.48	14.28
4	TDS	-	1500	185	190	192	195
5	DO	3.0	-	14.45	13.45	13.40	11.20
6	COD	200	-	214	210	184	169
7	Chloride	600	250	123	143	110	098
8	Sulphate	1000	400	674	685	550	534
9	NO ₃ - N	-	10	0.22	0.18	0.98	0.74
10	Fluoride	3.0	1.5	2.1	2.7	2.0	2.5
11	Phosphate	-	-	0.87	0.68	1.2	0.88

The electrical conductivity of all the samples was found to be higher indicating the presence of ionic substances and contaminants. The samples collected at Amrapura and Singrot (RW 4 and RW 5) showed very high electrical conductivity as compared to the other samples, exceeding 14 mS/cm. COD level in river samples (Chamunda nagar and Angad) exceeds the permissible limit indicating the presence of organic contaminants as against the ground water having the negligible amount of organic contaminants. The sulphate content was higher in all the samples exceeding the permissible limit of 400 mg/L set by WHO.

3

3.13. Simulation experiments for the transport of alizarin red in soil column

(a) Theory

The simulation experiments for any transport in soil can be done using readily available software. The simulation of transport of contaminants has been attempted by various authors [164-166]. Various software's are available free that can be used to understand this transport. The basis for this is essentially on water transport through the soil column.

Based on the water transport, the contaminant transport can also be simulated.

The partial differential equation for the water movement has been written by Richards [167] as below:

$$\frac{\partial \theta}{\partial t} = \frac{\partial}{\partial x} \left[K(h) \left(\frac{\partial h}{\partial x} - \sin(A) \right) \right]$$

Where θ is the volumetric water content, h is the matrix potential, x is the direction of flow, t is the time, $k(h)$ is the hydraulic conductivity of the soil at matrix potential h , $C(h)$ is the specific water capacity, $\sin(A)$ is the sine of the angle A between the direction of flow and the horizontal direction.

Initial condition for water:

The initial condition for the finite length of the soil column L is

$$h(x, 0) = h \text{ initial } (x) \quad 0 < x < L$$

For the semi infinite column

$$h(x, 0) = h \text{ initial} \quad x > 0$$

For the transport of water, three types of boundary conditions can be used to simulate the water movement in columns

At $X = 0$, the boundary conditions are

1) Constant potential of h_0

$$h(0, t) = h_0$$

2) Constant flux density q_0

$$-K(h) \left[\frac{\partial h}{\partial X} - \text{Sin}(A) \right]_{X=0} = q_0$$

At $X=L$ the boundary conditions are

1) Constant matrix potential of h_L

$$h(L, t) = h_L$$

2) Constant flux density q_L

$$-K(h) \left[\frac{\partial h}{\partial X} - \text{Sin}(A) \right]_{X=L} = q_L$$

3) Free drainage

$$\left[\frac{\partial h}{\partial X} \right]_{X=L} = 0$$

Flux density of water:

The flux density of water is the volume of the water flowing through the soil at a certain point of per unit cross sectional area of soil per unit time. The flux density of water $q(x,t)$ is given by the Darcy-Buckingham equation

$$q(X, t) = -K(h) \frac{\partial h}{\partial X}$$

The cumulative flux of water is the the total amount of water flowing past the inlet or outlet of the soil system during the simulation. It is given by

$$Q(X, t) = \int_0^t q(X, t) dt$$

Where $q(X,t)$ is the flux density of water.

Based on the above discussion, the application of freely available software “CHEMFLOW” for the simulation of contaminant transport is described below.

The movement of contaminant in this model is described by the convection-dispersion equation

$$\frac{\partial \theta c}{\partial t} + \frac{\partial \rho S}{\partial t} = \theta D \frac{\partial^2 C}{\partial x^2} - q \frac{\partial C}{\partial x} \quad (1)$$

Where $c = C(x,t)$ is the concentration of contaminant in the liquid phase, $S = S(x,t)$ concentration of contaminant in the solid phase, $D = D(x,t)$ is the dispersion coefficient, $\theta = \theta(x,t)$ is the volumetric water content, $q = q(x,t)$ is the superficial flow flux, $\rho = \rho(x,t)$ is the bulk density of the soil

The partitioning of contaminant between solid and liquid phase

$$S(x, t) = K(x)C(x, t) \quad (2)$$

Where $K(x)$ is the partition coefficient for the matrix.

Incorporating Equation 2 in 1 gives the following equation

$$\frac{\partial \theta R c}{\partial t} = \theta D \frac{\partial^2 C}{\partial x^2} - q \frac{\partial C}{\partial x}$$

Where R is the retardation factor of contaminant in the soil and is given by

$$R = 1 + \frac{\rho K}{\theta}$$

The following initial and boundary conditions can be written for this model are

$$C(x, 0) = C_{\text{initial}}(x) \quad 0 < x < L$$

$$S_f(x, 0) = 0$$

The boundary conditions at $x = 0$

1) Constant concentration of inflowing solution:

This is used in the simulation of contaminant entering the soil column with the known and constant concentration.

$$\left[-\theta D \frac{\partial C}{\partial x} + q(0, t)C\right]_{x=0} = q(0, t)C_s \quad \text{if } q(0, t) > 0$$

$$\left[-\theta D \frac{\partial C}{\partial x} + q(0, t)C\right]_{x=0} = 0 \quad \text{if } q(0, t) < 0$$

2) Constant concentration of contaminant in surface soil: This situation can be written as

$$C(0, t) = C_0$$

The boundary conditions at $X = L$ are given as below

1) Convective flow: This boundary condition is used to simulate movement of contaminant with the flowing water, irrespective of diffusion and dispersion. This can be written as

$$\left[\frac{\partial C}{\partial x}\right]_{x=L} = 0$$

2) Concentration of contaminant at the soil surface: This boundary condition specifies that the concentration of contaminant at the soil surface as

$$C(L, t) = C_L$$

Flux density of the contaminant is defined as the mass of the contaminant passing that position X in the soil per unit cross sectional area per unit time. The flux of contaminant is given as

$$f(x, t) = -\theta D \frac{\partial C}{\partial x} + qc$$

The cumulative flux of contaminant is the mass of contaminant moving out of the position of interest per unit cross sectional area of soil from $t = 0$ to $t =$ time of interest and it is given by the equation given below

$$F(x, t) = \int_0^t f(x, t) dt$$

Where $f(x, t)$ is the flux density of contaminant

Total mass of contaminant in the soil is the sum of the mass of the contaminant in the solid and liquid phases and it can be written as

$$mT(t) = m_l(t) + m_s(t)$$

Where the mass of the contaminant in the liquid phase is

$$m_l(t) = \int_0^L \theta(x, t) C(x, t) dx$$

and the mass of the contaminant in the solid phase is

$$m_s(t) = \int_0^L \rho(x) K(x) C(x, t) dx$$

Total concentration of contaminant is defined as the sum of the mass of contaminant in the soil solution and the mass of contaminant adsorbed on the soil and colloids.

This can be written as follows

$$C_T(x, t) = [\theta(x, t) + \rho(x)K(x)] C(x, t)$$

(b) Simulation experiment

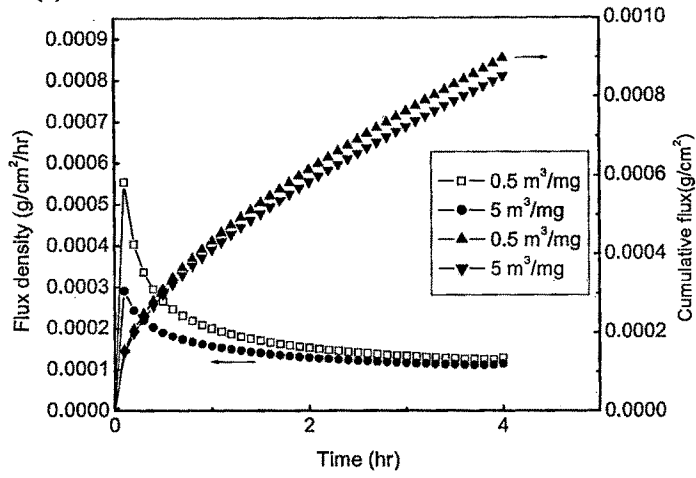
In these simulation experiments, the soil column having the finite length of 50 cm and width 4 cm is considered, through which constant concentration of 50 mg/L solution of alizarin red is passed. Then the dye was displaced from the soil column at the flow rate of 0.15 and 0.3 mL/min and the variation in the concentration of dye at the outlet were monitored. Time duration of 4 hr was selected as the time of interest for the simulation experiments.

Finite difference method has been used to obtain the numerical solution to the set of partial differential equations. In this simulation a set of mesh points is defined in the soil. The breakthrough curves are plotted in the form of total dye contaminant concentration against time. The parameters used in the simulation experiments are given in Table 3.37.

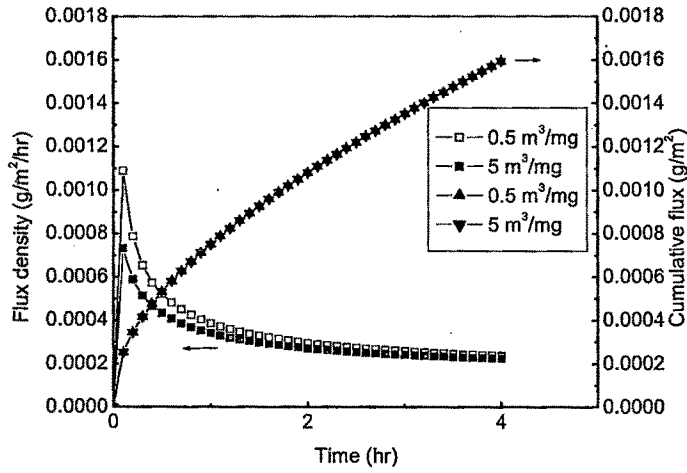
Table 3.37. Porous medium properties used in simulation experiments

Parameter	Value
Column length (cm)	50
Alizarin red dye concentration (g/L)	0.05
K_d (m ³ /mg)	0.5, 5.0
Flow rate (mL/hr)	9, 18
Dispersivity (cm)	02
Diffusion coefficient of contaminant in water (cm ² /hr)	0.03

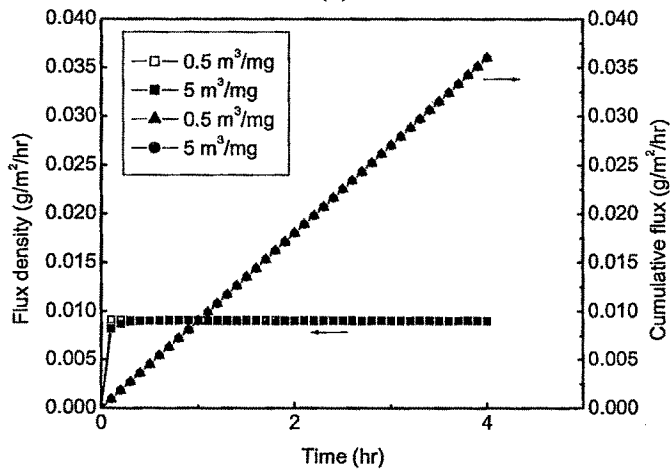
3.13.1. Effect of partition coefficient on the transport of alizarin red dye in (a) clay (b) silt and (c) sand



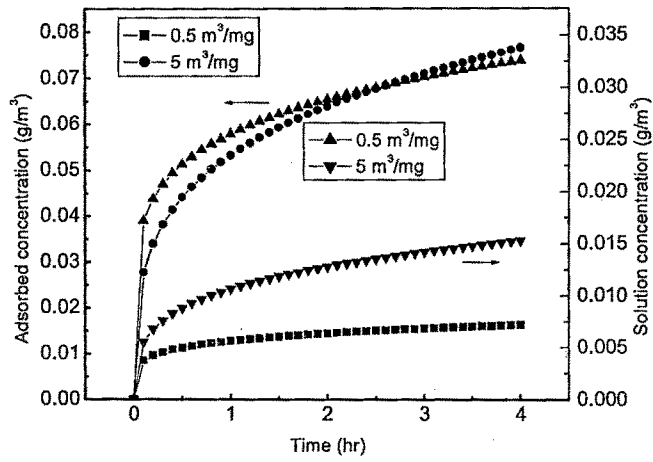
(a)



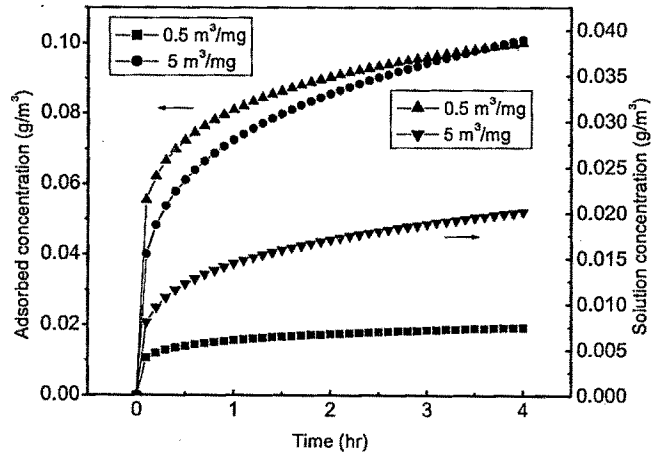
(b)



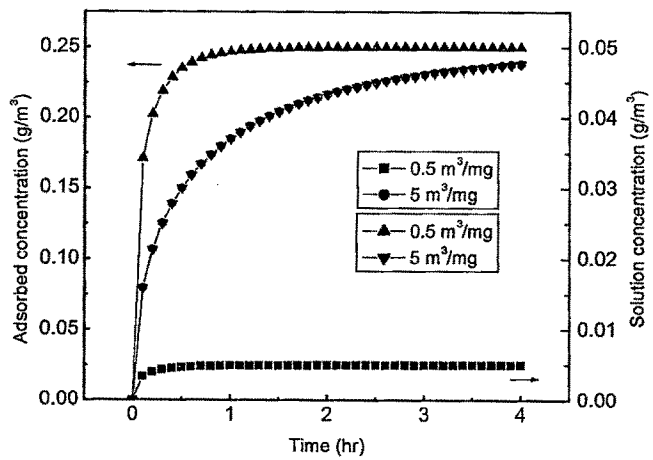
(c)



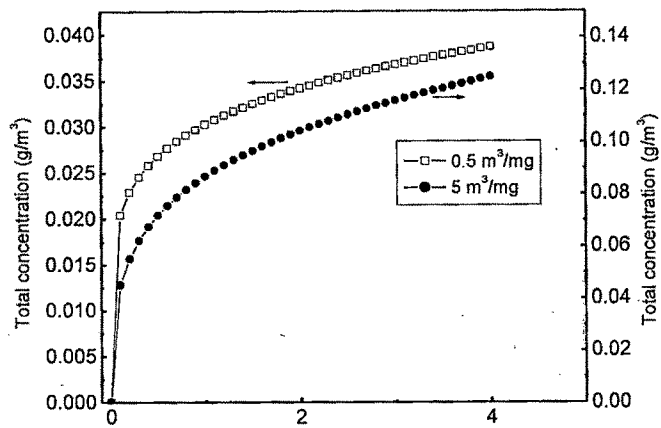
(a)



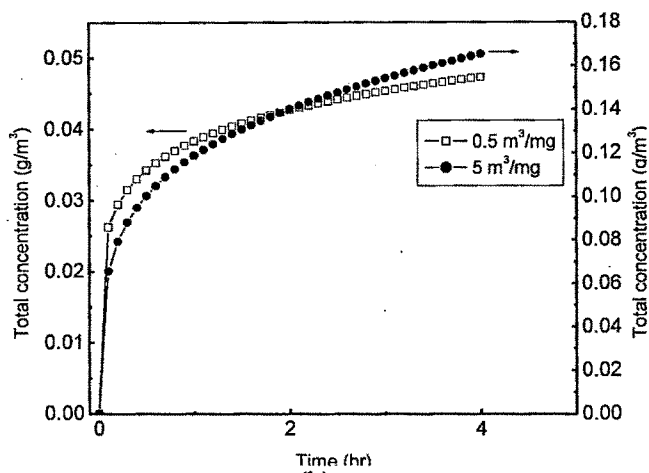
(b)



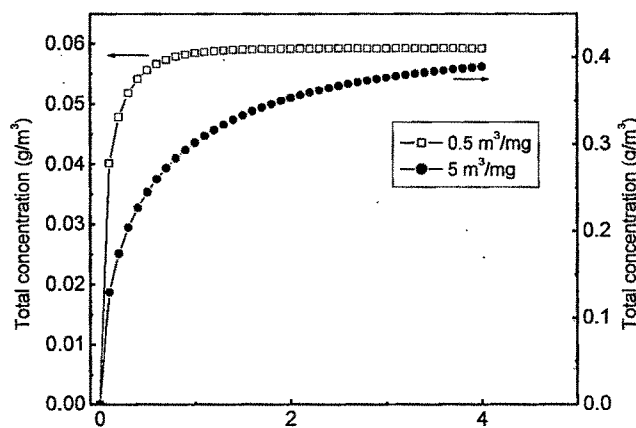
(c)



(a)



(b)



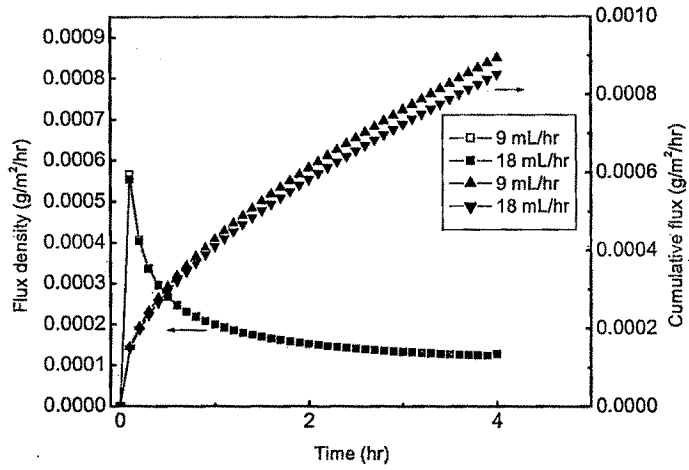
(c)

Figure 3.49. Effect of partition coefficient on the transport of alizarin red in (a) clay (b) silt and (c) sand

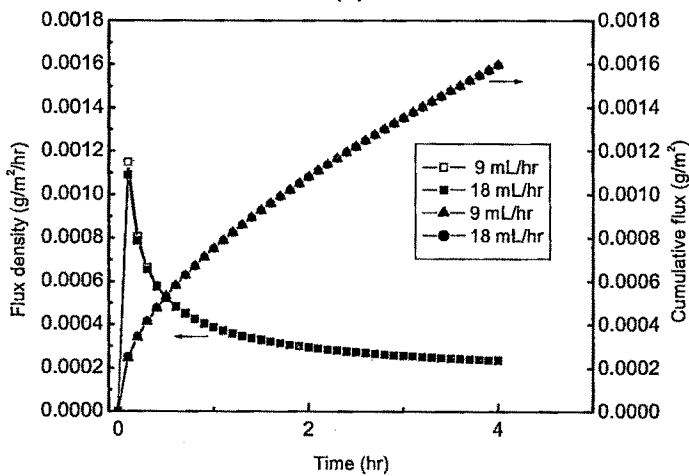
The flux density and cumulative flux and total concentration of alizarin red dye at the outlet is shown in Figure 3.49. It can be seen that the flux density of dye through the clay column is higher for the distribution coefficient of 0.5 than 5. The lower adsorption of dye on the clay matrix at $0.5 \text{ m}^3/\text{mg}$ leads to the increase in the flux density at 0.1 hr. In the case of silt matrix too, the flux density of chemicals is found to be higher for the K_d of $0.5 \text{ m}^3/\text{mg}$, suggesting the lower adsorption capacity of silt at low K_d . In contrast to this, the flux density of dye in sand columns is equal for the K_d of 0.5 and 5, with the maxima of flux density occurring at 0.1hr followed by equilibration. The simulation results also reveal the increase in the flux density of dye with the increase in particle size of soil constituents, with the higher flux density value for sand column followed by silt and clay. As the particle size of sand is bigger, the dye move through it unhindered leading to the high concentration. These simulation experiments suggest that the distribution of contaminants between liquid phase and solid phase is an important factor for the transport to occur and the mass transport of contaminants depends on their distribution.

The cumulative flux of alizarin red dye shows non-linearity for the clay and silt packed columns with the total cumulative mass of dye pass through silt column increasing two fold than the clay column. These results are in agreement with our laboratory column transport experiments which showed non linearity at the flow rate of 0.3 mL/min. In contrast to these results, linear behavior in the cumulative mass is observed for the dye passed through the sand column, suggesting the adsorption dependent transport of contaminants. The adsorbed concentration of dye also shows an increasing trend from silt to sand, with sand adsorbing chemicals more effectively than the silt and clay. The solution concentration at the outlet is found to be inversely proportional to the distribution coefficient values i.e. the solution concentration is higher at K_d $0.5 \text{ m}^3/\text{mg}$ than at $5 \text{ m}^3/\text{mg}$ and this is due to the strong association of contaminant with solid matrix. The total concentration curve is also showing the increasing trend in all three soils and the maximum concentration obtained for the sand. The simulation results corroborate well with laboratory column experiments as in both cases peak in the dye concentration was observed followed by decline in concentration.

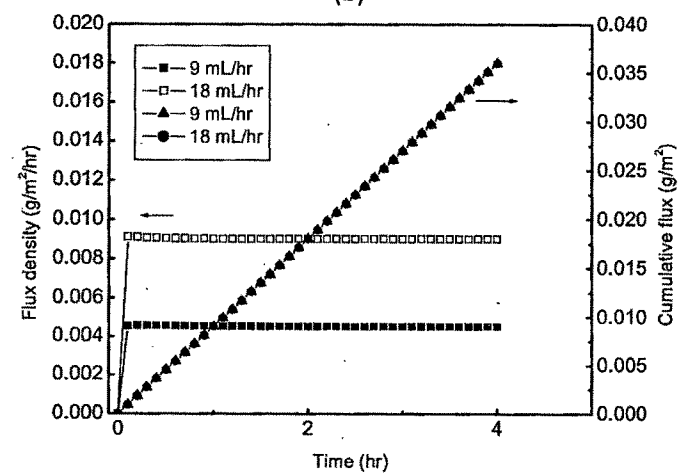
3.13.2. Effect of flow rate on the transport of alizarin red through (a) clay (b) silt & (c) sand (9 mL/hr and 18 mL/hr)



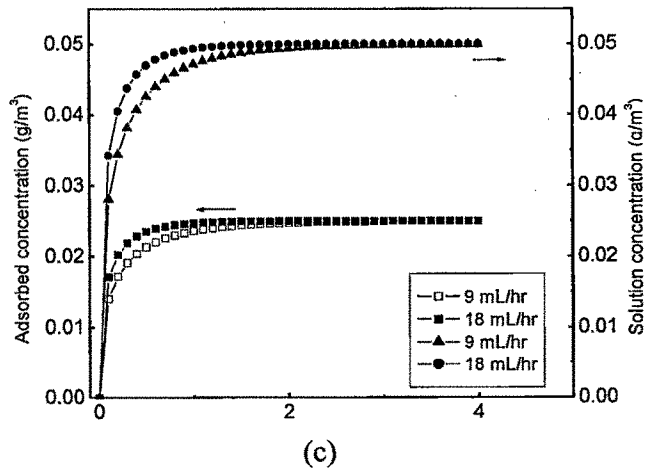
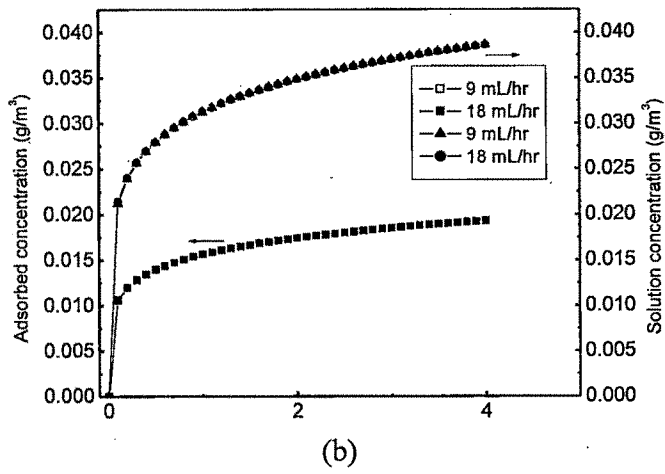
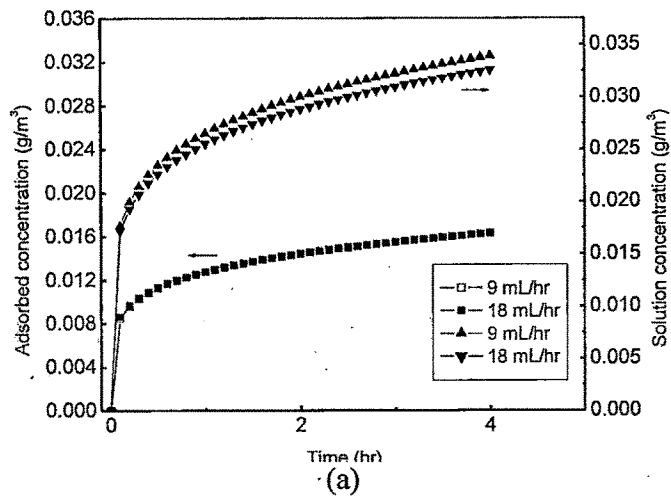
(a)

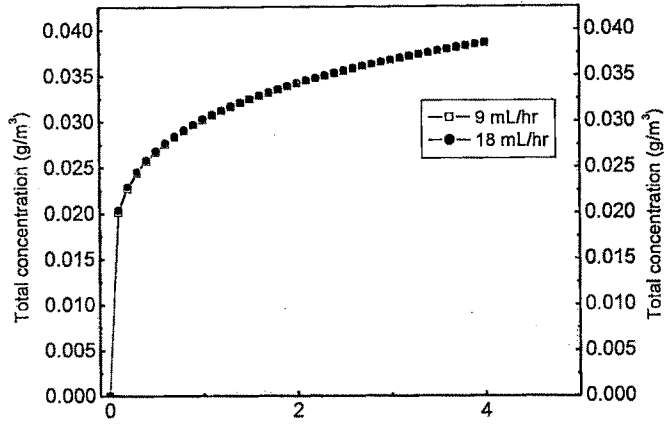


(b)

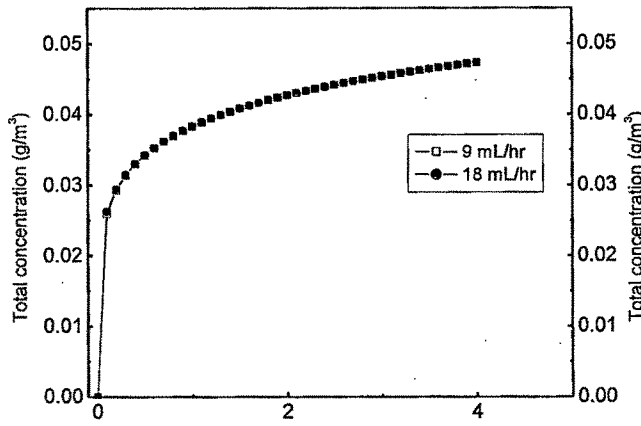


(c)

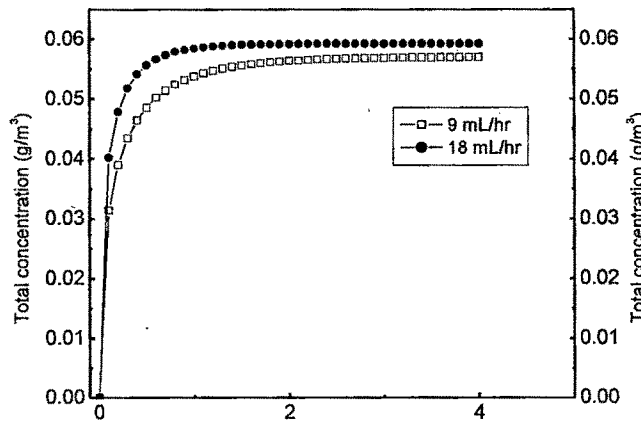




(a)



(b)



(c)

Figure 3.50. Effect of flow rate on the transport of alizarin red (9 mL/hr and 18 mL/hr)

The effect of flow rate on the transport of Alizarin red dye is given Figure 3.50. It can be seen that there is hardly any difference in the flux density is observed at the flow rate of 9 and 18 mL/hr in clay and silt soil. This simulation results suggest that flow rate doesn't influence the amount of transport of dye contaminants in natural porous media as much as expected. This simulation results are in line with our experimental results of the effect of flow rate on the transport of methylene blue in soil columns reported earlier.

In the case of sand column considerable difference in the flux density of chemicals is observed with maximum concentration occurring for the flow rate of 18 mL/hr and thereafter the curve attains the equilibrium. In this case also, the peak in the flow density of dye was observed as in the case of laboratory column experiments.

For the simulation experiments performed with flow rate of 9 and 18 mL/hr, the cumulative flux of alizarin red dye shows non-linearity for the clay and silt packed columns and linearity is observed for the dye passed through the sand column.

The adsorbed concentration of dye at the flow rate of 9 and 18 mL/hr is found to be same for each soil category and it indicates that the flow rate doesn't influence the adsorption and transport of dye in different soils. But, there exist a difference in the adsorbed amount of dye on soils, with sand showing maximum adsorption. The solution and total concentration of dye also shows the increasing trend for clay followed by silt and sand. The difference in the adsorbed concentration, solution concentration and total concentration for the flow rate of 9 & 18 mL/hr is relatively less. This shows that the flow rate doesn't influence the mass transport of contaminants in the soil column.

3.14. Remediation of water

Removal of contaminants from water is a much discussed topic today. The number adsorbents have been tried for the removal of contaminants from water. One among them is activated carbon which is perhaps the most widely used adsorbent for the removal of organic contaminants, which are biologically resistant. The methods used for the removal of contaminants include adsorption, coagulation, flotation and biological treatment. Of these methods adsorption is considered to be the most suitable and cost effective method.

The objective of our work is to remove the dyes and hexavalent chromium from aqueous solution using natural polymeric colloids as adsorbents.

3.14.1. Materials

The anionic alizarin red dye and cationic methylene blue were selected as potential organic contaminants in this study. These two dyes are selected because of their utility in textile industries and their frequent occurrence and high concentrations in textile effluents. The alizarin red dye is an anthraquinone derivative obtained from the root of the madder plant. It is commercially available and is used in textile dyeing industries. Methylene blue is a thiazine dye, which is widely used in colouring paper, dyeing of cotton and wools and hair dyes among others. Although the toxicity level of this dye is less, it causes the serious health problems to human beings such as breathing, vomiting and nausea.

The inorganic contaminant used in this study is Chromium trioxide (CrO_3) and its compounds are useful in common life. It is widely used in electroplating, tanning and anodizing industries, ferrous and nonferrous alloys, in refractories and chemicals. This hexavalent chromium is of particular concern because of its toxicity, carcinogenicity and high mobility in soil and aquatic system.

3.14.2. Separation of humic acid

Humic acid was isolated from soil by alkali extraction method. The brief extraction method is as follows. Soil sample was acidified with 1 M HCl to a pH of 1-2 at room temperature. Solution volume was adjusted with 0.1 M HCl to get a ratio of 8mL liquid/1g soil. Suspension was stirred for 30 min and allowed for settling, followed by

decantation of supernatant liquid. Then the soil residue was extracted with 1 M NaOH at a pH 11 for 24 h. Then the suspension was centrifuged at 600 rpm for 5 min. Supernatant solution was collected and acidified with 6M HCl to pH = 1.0 and then allowed to stand for overnight. The humic acid (precipitate) and fluvic acid (supernatant) were separated by centrifugation. Humic acid fraction was redissolved in 0.1 M KOH solution and centrifuged to remove suspended solids. Finally 6M HCl was added to reprecipitate the humic acid and used for further analysis.

3.14.3. Characterization of Humic acid

(a) FTIR spectroscopy

FT-IR spectra of humic materials were recorded on a FTIR (Shimadzu 8400 S) spectrophotometer and is shown in Figure 3.51. Humic samples were mixed with KBr and then ground with mortar and pestle for recording the spectra.

The FT-IR spectra of humic acids show a strong band at 3600 cm^{-1} indicating the presence of phenolic OH, alcoholic OH and carboxylic group. The absorption peaks at 2900 cm^{-1} is ascribed to C-H stretching of methyl groups. The absorption bands at 1700 cm^{-1} is due to the presence of stretching frequencies of C=O bonds of COOH groups. The band observed at 1015 cm^{-1} shows the presence of C-O stretching polysaccharide groups.

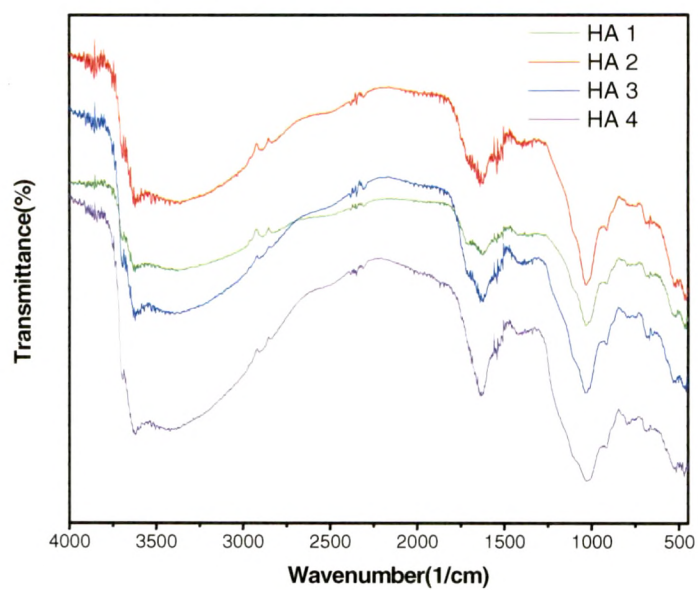


Figure 3.51. FTIR spectra of humic acid

(b) Thermogravimetric analysis (TGA)

Thermogravimetric analysis of humic acid samples was carried out using shimadzu under air atmosphere to find the decomposition temperature. The thermal decomposition of humic acids separated by alkali extraction method is given in Figure 3.52. Thermal analysis was carried out with platinum crucibles in an air atmosphere at a heating rate of 10°C per minute. From this Figure it is obvious that the all four humic samples loses absorbed water at 100°C. Carbon burns between 300- 550°C and leaves as oxygenated compounds. The observed percentage mass loss of humic sample 1 is higher than all other humic acids. The percentage mass loss of humic samples decreases with respect to depth in a manner that $HR1 > HR2 > HR3 > HR4$. This clearly shows that humic acid possess variable properties though they are separated from sediments in particular soil profile.

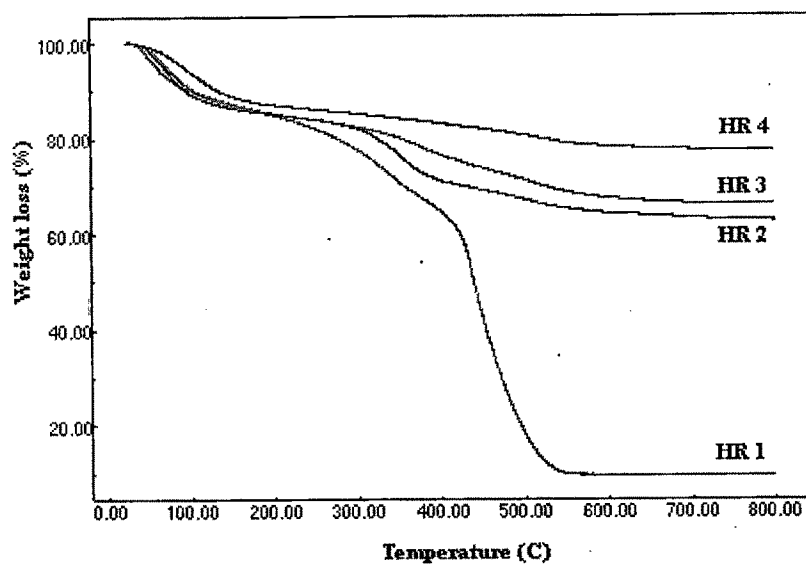


Figure 3.52. Thermogravimetry analysis (TGA) of humic acid

(c) Size of humic colloids

Particle size of humic colloids were measured by static light scattering technique equipped with Ga-As semi conductor laser at a wavelength range of 690 nm and is given in Table 3.38. It has been observed that the largest humic particles would exist in the range of approximately 110 nm at a concentration of 1-4 mg/mL. The particle size of humic substances determined by light scattering technique is in good agreement with the values reported by Osterberg and Mortensen [168].

Table 3.38. Size humic colloids

Sample	Particle size (nm)
HA 1	73.9
HA 2	82.0
HA 3	123.2
HA 4	59.6

3.14.4. Adsorption experiments

Adsorption of dye from their aqueous solutions by humic materials was measured by placing 20 mL of dye solution in contact with 5 mg of humic acids in a series of beakers. Total dye concentration range was varied from 20-100 mg/L and the chromium concentration range was 3-15 mg/L. Samples were stirred by using magnetic stirrer with constant speed to maintain the contents completely mixed for about 4 hr. After equilibration, samples were centrifuged at 1500 rpm for 15 minutes. The concentration of the supernatant solution was measured with UV-Visible spectrophotometer at a wavelength of 520 nm, 665 nm and 372 nm for the alizarin red, methylene blue and chromium respectively. The quantity of adsorbed dye on humic materials was calculated as the difference between initial concentration and concentration at equilibrium.

3.14.4.1. Adsorption Kinetics

In the case of kinetic experiments the same procedure described earlier was performed with initial concentrations ranging from 50- 200 mg/L. The volume of dye solution and the quantity of adsorbent taken was 50 mL and 20 mg respectively. The samples were withdrawn from the beaker at definite time intervals and analyzed for dye concentration with UV-Visible spectrophotometer. The amount of dye adsorbed at definite time intervals was determined by using the formula given below

$$Q_t = (C_0 - C_t)V/W$$

where C_0 and C_t are the initial and concentration of dye in the liquid phase at time t (mg/L) respectively. V is the volume of the dye solution (in liters) and W mass of the colloid adsorbent (g).

3.14.4.2. Effect of initial concentration

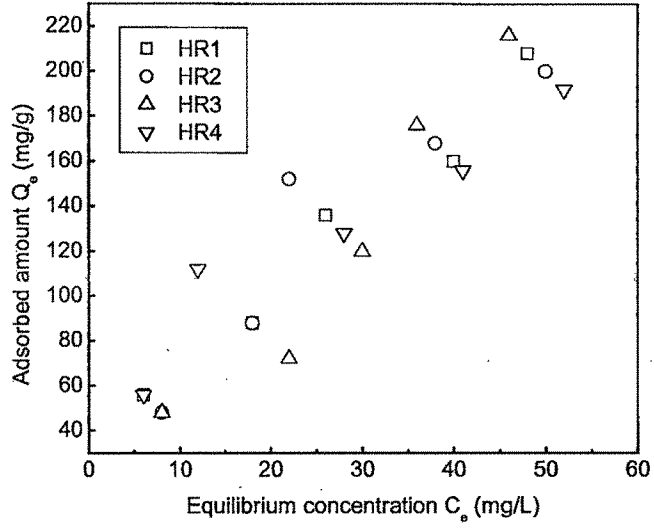
Effect of initial solution concentration was investigated at ambient conditions with measurements made after an equilibration time of 6 hr. The adsorption experiments were conducted by varying the initial solution concentration of methylene blue and alizarin red 20-100 mg/L at ambient conditions at temperature of $30 \pm 2^\circ\text{C}$ and the data is reported in Figure 3.53. It can be seen that with the increase in contaminant concentration in solution the amount adsorbed on humic colloid increases.

All sorption data were fitted to the logarithmic form of the Freundlich equation and the results are given in Table 3.39a. Adsorption of dye fits well to the Freundlich adsorption equation. Of the four humic samples selected for the adsorption studies, the HR 4 sample shows the highest adsorption capacity for the dye contaminants. It can be seen from table that the adsorption of alizarin red decreases in the following order HR 4>HR 3>HR 2>HR 1.

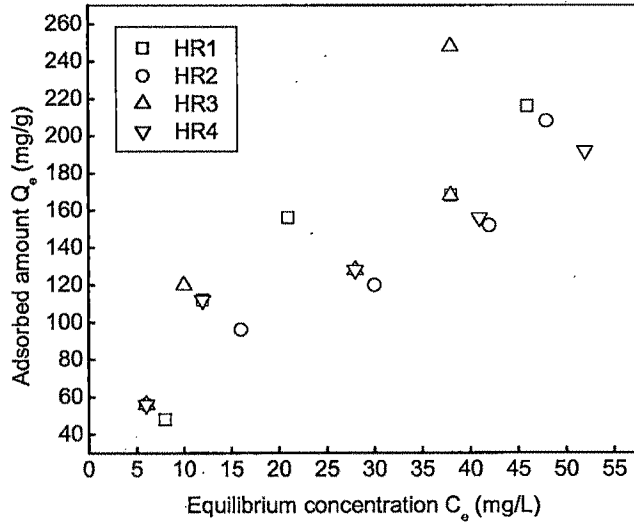
The results of Langmuir adsorption isotherm are given Table 3.39b. In this case adsorption capacity of humic acid for alizarin red decreased in the order HR 1>HR 3>HR 2>HR 4. This high amount of adsorption of contaminants suggests the potential use of humic colloids as an effective adsorbent for the removal of contaminants from contaminated water.



Methylene blue



Alizarin red



Chromium (VI) oxide

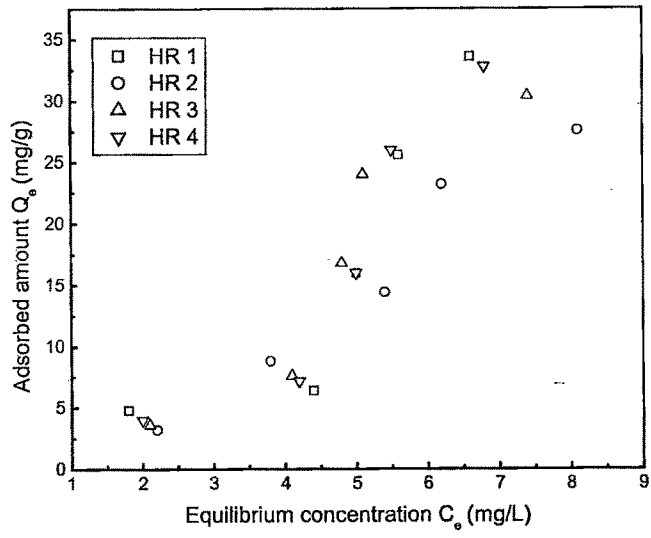


Figure 3.53. Adsorption of dyes and Cr(VI) on humic acid at different initial concentrations

Table 3.39. Adsorption of dyes and Cr(VI) on humic acid (a) Freundlich isotherm parameters

Sample	K _F (mg/g)/(L/mg)			N			R ²		
	AR	MB	Cr(VI)	AR	MB	Cr(VI)	AR	MB	Cr(VI)
HR 1	14.1	17.3	37.5	0.71	0.61	1.47	0.91	0.98	0.79
HR 2	19.4	9.77	46.2	0.56	0.79	0.54	0.97	0.96	0.74
HR 3	22.9	6.91	25.2	0.58	0.85	0.23	0.89	0.93	0.78
HR 4	25.1	25.1	60.9	0.50	0.50	0.75	0.95	0.95	0.72

(b) Langmuir isotherm parameters

Sample	Q ₀ (mg/g)			b (L/mg)			R ²		
	AR	MB	Cr(VI)	AR	MB	Cr(VI)	AR	MB	Cr(VI)
HR 1	416.6	357.1	37.1	0.10	0.11	37.1	0.79	0.87	0.45
HR 2	294.1	500.0	75.1	0.10	0.14	75.1	0.87	0.80	0.80
HR 3	303.0	2500	28.4	0.07	0.21	28.4	0.79	0.11	0.47
HR 4	250.0	250.0	69.9	0.08	0.08	69.9	0.96	0.96	0.53

3.14.4.3. Pseudo first order equation

The adsorbed amount of dye at different time intervals on colloids was calculated with the formula given below. The kinetics of dye adsorption on colloid was studied using the pseudo first order equation given below

$$dq/dt = K_1(q_e - q_t)$$

Where q_e is the amount of dye adsorbed at equilibrium per unit weight of adsorbent (mg/g), q_t is the amount of dye adsorbed at time t (mg/g) and K_1 is the adsorption constant. The linearized form of the above equation as a function of time is

$$\log (q_e - q_t) = \log q_e - K_1 t / 2.303$$

where k_1 is the first-order rate constant

Plots of the linearized equation were constructed and the constants were calculated from the slopes and intercepts of the plots of $\log (q_e - q_t)$ vs time. The correlation coefficient values were found to be low and the calculated q_e values did not agree with the experimental q_e values. Thus the adsorption of alizarin red and methylene blue does not follow pseudo first order kinetics.

3.14.4.4. Pseudo second order equation

The kinetics of adsorption of dye on colloid was studied using the pseudo second order equation given below

$$dq_t/dt = K(q_e - q_t)^2$$

where K is the pseudo second order rate constant (g/mg/h), q_e is the adsorbed amount of dye at equilibrium (mg/g) and q_t is the adsorbed amount of dye at time t (mg/g). Integrating the above equation for the boundary conditions $t=0$ to $t=t$ and $q_t=0$ to $q_t=q_t$, gives

$$1/(q_e - q_t) = 1/q_e + K t$$

The linear form of the above equation after integration is

$$t/q_t = 1/(Kq_e^2) + (1/q_e)t$$

The intercept and slope of the plot of t/q_t vs t gives the value of K and q_e respectively. The correlation coefficient values show that the pseudo second order kinetics fits well for the adsorption of methylene blue on humic acids and the results are shown in Table 3.40.

Table 3.40. Kinetics of adsorption of alizarin red and methylene blue

C_e (mg/L)	Methylene blue			Alizarin red		
	K (g/mg/h)	q_e (mg/g)	R	K (g/mg/h)	q_e (mg/g)	R
50	0.0245	0.0095	0.9886	0.0572	0.0020	0.3901
100	0.0306	0.0041	0.9651	0.0515	0.0026	0.8304
150	0.0170	0.0058	0.9908	0.0150	0.0047	0.9666
200	0.0147	0.0037	0.9212	-0.4695	0.2982	0.7969

The rate of adsorption of dyes on humic sample was determined at an initial concentration range of 50-200 mg/L and the results are shown in Figure 3.54. As shown in the Figure, equilibration time was found to be between four to six hours for the experiments performed with an initial concentration of 50mg/L to 200 mg/L. Pseudo second order rate constant (k) for the adsorption of alizarin red shows the decreasing trend except at 200 mg/L because at higher initial concentrations fractional adsorption is low. In the case of methylene blue rate constant (K) increases initially and then follows the decreasing trend with increasing concentration of dye. This shows that pseudo second order rate constant decreases non linearly with increasing initial concentration of dye solution.

The adsorption capacity at equilibrium (q_e) increased with increase in initial concentration of Alizarin red dye solution, but in the case of Methylene blue the adsorption capacity value q_e shows the decreasing trend except for the initial concentration of 100 mg/L.

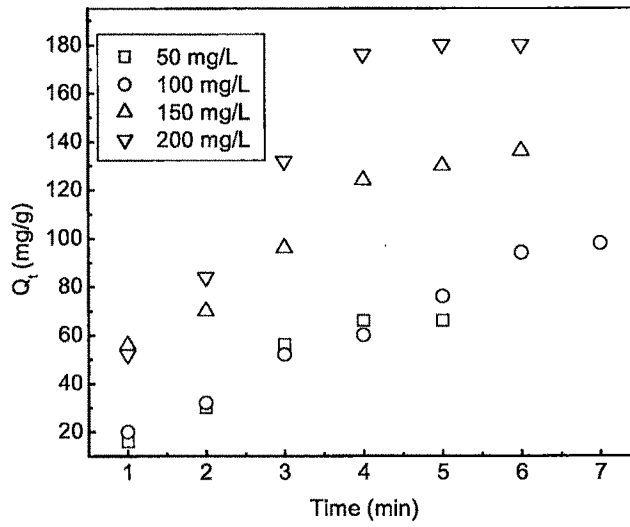
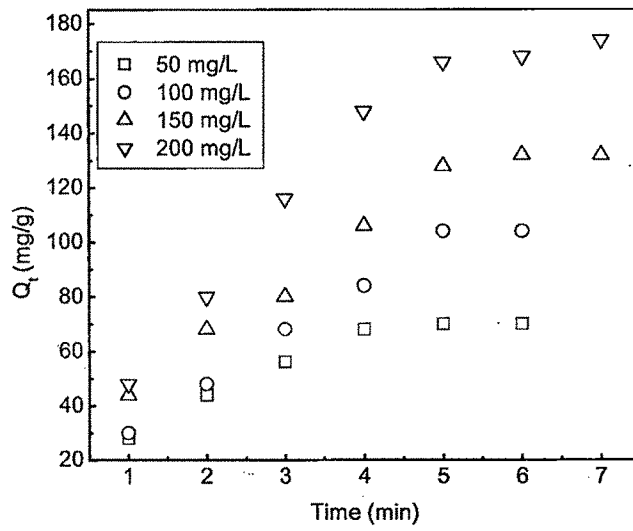


Figure 3.54. Effect of initial concentration vs time